

THE STUDY OF SCALE FORMATION IN OIL RESERVOIR DURING WATER
INJECTION AT HIGH-BARIUM AND HIGH-SALINITY FORMATION WATER

AMER BADR MOHAMMED BIN MERDHAH

UNIVERSITI TEKNOLOGI MALAYSIA

UNIVERSITI TEKNOLOGI MALAYSIA

DECLARATION OF THESIS / UNDERGRADUATE PROJECT PAPER AND COPYRIGHT

Author's full name: **AMER BADR MOHAMMED BIN MERDHAH**

Date of birth : **28/04/1973**

Title : **THE STUDY OF SCALE FORMATION IN OIL
RESERVOIR DURING WATER INJECTION AT HIGH-
BARIUM AND HIGH-SALINITY FORMATION WATER**

Academic Session : **2007/2008**

I declare that this thesis is classified as :

- | | | |
|-------------------------------------|---------------------|--|
| <input type="checkbox"/> | CONFIDENTIAL | (Contains confidential information under the Official Secret Act 1972) |
| <input type="checkbox"/> | RESTRICTED | (Contains restricted information as specified by the organization where research was done) |
| <input checked="" type="checkbox"/> | OPEN ACCESS | I agree that my thesis to be published as online open access (full text) |

I acknowledged that Universiti Teknologi Malaysia reserves the right as follows:

1. The thesis is the property of Universiti Teknologi Malaysia.
2. The Library of Universiti Teknologi Malaysia has the right to make copies for the purpose of research only.
3. The Library has the right to make copies of the thesis for academic exchange.

Certified by :

SIGNATURE

SIGNATURE OF SUPERVISOR

02076291
(NEW IC NO. /PASSPORT NO.)

PROF. DATO. DR. ABU AZAM MOHD. YASSIN
NAME OF SUPERVISOR

Date : **21 November 2007**

Date : **21 November 2007**

NOTES : * If the thesis is CONFIDENTIAL or RESTRICTED, please attach with the letter from the organization with period and reasons for confidentiality or restriction.

THE STUDY OF SCALE FORMATION IN OIL RESERVOIR DURING WATER
INJECTION AT HIGH-BARIUM AND HIGH-SALINITY FORMATION WATER

AMER BADR MOHAMMED BIN MERDHAH

A thesis submitted in fulfilment of the
requirements for the award of the degree of
Master of Engineering (Petroleum)

Faculty of Chemical and Natural Resources Engineering
Universiti Teknologi Malaysia

November 2007

ACKNOWLEDGMENT

First and foremost I would like express my thanks to Almighty ALLAH on successful completion of this research work and thesis.

I hereby, express my sincere and profound gratitude to my supervisor Professor Dato' Dr. Abu Azam Mohd.Yassin for his continuing assistance, support, guidance, and understanding throughout my graduate studies. His trust, patience, knowledge, great insight, modesty, and friendly personality have always been an inspiration for me and will deeply influence my career and future life.

The author is grateful to the Faculty of Chemical and Natural Resources Engineering, UTM for the support and facilities provided to carry out the experimental work. The author is also grateful to the staff of the Reservoir Engineering Laboratory for their support, assistance and friendly treatment that not only facilitated the work, but also made it pleasant.

My fellow postgraduate students should also be recognized for their support, especially Mazen Ahmed Moherei. I am grateful to all my family members.

ABSTRACT

Scale deposition is one of the most serious oil field problems that afflict water injection systems primarily when two incompatible waters are involved. Two waters are incompatible if they interact chemically and precipitate minerals when mixed. Typical examples are sea water, with high concentration of sulfate ion and formation waters, with high concentrations of calcium, barium, and strontium ions. Mixing of these waters, therefore, could cause precipitation of calcium sulfate, barium sulfate and/or strontium sulfate. This study was conducted to investigate the permeability reduction caused by deposition of calcium, strontium, and barium sulfates in sandstone cores from mixing of injected sea water and formation water that contained high concentration of calcium, barium, and strontium ions at various temperatures (50 - 80 °C) and differential pressures (100 - 200 psig). The solubility of common oil field scales formed and how their solubilities were affected by changes in salinity and temperatures (40 - 90 °C) were also studied. The morphology and particle size of scaling crystals formed as shown by Scanning Electron Microscopy (SEM) were also presented. The results showed that a large extent of permeability damage caused by calcium, strontium, and barium sulfates that deposited on the rock pore surface. The rock permeability decline indicates the influence of the concentration of calcium, barium, and strontium ions. At higher temperatures, the deposition of CaCO_3 , CaSO_4 , and SrSO_4 scales increases and the deposition of BaSO_4 scale decreases since the solubilities of CaCO_3 , CaSO_4 , and SrSO_4 scales decreases and the solubility of BaSO_4 increases with increasing temperature. The deposition of CaSO_4 , SrSO_4 , and BaSO_4 scales during flow of injection waters into porous media was shown by Scanning Electron Microscopy (SEM) micrographs.

ABSTRAK

Pemendapan kerak ialah satu daripada masalah medan minyak yang paling serius dalam sistem suntikan air terutama apabila dua larutan tidak secocok bercampur. Dua larutan dikatakan tidak secocok jika kedua-duanya berinteraksi secara kimia dan termendap apabila bercampur. Sebagai contoh, campuran air laut dengan kepekatan ion sulfat yang tinggi dan air formasi dengan kepekatan ion kalsium, barium, dan strontium yang tinggi. Seterusnya, gabungan larutan ini menyebabkan berlakunya pemendapan CaSO_4 , BaSO_4 , dan/atau SrSO_4 . Eksperimen yang dijalankan adalah untuk menyiasat pengurangan ketertelapan yang disebabkan oleh pemendapan kalsium, strontium, dan barium sulfat di dalam teras batu pasir dengan menggabungkan air laut suntikan dengan air formasi yang mengandungi kepekatan kalsium, strontium, dan ion barium pada pelbagai suhu (50 – 80 °C) dan perbezaan tekanan (100 - 200 psig). Keterlarutan kerak yang terbentuk di medan minyak dan bagaimana larutan tersebut dipengaruhi oleh perubahan paras kandungan garam dan suhu (40 – 90 °C) turut dikaji. Morfologi dan saiz zarah kerak kristal yang diperoleh daripada Imbasan Mikroskop Elektron (SEM) turut diketengahkan. Keputusan menunjukkan bahawa pengurangan ketertelapan yang ketara adalah disebabkan oleh kalsium, strontium, dan barium sulfat yang termendap pada permukaan liang batu. Penyusutan ketertelapan batuan menunjukkan kesan kepekatan ion kalsium, strontium, dan barium. Pada suhu yang lebih tinggi, kerak bagi CaCO_3 , CaSO_4 , dan SrSO_4 meningkat, manakala kerak BaSO_4 menurun kerana keterlarutan CaCO_3 , CaSO_4 , dan SrSO_4 menurun dan keterlarutan BaSO_4 pula meningkat dengan kenaikan suhu. Pembentukan CaSO_4 , SrSO_4 , dan BaSO_4 semasa pengaliran air suntikan ke dalam medium poros dibuktikan menerusi penggunaan Imbasan Mikroskop Elektron (SEM) mikrograf.

TABLE OF CONTENTS

CHAPTER	TITLE	PAGE
	ACKNOWLEDGEMENTS	ii
	ABSTRACT	iii
	ABSTRAK	iv
	TABLE OF CONTENTS	v
	LIST OF TABLES	ix
	LIST OF FIGURES	x
1	INTRODUCTION	1
	1.1 Introduction	1
	1.2 Common Oilfield Scales	2
	1.3 Scale Deposition	3
	1.4 Source of Oilfield Scale	4
	1.5 Problem Statement	5
	1.6 Objective of the Study	5
	1.7 Scope of the Study	6
2	LITERATURE REVIEW	7
	2.1 Introduction	7
	2.2 An Overview of Formation Damage	7
	2.2.1 Occurrence of Formation Damage	12
	2.3 Waterflooding	13
	2.3.1 Scale Formation along the Injection Water Path in Waterflood Operations	15
	2.3.2 Where Does Oilfield Scale Form?	17

2.4	The Scaling Problem in Oilfields	19
2.5	Solubility of Scale formation	24
2.5.1	Calcium, Strontium, Barium Sulfates, and Calcium Carbonate Solubilities	26
2.5.1.1	Effect of Supersaturation	27
2.5.1.2	Effect of Temperature	28
2.5.1.3	Effect of Pressure	30
2.5.1.4	Effect of Ionic Strength	31
2.5.1.5	Effect of PH	32
2.5.1.6	Effect of Carbon Dioxide Partial Pressure	32
2.5.2	Zinc Sulfide, Lead Sulfide, and Iron Sulfide Solubilities	33
2.6	Oilfield Scale Types	34
2.6.1	Calcium Carbonate Scales	34
2.6.2	Calcium Sulfate Scales	36
2.6.3	Barium Sulfate Scale	37
2.6.4	Strontium Sulfate Scale	39
2.6.5	Sources of Zinc and Lead and the Mechanism of Sulfide Formation	39
2.6.6	Iron Sulfide Scale	41
2.7	Scale Prevention and Removal	41
2.7.1	Prevention Scale Formation	41
2.7.1.1	Operational Prevention	42
2.7.2	Scale Control Chemicals	42
2.7.3	Scale Removal Methods	45
2.7.3.1	Calcium Carbonate	45
2.7.3.2	Calcium Sulfate	46
2.7.3.3	Barium Sulfate	46
2.8	Scale Prediction	47
2.8.1	Laboratory Evaluation	47
2.8.2	Modeling Development	55
2.9	Summary	60

3	METHODOLOGY	61
3.1	Introduction	61
3.2	Materials Used	61
3.2.1	Porous Medium	61
3.2.2	Brines	63
3.3	Equipment Set-up	64
3.3.1	Core Holder	65
3.3.2	Fluid Injection Pump	66
3.3.3	Transfer Cell	67
3.3.4	Oven	68
3.3.5	Pressure Transducer	68
3.3.6	Laboratory Thermal Equipment (Water Bath)	69
3.3.7	Vacuum Pump	69
3.3.8	A Core Cutter Purchased	70
3.3.9	Soxhlet Extractor	70
3.3.10	Memmert Universal Oven	71
3.3.11	Viscometer	71
3.3.12	Auxiliary Equipment and Tools	72
3.4	Experimental Procedure	72
3.4.1	Beaker Test	72
3.4.2	Core Test	74
3.4.2.1	Core Saturation	74
3.4.2.2	Porosity Measurement	75
3.4.2.3	Initial Permeability Measurement	75
3.4.2.4	Flooding Experiment	76
3.4.2.5	Scanning Electron Microscopy (EM)	77
4	RESULTS AND DISCUSSION	78
4.1	Beaker Test	78
4.2	Core Test	82
4.2.1	Calcium and Strontium Sulfates Experiments	83

4.2.1.1	Extend of Permeability Damage	83
4.2.1.2	Decline Trend of Permeability Ratio	85
4.2.1.3	Effect of Temperature	85
4.2.1.4	Effect of Differential Pressure	89
4.2.1.5	Effect of Concentration	93
4.2.2	Barium Sulfate Experiments	97
4.2.2.1	Extend of Permeability Damage	98
4.2.2.2	Decline Trend of Permeability Ratio	99
4.2.2.3	Effect of Temperature	99
4.2.2.4	Effect of Differential Pressure	103
4.2.2.5	Effect of Concentration	107
4.3	Scanning Electron Microscopy Analysis	113
5	CONCLUSIONS AND RECOMMENDATIONS	117
5.1	Conclusion	117
5.2	Recommendations	119
	REFERENCES	120
	APPENDICES A - E	132 - 164

LIST OF TABLES

TABLE NO.	TITLE	PAGE
1.1	Most common oilfield scales	3
3.1	Physical properties of sandstone cores used in this study	62
3.2	The ionic compositions of synthetic formation and injection waters	64
3.3	Compounds of synthetic formation and injection waters	64
4.1	Solubility of CaCO_3 at various temperatures	80
4.2	Solubility of CaSO_4 at various temperatures	80
4.3	Solubility of SrSO_4 at various temperatures	80
4.4	Solubility of BaSO_4 at various temperatures	81

LIST OF FIGURES

FIGURE NO.	TITLE	PAGE
2.1	Diagram indicating changes which could produce scale at different locations	16
2.2	Locations throughout the flow system where scale deposition may take place	19
2.3	Solubilities of common scales	27
2.4	Calcium sulfate solubility in water	30
2.5	Relative solubilities of three sulfates in brine	32
2.6	Comparison of zinc, lead, and iron sulfide solubility in 1M NaCl brine at 25 °C.	34
3.1	Schematic of the core flooding apparatus	65
3.2	Photograph of the core flooding apparatus	65
3.3	Core holder	66
3.4	Double- piston plunger pump	67
3.5	Stainless steel transfer cell	67
3.6	A temperature controlled oven	68
3.7	Pressure transducer with a digital display	68

3.8	A temperature controlled water bath	69
3.9	Vacuum pump	69
3.10	Sandstones cutting equipment	70
3.11	Soxhlet extractor	70
3.12	Memmert universal oven	71
3.13	Brookfield viscometer with a circulated temperature water bath	71
3.14	Hot plate	73
3.15	Equipments of core saturation	75
4.1	Solubility of CaCO_3 is largely dependent on temperature	81
4.2	CaSO_4 solubility is dependent on temperature	81
4.3	SrSO_4 solubility is dependent on temperature	82
4.4	BaSO_4 solubility is dependent on temperature	82
4.5	Variation of permeability ratio as a function of time showing the effect of concentration at 100 psig and 50 °C	84
4.6	Variation of permeability ratio as a function of time showing the effect of concentration at 200 psig and 80 °C	85
4.7	Variation of permeability ratio as a function of time showing the effect of temperature at 100 psig	86
4.8	Variation of permeability ratio as a function of time showing the effect of temperature at 150 psig	87
4.9	Variation of permeability ratio as a function of time showing the effect of temperature at 200 psig	87

4.10	Variation of permeability ratio as a function of time showing the effect of temperature at 100 psig	88
4.11	Variation of permeability ratio as a function of time showing the effect of temperature at 150 psig	88
4.12	Variation of permeability ratio as a function of time showing the effect of temperature at 200 psig	89
4.13	Variation of permeability ratio as a function of time showing the effect of differential pressure at 50 °C	90
4.14	Variation of permeability ratio as a function of time showing the effect of differential pressure at 70 °C	91
4.15	Variation of permeability ratio as a function of time showing the effect of differential pressure at 80 °C	91
4.16	Variation of permeability ratio as a function of time showing the effect of differential pressure at 50 °C	92
4.17	Variation of permeability ratio as a function of time showing the effect of differential pressure at 70 °C	92
4.18	Variation of permeability ratio as a function of time showing the effect of differential pressure at 80 °C	93
4.19	Variation of permeability ratio as a function of time Showing the effect of concentration at 100 psig and 70 °C	94
4.20	Variation of permeability ratio as a function of time showing the effect of concentration at 100 psig and 80 °C	94
4.21	Variation of permeability ratio as a function of time showing the effect of concentration at 150 psig and 50 °C	95

4.22	Variation of permeability ratio as a function of time showing the effect of concentration at 150 psig and 70 °C	95
4.23	Variation of permeability ratio as a function of time showing the effect of concentration at 150 psig and 80 °C	96
4.24	Variation of permeability ratio as a function of time showing the effect of concentration at 200 psig and 50 °C	96
4.25	Variation of permeability ratio as a function of time showing the effect of concentration at 200 psig and 70 °C	97
4.26	Variation of permeability ratio as a function of time showing the effect of concentration at 100 psig and 80 °C	98
4.27	Variation of permeability ratio as a function of time showing the effect of concentration at 200 psig and 50 °C	99
4.28	Variation of permeability ratio as a function of time showing the effect of temperature at 100 psig	100
4.29	Variation of permeability ratio as a function of time showing the effect of temperature at 150 psig	101
4.30	Variation of permeability ratio as a function of time showing the effect of temperature at 200 psig	101
4.31	Variation of permeability ratio as a function of time showing the effect of temperature at 100 psig	102
4.32	Variation of permeability ratio as a function of time showing the effect of temperature at 150 psig	102
4.33	Variation of permeability ratio as a function of time showing the effect of temperature at 200 psig	103

4.34	Variation of permeability ratio as a function of time showing the effect of differential pressure at 50 °C	104
4.35	Variation of permeability ratio as a function of time showing the effect of differential pressure at 70 °C	105
4.36	Variation of permeability ratio as a function of time showing the effect of differential pressure at 80 °C	105
4.37	Variation of permeability ratio as a function of time showing the effect of differential pressure at 50 °C	106
4.38	Variation of permeability ratio as a function of time showing the effect of differential pressure at 70 °C	106
4.39	Variation of permeability ratio as a function of time showing the effect of differential pressure at 80 °C	107
4.40	Variation of permeability ratio as a function of time showing the effect of concentration at 100 psig and 50 °C	108
4.41	Variation of permeability ratio as a function of time showing the effect of concentration at 150 psig and 50 °C	108
4.42	Variation of permeability ratio as a function of time showing the effect of concentration at 100 psig and 70 °C	109
4.43	Variation of permeability ratio as a function of time showing the effect of concentration at 150 psig and 70 °C	109
4.44	Variation of permeability ratio as a function of time showing the effect of concentration at 200 psig and 70 °C	110
4.45	Variation of permeability ratio as a function of time showing the effect of concentration at 150 psig and 80 °C	110

4.46	Variation of permeability ratio as a function of time showing the effect of concentration at 200 psig and 80 °C	111
4.47	Variation of permeability ratio as a function of time showing the effect of concentration at 200 psig and 50 °C	111
4.48	Variation of permeability ratio as a function of time showing the effect of concentration at 200 psig and 80 °C	112
4.49	Variation of permeability ratio as a function of time showing the effect of concentration at 100 psig and 50 °C	112
4.50	Variation of permeability ratio as a function of time showing the effect of concentration at 100 psig and 80 °C	113
4.51	SEM image of an unscaled sandstone cores	114
4.52	SEM image of BaSO ₄ scale in sandstone core at 200 psig and 50 °C	115
4.53	SEM image of CaSO ₄ and SrSO ₄ scales in sandstone core at 200 psig and 80 °C	116

LIST OF APPENDICES

APPENDIX	TITLE	PAGE
A	Summary of Previous Experimental Works	132
B	Experimental Data and Results of Barium Sulfate	136
C	Experimental Data and Results of Calcium and Strontium Sulfates	146
D	Effects of Temperature, Concentration of Brine, and Differential Pressures on Permeability Reduction by Deposition of Barium Sulfate	156
E	Effects of Temperature, Concentration of Brine, and Differential Pressures on Permeability Reduction by Deposition of Calcium and Strontium Sulfates	164

CHAPTER 1

INTRODUCTION

1.1 Introduction

The injection of seawater into oilfield reservoirs to maintain reservoir pressure and improve secondary recovery is a well established mature operation. Moreover, the degree of risk posed by deposition of mineral scales to the injection and production wells during such operations has been much studied.

Scale formation in surface and subsurface oil and gas production equipment has been recognized to be a major operational problem. It has been also recognized as a major cause of formation damage either in injection or producing wells. Scale contributes to equipment wear and corrosion and flow restriction, thus resulting in a decrease in oil and gas production.

Experience in the oil industry has indicated that many oil wells have suffered flow restriction because of scale deposition within the oil producing formation matrix and the downhole equipment, generally in primary, secondary and tertiary oil recovery operation as well as scale deposits in the surface production equipment.

There are other reasons why scale forms, and the amount and location of which are influenced by several factors. And, supersaturation is the most important reason behind mineral precipitation.

A supersaturated condition is the primary cause of scale formation and occurs when a solution contains dissolved materials which are at higher concentrations than their equilibrium concentration. The degree of supersaturation, also known as the scaling index, is the driving force for the precipitation reaction and a high supersaturation condition, therefore, implies higher possibilities for salt precipitation.

Scale can occur at/or downstream of any point in the production system, at which supersaturation is generated. Supersaturation can be generated in single water by changing the pressure and temperature conditions or by mixing two incompatible waters. Changes in temperature, pressure, pH, and CO₂/H₂S partial pressure could also contribute to scale formation (Mackay *et al.*, 2003; Moghadasi *et al.*, 2003a).

This chapter gave an introduction to the most common scales encountered in oil field operations, scale deposition, and source of oil field scale. The problem statement, objectives, and scope of the study were also presented.

1.2 Common OilField Scales

The most common oilfield scales are listed in Table 1.1, along with the primary variables that affect their solubility (Moghadasi *et al.*, 2003a). These scales are sulfates such as calcium sulfate (anhydrite, gypsum), barium sulfate (barite), and strontium sulfate (celestite) and calcium carbonate. Other less common scales have also been reported such as iron oxides, iron sulfides and iron carbonate.

Table 1.1: Most common oilfield scales

Name	Chemical Formula	Primary Variables
Calcium Carbonate	CaCO_3	Partial pressure of CO_2 , temperature, total dissolved salts, pH
Calcium Sulfate: Gypsum Hemihydrate Anhydrite	$\text{CaSO}_4 \cdot 2\text{H}_2\text{O}$ $\text{CaSO}_4 \cdot 1/2\text{H}_2\text{O}$ CaSO_4	Temperature, total dissolved salts, pressure
Barium Sulfate	BaSO_4	Temperature, pressure
Strontium Sulfate	SrSO_4	Temperature, pressure, total dissolved salts
Iron Compounds: Ferrous Carbonate Ferrous Sulfide Ferrous Hydroxide Ferrous Hydroxide	FeCO_3 FeS $\text{Fe}(\text{OH})_2$ $\text{Fe}(\text{OH})_3$	Corrosion, dissolved gases, pH

1.3 Scale Deposition

Scale deposition in surface and subsurface oil and gas production equipment has been recognized. Scale deposition is one of the most important and serious problems that inflict oil field water injection systems. Scale limits and sometimes blocks oil and gas production by plugging the oil-producing formation matrix or fractures and perforated intervals. It can also plug production lines and equipment and impair fluid flow. The consequence could be production-equipment failure, emergency shutdown, increased maintenance cost, and overall decrease in production efficiency. The failure of these equipments could result in safety

dangers. In case of water injection systems, scale could plug the pores of the formation and results in injectivity decline with time (Yuan and Todd, 1991; Bayona, 1993; Asghari and Kharrat, 1995; Andersen *et al.*, 2000; Paulo *et al.*, 2001; Voloshin *et al.*, 2003).

Scale deposition can occur from one type of water because of supersaturation with scale-forming salts attributable to changes in the physical conditions under which the water exists. Scale also can deposit when two incompatible waters are mixed and supersaturation is reached (Nassivera and Essel, 1979; Read and Ringen, 1982; Vetter *et al.*, 1982; Todd and Yuan, 1992; Moghadasi *et al.*, 2003b; Moghadasi *et al.*, 2004b).

1.4 Source of OilField Scale

The chief source of oilfield scale is mixing of incompatible waters. Two waters are called incompatible if they interact chemically and precipitate minerals when mixed. A typical example of incompatible waters are sea water with high concentration of SO_4^{-2} and low concentrations of Ca^{+2} , $\text{Ba}^{+2}/\text{Sr}^{+2}$, and formation waters with very low concentrations of SO_4^{-2} but high concentrations of Ca^{+2} , Ba^{+2} and Sr^{+2} . Mixing of these waters, therefore, causes precipitation of CaSO_4 , BaSO_4 , and/or SrSO_4 . Field produced water (disposal water) can also be incompatible with seawater. In cases where disposal water is mixed with seawater for re-injection, scale deposition is possible (Bayona, 1993; Andersen *et al.*, 2000; Bedrikovitsky *et al.*, 2001; Stalker *et al.*, 2003; Paulo *et al.*, 2001).

During the production, the water is drained to the surface and suffers from significant pressure drop and temperature variations. The successive pressure drops lead to release of the carbon dioxide with an increase in pH value of the produced water and precipitation of calcium carbonate (Mackay, 2003).

Zinc sulfide scale is more likely when zinc ion source mixes with the hydrogen sulfide-rich source within the near wellbore or the production tubing during fluid extraction. Lead and zinc sulfide scales have recently become a concern in a number oil and gas fields. These deposits have occurred within the production tubing and topside process facilities (Collins and Jordan, 2003).

1.5 Problem Statement

Seawater is injected into the reservoir for the purpose of pressure maintenance and improves secondary recovery in offshore production location. Seawater contains significant concentration of sulfate ion while formation water is rich in divalent cations such as Ca^{++} , Sr^{++} , and Ba^{++} . When these two incompatible waters mix, unstable, supersaturated brine is created which precipitates calcium sulfate, strontium sulfate, and barium sulfate within the reservoir rock. Such scale deposition could have adverse effects on reservoir performance, primarily through damaging reservoir permeability.

1.6 Objective of the Study

The objectives of this study were:

- (i) To investigate permeability reduction by deposition of scale in a sample of Malaysia sandstone core.
- (ii) To know the solubilities of scale formed and how their solubilities were affected by the changes in salinity and temperature.

1.7 Scope of the Study

The scopes of this study were divided into three sections:

- (1) A laboratory investigation of scale formation in a typical Malaysia sandstone cores, resulting from the mixing of injected and formation waters at the condition of high-salinity (high concentration of calcium and strontium) and high concentration of barium. Temperatures (50 – 80 °C) and differential pressures (100 – 200 psig) effects were conducted to give insight into the nature of the scale and its effect on rock permeability.
- (2) The solubility of scale formed at various temperatures (40 – 90 °C) and concentrations were also studied.
- (3) The particle size and the morphology of scale deposition were observed using Scanning Electron Microscopy (SEM).

CHAPTER 2

LITERATURE REVIEW

2.1 Introduction

Scale deposition in waterflooding operations often results from the incompatibility of injected and formation waters. This chapter describes an overview of the formation damage, scale formation along the injection water path in waterflood operations, scaling problems encountered in the oilfields, solubility of scale, oilfield scale types, scale control chemicals, and laboratory investigations of scale in different media and procedures used to predict scale are presented.

2.2 An Overview of Formation Damage

Formation damage occurs during the life of many wells. Loss of well performance because of formation damage has been the subject of several review articles. Fines migration, inorganic scale, emulsion blockage, asphaltene, and other organic deposition are a few mechanisms that can cause formation damage (Nasr-El-Din, 2003).

The success of oil recovery is strongly influenced by whether the reservoir permeability can be kept intact or even improved. Permeability changes in petroleum reservoirs have received a great deal of concern by the oil and gas industry. This problem is termed as formation damage. It can occur during almost any stage of petroleum exploration and production operations.

The formation damage in scaled-up production wells caused by incompatibility of injected and formation waters have long been known. Permeability decline due to precipitate of salts. Among the most onerous of all scaling species is that of sulfates, particularly barium and strontium sulfates (Oddo and Tomson, 1994).

Due to the extensive use of water injection for oil displacement and pressure maintenance in the oilfield, many reservoirs experience the problem of scale deposition when injection water begins to breakthrough.

In most cases, the scaled-up wells are caused by the formation of sulfate and carbonate scales of calcium and strontium. Because of their proportionate hardness and low solubility, there are restricted processes available for their removal and preventive measures such as the *squeeze* inhibitor treatment must be taken. It is therefore important to gain a proper understanding of the kinetics of scale formation and its detrimental effects on formation damage under both inhibited and uninhibited conditions (Moghadasi *et al.*, 2003b).

According to Moghadasi *et al.* (2004a), formation damage is a general terminology referring to the impairment of the permeability of petroleum bearing formations by various adverse processes. Formation damage is an undesirable operational and economic problem that can happen during the several phases of oil and gas recovery from subsurface reservoirs involving drilling, production, hydraulic fracturing and workovers operations.

Formation damage is a costly headache to the oil and gas industry. The fundamental processes causing damage in petroleum bearing formations are: hydrodynamic, physico-chemical, chemical, thermal, and mechanical.

Two phenomena can change the permeability of the rock. One is change of porosity. This phenomenon is due to the swelling of clay minerals or deposition of solids in the pore body. The other is the plugging of pore throats. The narrow passages govern the ease of fluid flow through porous media. If they are blocked,

the permeability of the porous rock will be low even though the pore space remains large.

Either organic or inorganic matter may cause the plugging of pore throats. The organic induced damage is due to the formation of high viscosity hydrocarbon scale when temperature and pressure conditions in the reservoirs are changed. The inorganic damage involves release and capture of particulate including in-situ fines and precipitates from chemical reactions.

The mechanisms that trigger the formation damage can be categorized into three major processes (Leone and Scott, 1988):

(1) Hydrodynamic

A mechanical force mobilizes loosely attached fine particles from the pore surface by exerting a pressure gradient during fluid flow. The movement of many different types of fines including clay minerals, quartz, amorphous silica, feldspars, and carbonates may cause mechanical fine migration damage.

(2) Physicochemical

This mechanism is caused by the water sensitivity clays. Clays exist in equilibrium with the formation brines until the ionic composition and concentration of the brine is altered (Crowe, 1986). Permeability declines because the swollen clay occupies more of the pore space, but more often occurs because of fines released by the swelling.

(3) Geochemical

The injected fluid may not be compatible with the native pore fluid during treatment of reservoirs or waterflooding. This incompatibility results in chemical none equilibrium in the porous system. Ions in the source water may react with ions in the reservoir fluids to form solid precipitates downstream in the porous system to plug pore throats or to deposit onto pore wall resulting in porosity reduction.

Mineral scale formation and deposition on downhole and surface equipment is a major source of cost and reduce production to the oil industry. Solid scale formation mainly results from changes in physical-chemical properties of fluids (i.e., pH, partial pressure of CO₂, temperature, and pressure) during production or from chemical incompatibility between injected and formation waters (Collins *et al.*, 2005).

Precipitation of mineral scales causes many problems in oil and gas production operations: formation damage, production losses, increased workovers in producers and injectors, poor injection water quality, and equipment failures due to under-deposit corrosion. The most common mineral scales are sulfate and carbonate-based minerals. However, scale problems are not limited to these minerals and there have recently been reports of unusual scale types such as zinc and lead sulfides (Collins and Jordan, 2003).

The formation of mineral scale in production facilities is a relatively common problem in the oil industry. Most scale forms either by pressure and temperature changes that favor salt precipitation from formation waters, or when incompatible waters mix during pressure maintenance or waterflood strategies. Scale prevention is achieved by performing *squeeze* treatments in which chemical scale inhibitors are injected in the producers near wellbore.

Mechanisms by which a precipitate reduces permeability include solids depositing on the pore walls because of attractive forces between the particles and the surface of the pore, a single particle blocking a pore throat, and several particles bridging across a pore throat. The characteristics of the precipitate influence the extent of formation damage. Such conditions as a large degree of supersaturation, the presence of impurities, a change in temperature, and the rate of mixing control the quantity and morphology of the precipitating crystals (Allaga *et al.*, 1992).

In the North Sea, the universal use of sea water injection as the primary oil recovery mechanism and for pressure maintenance means that problems with sulfate

scale deposition, mainly barium and strontium, are likely to be present at some stage during the production life of the field (Wat *et al.*, 1992).

Formation damage studies are executed for understanding of these processes via laboratory and field testing, development of mathematical models via the description of fundamental mechanisms and processes. Mineral scale formation is one of the main mechanisms of formation damage.

Moreover, the formation of mineral scale associated with the production of hydrocarbons has always been a concern in oilfield operation. Depending on the nature of the scale and on the fluid composition, the deposition can occur inside the reservoir which causes formation damage (Khatib, 1994; Krueger, 1986; Lindlof and Stoffer, 1983; Moghadasi *et al.*, 2003a) or in the production facilities where blockage can cause severe operational problems.

Furthermore, the two main types of scale which are commonly found in the oilfield are carbonate and sulfate scales. Whilst the formation of carbonate scale is associated with the pressure and pH changes of the production fluid, the occurrence of sulfate scale is mainly due to the mixing of incompatible brines, i.e. formation water and injection water.

According to Bagci *et al.* (2000), formation damage is a well-known phenomenon in many waterflooding operations. This damage depends on many factors, such as the quality of the injected water and rock mineralogical composition. Movement of particles in reservoirs has long been recognized to cause formation damage.

Nevertheless, during drilling and production operations, these fine particles could have been incorporated in the formation during geological deposition or can be introduced into the formation. Investigations and diagnosis of specific problems indicate that the reasons are usually associated with either the physical movement of

fine particles, chemical reactions, or a combination of both. In addition, formation damage may happen from the fine particles introduced with the injection water.

2.2.1 Occurrence of Formation Damage

During petroleum exploration and production, when fluids are introduced into a porous rock, its original purpose is to increase the recovery of hydrocarbon. However, because the incompatibility between injected and native fluids, change of reservoir rock properties can often be expected. During various oil exploitation activities, the following sections describe the potential causes of formation damage (Moghadasi *et al.*, 2002):

(1) Drilling

During drilling, higher pressure is required in the wellbore to control the formation being penetrated, the pressure differential will result in invasion of mud solids and mud filtrate into reservoir rock near wellbore. Solid invasion is strongly influenced by particle size and pore throat size distribution.

(2) Production

During the oil and gas production the temperature and pressure in reservoirs are constantly altering. Organic scale such as asphaltenes and paraffin waxes may deposit outside of the crude oil to plug the formation. Inorganic salts such as calcium carbonate and barium sulfate may also precipitate out of the aqueous phase to block flow paths. The great pressure gradient near the wellbore often is capable of mobilizing fines residing on the surface of pore wall around the producing wells to cause fines migration.

(3) Water Flooding

Combination of the injected water with the indigenous reservoir fluids is an important factor that influences the success of a waterflooding program. The ions contained in the injected fluid may react with the ions in the native fluid to insoluble precipitates.

(4) Stimulation

Most stimulation operations involve chemical treatments. Reactions of different kinds occur when chemicals are introduced into formations. Some of the reactions have adverse effects on formation permeability.

2.3 Waterflooding

Water injection to improve oil recovery is a long-standing practice in the oil industry. Pressure maintenance by water injection in some reservoirs may be considered satisfactory for oil recovery. The main objective of waterflooding is to place water into a rock formation at desired rate and pressure with minimal expense and trouble.

This objective, however, could not be achieved unless water has certain characteristics. The water, therefore, should be treated and conditioned before injection. This treatment should solve problems associated with the individual injection waters, including suspended matter, corrosivity of water scale deposition, and microbiological fouling and corrosion.

Pressure maintenance by sea water injection is planned for major North Sea oil reservoir. Sea water is proposed to be injected, where possible, into water saturated formations underlying the reservoir. Analyses of the water composition indicate that scale formation may occur by two possible mechanisms. One, changing pH and temperature conditions for sea water may precipitate insoluble salts. Two, the mixing of sea water and formation water may cause precipitation of solids. Both mechanisms could result in damage to the near wellbore formation (Read and Ringen 1982).

According to Vetter *et al.* (1982), two of the more difficult problems in designing a proper waterflood operation are:

- (1) The predetermination of chemical incompatibilities of waters used in the flood and

- (2) The forecast of these incompatibility effects on future field operations. This forecast should cover the type, extent, and location of all future damages resulting from chemical incompatibility problems.

The chemical incompatibility of injected seawater and formation water has prompted deposition of barium and strontium sulfate scales in producing wells of the Namorado field. The precipitation squeeze process was chosen as a means of preventing scale formation in this field (Bezerra *et al.*, 1990).

Sea water and formation water can become mixed during water injection both around an injection well, and also after breakthrough of injection water into production wells. Injection wells will mainly form scale in the pores of the formation rock. Production wells may form scales both within the formation and in the well tubular and process equipment.

The selection of the injection water is a critical factor when waterflood operations are planned. The most obvious (and the cheapest) source of water is the sea water in offshore oilfields; in onshore fields, waters from shallow aquifers are normally used for injection. River water is used only when no other source is available due to the high content of suspended matter and microorganisms usually present.

In all cases, the prior condition for good injection water is that it must not impair well injectivity and reservoir fluid characteristics. Injection water must be free of suspended particles, organic matter, oxygen, and acid gases (CO₂ and H₂S) before it is pumped into the injection wells (Betero *et al.*, 1988).

2.3.1 Scale Formation along the Injection Water Path in Waterflood Operations

At the injection wellhead, injection water temperature is usually much lower than reservoir temperature. When it travels down the injection well string, the water cools the surrounding formations, and its temperature and pressure increase. If the water is saturated at surface conditions with salts whose solubility decreases with increasing temperatures (e.g. anhydrite), scale may form along the well string. As the water enters the reservoir, three main phenomena occur (Bertero *et al.*, 1988):

- (a) Along the water flow path, temperature increases due to heat exchange with the reservoir rock and fluids.
- (b) Pressure decreases along the flow path.
- (c) Injection water mixes with reservoir brine.

Scale precipitation from the injection water may happen behind the mixing zone as a consequence of temperature and pressure changes. This is particularly true for waters containing salts whose solubility decreases with increasing temperature and decreasing pressure. Reservoir brine is present in forward position to the mixing zone in the rock pores. Behind the mixing zone, only injected water in equilibrium at local temperature and pressure (with residual oil) exists.

In the mixing zone, precipitation of insoluble salts may occur due to the interaction, at local temperature and pressure, of chemical species contained in the injection water with chemical species present in the reservoir brine. The remaining clear water moves ahead and mixes with reservoir brine at different pressure, due to which scale precipitation take place again. This cycle is repeated until the remaining clear water reaches a production well.

Pressure and temperature decrease along the flow string up to the surface in the production well, and further changes in thermodynamic conditions occur in the surface

equipment. This may again result in scale formation. Normally, these scales do the most damage in the wellbore when there are major falls in pressure but hardly any temperature changes (Khelil *et al.*, 1979). Figure 2.1 gives some indication of which changes occur at which part of an oilfield (Moghadasi *et al.*, 2004b).

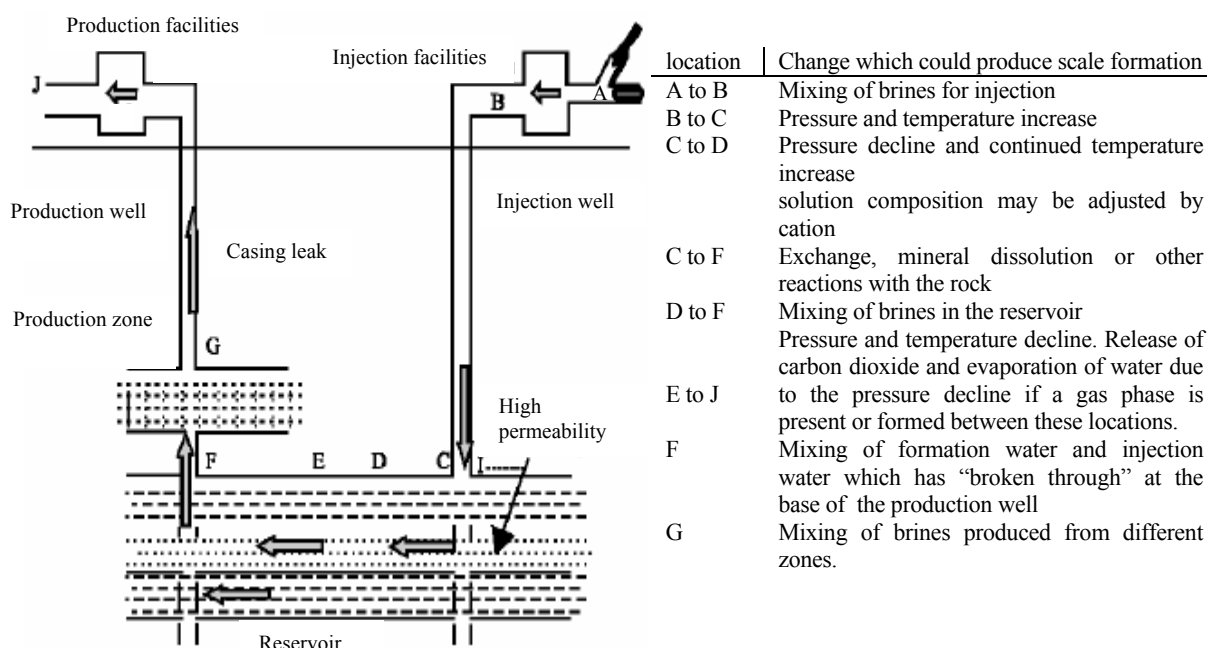


Figure 2.1 Diagram indicating changes which could produce scale at different locations (Moghadasi *et al.*, 2004b)

Seawater injection is common in North Sea field developments. The often layered nature of the reservoir results in early water breakthrough. The chemical incompatibility between injected seawater and formation water makes BaSO_4 and related scale deposition possible at various producing wells and facilities in North Sea operations.

Injected water may also mix with formation water in the near wellbore area, causing possible resistance to flow. The presence of strontium and barium ions in some formation water necessitates the examination of the possible formation damage resulting from solid solution formation of barium sulfate and strontium sulfate (Todd and Yuan, 1990).

2.3.2 Where Does Oilfield Scale Form?

The scaling reaction depends on there being adequate concentrations of sulfate ions in the injected seawater, and barium, strontium, and calcium divalent cations in the formation brine to generate sulfate scale or on there being enough bicarbonate and calcium ions to generate carbonate scale.

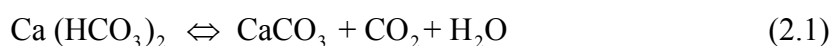
Therefore scale precipitation may occur wherever there is mixing of incompatible brines, or there are changes in the physical condition such as pressure decline. An overview of all the possible scale formation environments for seawater, aquifer, natural depletion and produced water re-injection is presented in Figure 2.2 (Jordan and Mackay, 2005; Jordan *et al.*, 2006a).

- (a) Prior to injection, for example if seawater injection is supplement by produced water re-injection (PWRI).
- (b) Around the injection well, as injection brine enters the reservoir, contacting formation brine.
- (c) Deep in formation, due to displacement of formation brine by injected brine, or due to meeting flow paths.
- (d) As injection brine and formation brine converge towards the production well, but beyond the radius of a squeeze treatment.
- (e) As injection brine and formation brine converge towards the production well, and within the radius of a squeeze treatment.
- (f) In the completed interval of a production well, as one brine enters the completion, while other brine is following up the tubing from a lower section, or as fluid pressure decreases.
- (g) At the junction of a multilateral well, where one branch is producing single brine and the other branch is producing incompatible brine.

- (h) At a subsea manifold, where one well is producing single brine and another well is producing different brine.
- (i) At the surface facilities, where one production stream is flowing one brine and another production stream is flowing another brine.
- (j) During aquifer water production and processing for re-injection could lead to scale formation within self-scaling brine or mixing with incompatible formation brine.
- (k) During pressure reduction and/or an increase in temperature within any downhole tube or surface processing equipment, leading to the evolution of CO₂ and to the generation of carbonate and sulfide scale if the suitable ions are present. Temperature reductions could lead to the formation of halite scales if the brine was close to saturation under reservoir conditions.

Oilfield scales are inorganic crystalline deposits that form as a result of the precipitation of solids from brines present in the reservoir and production flow system. The precipitation of these solids occurs as the result of changes in the ionic composition, pH, pressure, and temperature of the brine. There are three principal mechanisms by which scales form in both offshore and onshore oil field system (Mackay, 2005; Jordan and Mackay, 2005 and Collins *et al.*, 2006):

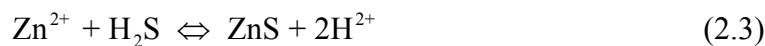
- (1) Decrease in pressure and/or increase in temperature of a brine, goes to a reduction in the solubility of the salt (most commonly these lead to precipitation of carbonate scales, such as CaCO₃).



- (2) Mixing of two incompatible brines (most commonly formation water rich in cations such as barium, calcium and/or strontium, mixing with sulfate rich seawater, goes to the precipitation of sulfate scales, such as BaSO₄).



Other fluid incompatibilities include sulfide scale where hydrogen sulfide gas mixes with iron, zinc or lead rich formation waters:



- (3) Brine evaporation, resulting in salt concentration increasing above the solubility limit and goes to salt precipitation (as may occur in HP/HT gas wells where a dry gas stream may mix with a low rate brine stream resulting in dehydration and most commonly the precipitation of NaCl).

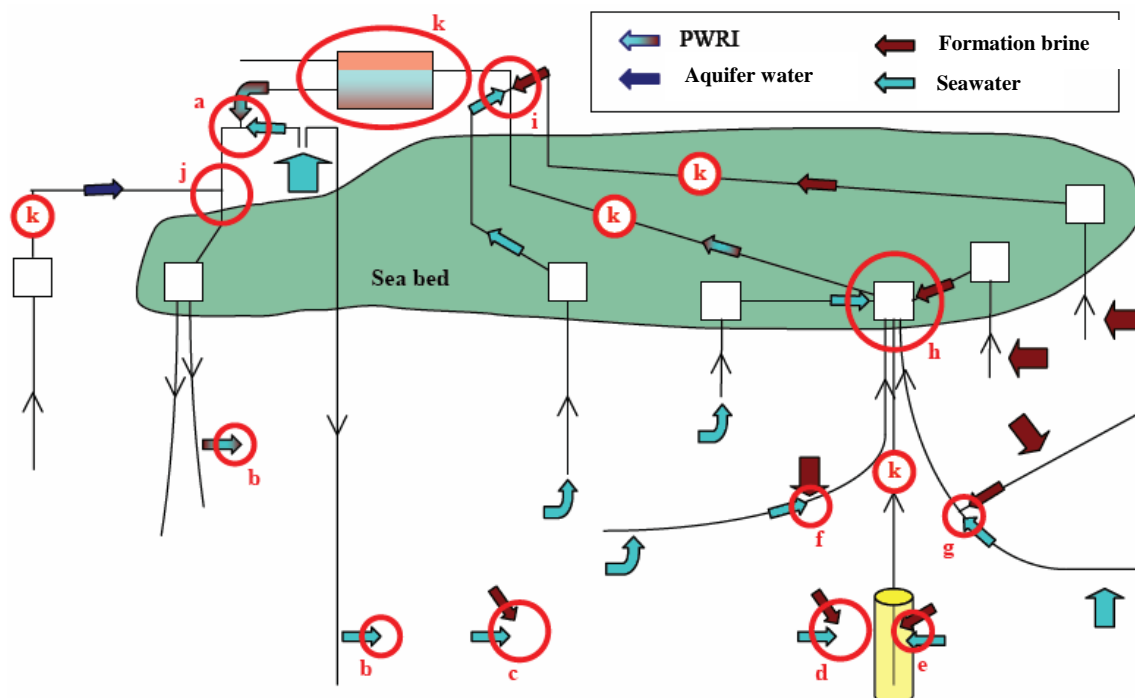


Figure 2.2 Locations throughout the flow system where scale deposition may take place (Jordan *et al.*, 2006a)

2.4 The Scaling Problem in OilFields

Scaling deposition is one of the most serious problems where water injection systems are engaged in. Generally, scale deposited in downhole pumps, tubing, casing flowlines, heater treaters, tanks, and other production equipment and facilities.

Scale formation is a major problem in the oil industry. They may occur downhole or in surface facilities. The formations of these scales plug production lines and equipment and impair fluid flow. Their consequence could be production-equipment failure, emergency shutdown, increased maintenance cost, and an overall decrease in production efficiency. The failure of production equipment and instruments could result in safety hazards (Yeboah *et al.*, 1993).

According to Bertero *et al.* (1988), one of the problems encountered in water flooding projects is scale formation caused by chemical incompatibility between potential injection waters and reservoir brine. Chemical compatibility evaluation through laboratory experiments on cores at reservoir conditions is of limited value because only first-contact phenomena are reproduced.

For a scale layer to be built up, the supersaturated formation water should contact the walls of the production equipment. The tendency for scale to be deposited, therefore, will be low, if the crude has a low water cut and if the water is finely dispersed in the oil.

The rate of scale deposition is approximately proportional to the rate of free water production. Depending upon where the formation water becomes supersaturated, scale may be deposited in the flow line only, in both flow line and tubing, and in some cases even in the perforations and in the formation near the wellbore.

The formation of inorganic mineral scale within onshore and offshore production facilities around the world is a relatively common problem. Scale can form from a single produced connate or aquifer water due to changes in temperature and pressure, or when two incompatible waters mix. An example of the latter would be seawater support of a reservoir where the formation water is rich in cations (Ba, Sr, and Ca) and the injection water is rich in anions (SO₄).

The production of such comingled fluids results in the formation of inorganic scale deposits. The types of scale and their solubility is a function of the water chemistry and physical production environment.

Oilfield scales costs are high due to intense oil and gas production decline, frequently pulling of downhole equipment for replacement, re-perforation of the producing intervals, re-drilling of plugged oil wells, stimulation of plugged oil-bearing formations, and other remedial workovers through production and injection wells. As scale deposits around the wellbore, the porous media of formation becomes plugged and may be rendered impermeable to any fluids.

The production problems caused by mineral scale in oil production operations have long been known. Among the most onerous of all scaling problems is that of sulfate scales, particularly barium sulfate scale. This is a difficult scaling problem because of the low solubility of barium sulfate in most fluids and the commensurate low reactivity of most acids with barium sulfate scale.

Deposition of barium sulfate into a continuous scale surface on production tubular exposes very little surface area for treatment by chemicals, and therefore this scale is almost impossible to remove once it is deposited. The most popular approach to addressing the barium sulfate scale problem has been to retard or prevent the formation of this scale in the first place (McElhiney *et al.*, 2001).

Many case histories of oil well scaling by calcium carbonate, calcium sulfate, strontium sulfate, and barium sulfate have been reported (Mitchell *et al.*, 1980; Lindlof and Stoffer, 1983; Vetter *et al.*, 1987; Shuler *et al.*, 1991). Problems in connection to oil well scaling in the Russia where scale has seriously plugged wells and are similar to cases in North Sea fields have been reported (Mitchell *et al.*, 1980).

Oilfields scale problems have occurred because of waterflooding in Saudi oil fields, Algeria, Indonesia in south Sumatra oilfields, and Egypt in el-Morgan

oilfield where calcium and strontium sulfate scales have been found in surface and subsurface production equipment (El-Hattab, 1982). The following is a brief explain of scaling cases reported in the literature.

Bezemer and Bauer (1969) mentioned the main difficulties encountered in the South Sumatran fields (Indonesia) due to the deposition of calcium carbonate scale have been restriction of flow through tubing and flow lines, wear and abrasion of plungers and liners, and stuck plungers or wellhead valves, so far, the only methods of combating the scale problem have been routine acidizing and well pulling. As for the pumping wells, it was estimated that some 50 percent of the total well pulling effort was directly attributable to scale deposition.

Mitchell *et al.* (1980) described scale problems occurring in the Forties field could be attributed two major factors:

- (1) Commingling of forties formation and injection waters could precipitate both barium and strontium sulfates.
- (2) Precipitation of calcium carbonate scale from formation water due to variations in pressure and temperature in production systems.

Brown *et al.* (1991) mentioned barium sulfate scale formation was a major problem could occur readily in the wellbores of the Forties field when produced water containing a high barium ion concentration mixed with injection seawater of a high sulfate ion concentration. Barium sulfate scale has been found in the topsides equipment, production header and water handling plant.

It is also found downhole, deposited on the production tubing and liner resulting in reduced bore sizes and associated loss of production. Typically scale formation begins with the onset of sea water breakthrough into a wellbore and can lead to very rapid production declines.

Todd and Yuan (1992) described barium sulfate scale occurrence was a severe production problem in North Sea oil operations. Barium sulfate is often accompanied by strontium sulfate to form a completely mixed scale called (Ba, Sr) SO₄ solid solution. Sulfate-anion-rich seawater injected into the reservoir formation subsequently mixed with formation water, which contains excessive barium and strontium.

Bayona (1993) reported two major problems with seawater injection in the north Uthmaniyah section of the Ghawar field in Saudi Arabia. The first is maintenance of acceptable water quality to prevent excessive losses of well injectivity and the second is control of plugging in the pores and corrosion at a reasonable level in the equipment due to which excessive losses of well injectivity occur. The only cause of these losses is the deposition of scales due to the presence of salts in the injection water.

Asghari and Kharrat (1995) mentioned water injectivity loss in the Siri field in Iran from an initial injection rate of 9100 bbl/day to 2200 bbl/day within six years of injection. Field and laboratory data indicated that loss of injectivity was the result of permeability reduction caused by fine particles migration and deposition in the rock pores.

Salman *et al.* (1999) conducted a study in order to predict the possibility of scale formation when seawater was injected into the northern Kuwaiti oilfields for reservoir pressure maintenance. Results indicated that the seawater was likely to be self-scaling with respect to calcium carbonate under production reservoir conditions but could become a problem when the system underwent temperature and pressure changes.

Paulo *et al.* (2001) described Sulfate scale deposition is a common problem in the Alba field in the North Sea resulted from injected seawater mixing with aquifer brines. The problem is most severe in and around the injection and

production well bores and can cause considerable disruption to hydrocarbon production after water breakthrough.

Voloshin *et al.* (2003) presented an overview of scale problems encountered in Western Siberian oilfields where formation pressure was maintained by injecting water (Senoman, fresh and Podtovarnaya water). Electric submersible pumps (ESPs) and rod pumps were used to lift reservoir fluids to surface.

Moreover, scale was one of the main reasons for failure of ESPs, which were widely used in the West Siberian oil fields. Investigation showed that carbonate deposit (calcite) was the main culprit, along with mechanical impurities. Iron deposits were present too. In 2003, many thousands of wells compromised by scale in Western Siberian oilfields.

Moghadasi *et al.* (2003a) described scale formation in the Iranian oilfields has been recognized to be a major operational problem causing formation damage either at injection or producing wells. Scale contributes to equipment wear and corrosion and flow restrictions, thus resulting in a decrease in oil and gas production.

Strachan *et al.* (2004) reported barium sulfate scale was a major problem in the BP Magnus field, even at low water cuts (<1%). In the late 1990's, BP Magnus adopted a policy of executing pre-emptive scale squeeze treatments on newly completed wells to prevent scale deposition and maintain well productivity on water breakthrough.

2.5 Solubility of Scale Formation

Solubility is defined as the limiting amount of solute that can dissolve in a solvent under a given set of physical conditions. When a sufficiently large amount of solute is maintained in contact with a limited amount of solvent, dissolution occurs continuously till the solution reaches a state when the reverse process

becomes equally important. This reverse process is the return of dissolved species (atoms, ions, or molecules) to the undissolved state, a process called precipitation.

Dissolution and precipitation occur continuously and at the same rate, the amount of dissolved solute present in a given amount of solvent remains constant with time. The process is one of dynamic equilibrium and the solution in this state of equilibrium is known as a saturated solution. The concentration of the saturated solution is referred to as the solubility of the solute in the given solvent. Thus solubility of a solute is defined as its maximum concentration which can exist in solution under a given set of conditions of temperature, pressure and concentration of other species in the solution.

A solution that contains less solute than required for saturation is called an unsaturated solution. A solution, whose concentration is higher than that of a saturated solution due to any reason, such as change in other species concentration, temperature, etc., is said to be supersaturated. When the temperature or concentration of a solvent is increased, the solubility may increase, decrease, or remain constant depending on the nature of the system. For example, if the dissolution process is exothermic, the solubility decreases with increased temperature; if endothermic, the solubility increases with temperature.

Both unsaturated and saturated solutions are stable and can be stored indefinitely whereas supersaturated solutions are generally unstable. However, in some cases, supersaturated solutions can be stored for a long time without exhibiting any change and the period for which a supersaturated solution can be stored depends on the degree of departure of such a solution from the saturated concentration and on the nature of the substances in the solution. There are two solubilities of scales:

- (1) Calcium, strontium, barium sulfates, and calcium carbonate solubilities.
- (2) Zinc sulfide, lead sulfide, and iron sulfide solubilities.

There follows a brief description of each solubility.

2.5.1 Calcium, Strontium, Barium Sulfates, and Calcium Carbonate Solubilities

The chemical species of interest to us are present in aqueous solutions as ions. Certain combinations of these ions lead to compounds, which have very little solubility in water. The water has a limited capacity for maintaining those compounds in solution and once this capacity (i.e. solubility) is exceeded, the water becomes supersaturated; and the compounds precipitate from solution as solids. The solubilities of typical oilfield scales are given in Figure 2.3 (Connell, 1983).

Although the solubility curves (Figure 2.3) of these crystalline forms versus temperature show that above about 40 °C (104 °F), anhydrite is the chemically stable form, it is known from experience that gypsum is the form most likely to precipitate up to a temperature of about 100 °C (212 °F). Above this temperature, hemihydrate becomes less soluble than gypsum and will normally be the form precipitated. This, in turn, can dehydrate to form a scale at temperatures below 100 °C and hemihydrate forms above this temperature (Connell, 1983).

Therefore, precipitation of solid materials, which may form scale, will occur if:

- (1) The water contains ions, which are capable of forming compounds of limited solubility.
- (2) There is a change in the physical conditions or water composition, lowering the solubility.

Factors that affect scale precipitation, deposition and crystal growth can be summarized as: supersaturation, temperature, pressure, ionic strength, evaporation, contact time, and pH. Effective scale control should be one of the primary objectives

of any efficient water injection and normal production operation in oil and gas fields. There follows a brief description of some factors.

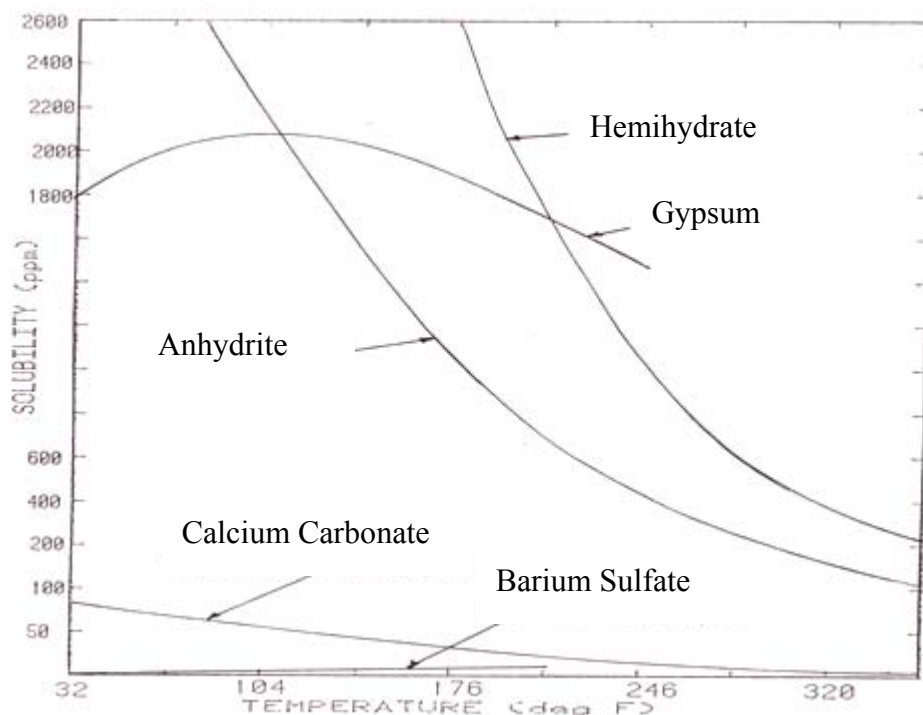


Figure 2.3 Solubilities of common scales (Connell, 1983)

2.5.1.1 Effect of Supersaturation

Supersaturation is the most important reason behind mineral precipitation. A supersaturated is the primary cause of scale formation and occurs when a solution contains dissolved materials which are at higher concentrations than their equilibrium concentration. The degree of supersaturation, also known as the scaling index, is the driving force for the precipitation reaction and a high supersaturation, therefore, implies high possibilities for salt precipitation.

Since the solubility of the sulfates of calcium, strontium, and barium can all be estimated, the amount of supersaturation of each can be predicted for any given system of different waters. Caution, however, must be exercised when working with estimated values of solubility and supersaturation.

Many different variables, including temperature, pressure, other ions, pH, turbulence, rate of kinetics of precipitation, and seeding or nucleation all have an effect on the behavior of mixtures of incompatible waters. Some of these variables are beyond the scope of definition in an oilfield situation. They introduce unknown factors that make any estimate of solubility, supersaturation, and the likelihood of precipitation and scaling uncertain.

According to Lindlof and Stoffer (1983), strontium sulfate solubility is decreased by the common ion effect; the supersaturation becomes a disproportionately higher percentage of total strontium sulfates in the solution. The supersaturation represents the amount of strontium sulfate present in excess of the solubility and thus represents the amount available for precipitation from solution and possible scaling. The supersaturation exists in a metastable state and, as such, the manner in which it exists in solution or comes out of solution by crystallization and precipitation is entirely unpredictable.

2.5.1.2 Effect of Temperature

Heating the reservoir water tends to precipitate calcium sulfate, since it can be seen from Figure 2.3 that calcium sulfate is less soluble at higher temperatures. Calcium sulfate is often observed on the fire tubes of heater theaters. Calcium carbonate also tends to precipitate more at decrease in solubility at higher temperatures. Although this increase can be several-fold, solubility still remains at a low level (Connell, 1983).

Contrary to the behaviour of most materials, calcium carbonate becomes less soluble as temperature increases. The hot water is more likely the CaCO_3 precipitation. Hence, water, which is nonscaling at the surface, may result in scale formation in the injection well if the downhole temperature is sufficiently high.

According to Oddo *et al.* (1991), calcium carbonate solubility has an inverse relationship with temperature or stated more simply, CaCO₃ scale becomes more insoluble with increasing temperature and a solution at equilibrium with CaCO₃ will precipitate the solid as the temperature is increased. The tendency to form CaCO₃ also increases with increasing pH (as the solution becomes less acid). The decrease in total pressure around the pumps allows dissolved carbon dioxide to escape from solution as a gas causing an increase in pH with a subsequent increase in the tendency to form solid.

Landolt-bornstien (1985) (cited in Moghadasi *et al.*, 2004b) showed the effect of temperature on solubility of calcium sulfate. Gypsum solubility increases with temperature up to about 40 °C, and then decreases with temperature. Note that above about 40 °C, anhydrite becomes less soluble than gypsum, so it could reasonably be expected that anhydrite might be the preferred form of calcium sulfate in deeper, hotter wells.

Actually, the temperature at which the scale changes from gypsum to anhydrite or hemihydrate is a function of many factors, including pressure, dissolved solids concentration, flow conditions and the speed at which different forms of calcium sulfate can precipitate out from solution.

Prediction which form of calcium sulfate will precipitate under a given set of conditions is very difficult. Even though an anhydrite precipitate might be expected above 40 °C in preference to gypsum due to its lower solubility, gypsum may be found at temperature up to 100 °C. It is often difficult to precipitate anhydrite directly from solution, but with the passage of time, gypsum can dehydrate to form anhydrite. Above 100 °C, anhydrite will precipitate out directly in a stirred or flowing system.

Calcium sulfate is one of several soluble salts commonly deposited from oil field waters. That deposition is the result of a supersaturated condition approaching equilibrium by precipitating some of its dissolved salt burden. Precipitation

continues until stability has been achieved. Figure 2.4 shows solubility of the three most common forms in distilled water as a function of temperature (Carlberg and Matthews, 1973).

Barium sulfate solubility increased with temperature increase, with increase ionic strength of brine, and with pressure. Barium sulfate precipitation was affected most strongly by temperature (Moghadasi *et al.*, 2003a).

Jacques and Bourland (1983) described a solubility study of strontium sulfate in sodium chloride brine. His study showed that the solubility of strontium sulfate increased with increasing ionic strength and decreased with increasing temperature.

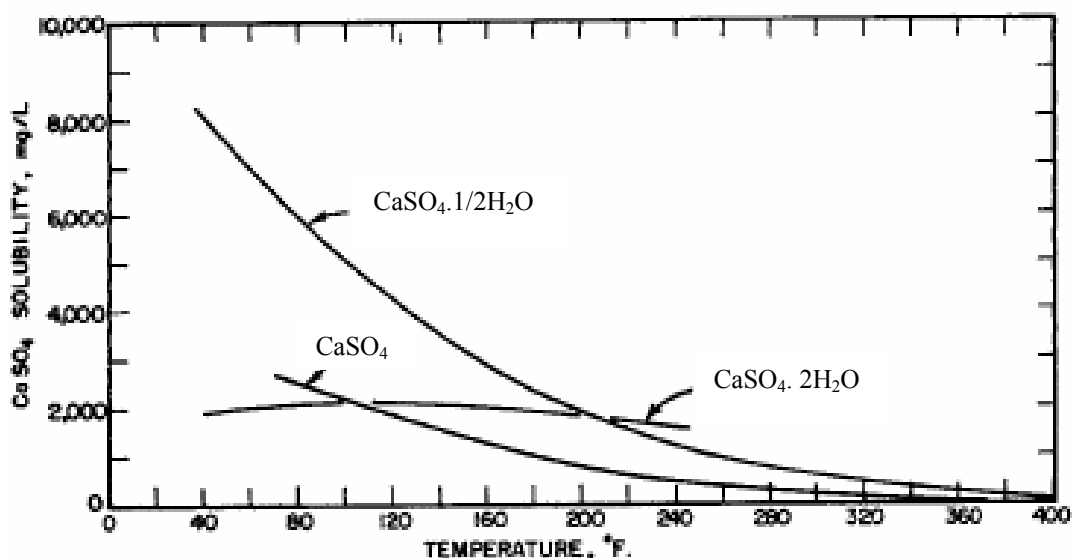


Figure 2.4 Calcium sulfate solubility in water (Carlberg and Matthews, 1973)

2.5.1.3 Effect of Pressure

The sulfates of calcium, barium and strontium are more soluble at higher pressures. Consequently, formation water will often precipitate a sulfate scale when pressure is reduced during production. The scale may deposit round the wellbore, at the perforations, or in the downhole pump (if used). Barium sulfate is common at

perforations or downstream of chokes, where the pressure is reduced considerably (Connell, 1983).

A drop in pressure can cause calcium sulfate deposition. The reason is quite different from that for calcium carbonate. The presence or absence of CO₂ in solution has little to do with calcium sulfate solubility. The solubility of scale formation in a two-phase system increases with increased pressure for two reasons (Moghadasi, 2004b):

- (1) Increased pressure increases the partial pressure of CO₂ and increases the solubility of CaCO₃ in water.
- (2) Increased pressure also increases the solubility due to thermodynamic considerations.

2.5.1.4 Effect of Ionic Strength

The solubility of calcium sulfate is strongly affected by the presence and concentration of other ions in the system. The solubility of calcium sulfate is an order of magnitude larger than that of strontium sulfate, with in turn is about one and one-half orders of magnitude larger than that of barium sulfate, as shown in Figure 2.5.

For example, Figure 2.5 indicates that the solubility of strontium sulfate can be larger than 950 mg/l. This solubility, however, is true only when the solution is stoichiometrically balanced i.e., when the number of strontium ions equals the number of sulfate ions. If an excess of either ion is introduced, the solubility is depressed remarkably. This is known as the common ion effect (Lindlof and Stoffer, 1983). The solubility reaches a maximum in highly concentrated brines.

2.5.1.5 Effect of pH

The amount of CO_2 present in the water affects the pH of the water and the solubility of calcium carbonate. However it really does not matter what causes the acidity or alkalinity of the water. The lower the pH, the less likely is CaCO_3 precipitation. Conversely, the higher pH, the more likely that precipitation will occur (Moghadasi, 2004b).

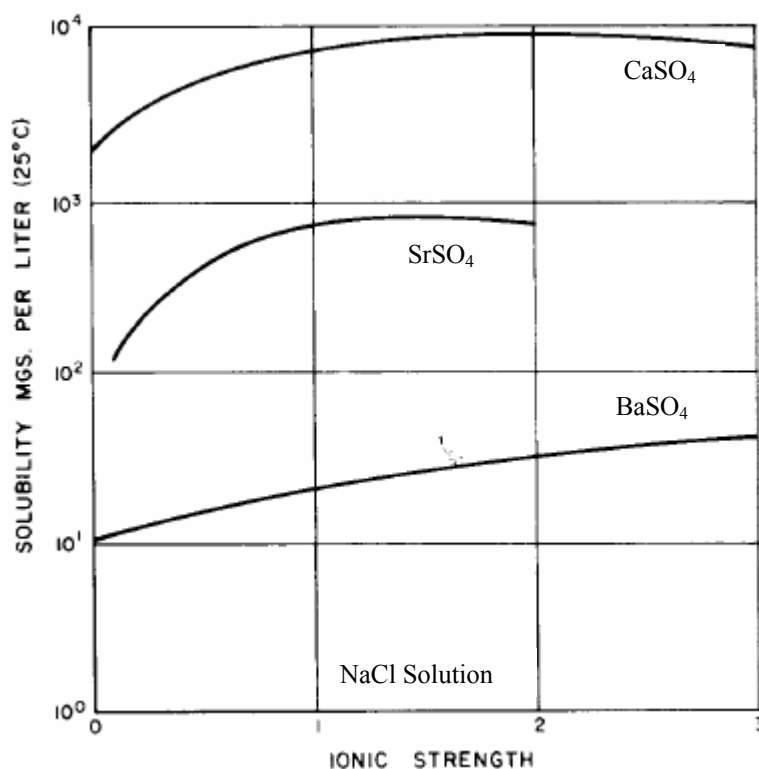


Figure 2.5 Relative solubilities of three sulfates in brine (Lindlof and Stoffer, 1983)

2.5.1.6 Effect of Carbon Dioxide Partial Pressure

As opposed to most sulfate scales, the prediction of carbonate scales requires not only the consideration of pressure, temperatures, and water composition, but also the knowledge on the chemical reactions within the brine and CO_2 in the gas phase. Most oilfield reservoirs contain carbonate mineral cements and carbon dioxide, therefore the formation water is normally saturated with calcium carbonate under

reservoir conditions where the temperature can be as high as 200 °C and the pressure up to 30 MPa (Moghadasi, 2004b).

Solubility of calcium carbonate is greatly influenced by the carbon dioxide content of the water. CaCO_3 solubility increases with increased CO_2 partial pressure. The effect becomes less pronounced as the temperature increases. The reverse is also true. It is one of the major causes of CaCO_3 scale deposition.

At any point in the system where a pressure drop is taken, the partial pressure of CO_2 in the gas phase decreases, CO_2 comes out of solution, and the pH of the water rises. The amount of CO_2 that will dissolve in water is proportional to the partial pressure of CO_2 in the gas over the water (Moghadasi, 2004b).

2.5.2 Zinc Sulfide, Lead Sulfide, and Iron Sulfide Solubilities

Lead and zinc sulfide solubility is much lower even than iron sulfide, which is the common sulfide in oil field environments. The very low solubility of lead and zinc sulfide would make it unlikely that zinc/lead and sulfide ions could exist together in solution for any length of time.

It is more likely that the zinc/lead ion source mixes with the hydrogen sulfide-rich source within the near wellbore or the production tubing during fluid extraction; from then on, changes in temperature, solution pH, and residence time control where scales deposit within the process system.

For example, in a 1M (mole/dm^3) NaCl brine solution as presented in Figure 2.6 at pH = 5 the solubility of iron sulfide is 65 ppm, whereas lead and zinc sulfides are 0.002 ppm and 0.063 ppm respectively. Depending on the exact brine conditions, the solubility of zinc sulfide is between 30 to 100 times more soluble than lead sulfide. As with iron sulfide, the solubility of both lead and zinc sulfide increases with increasing solution pH (Collins and Jordan, 2001).

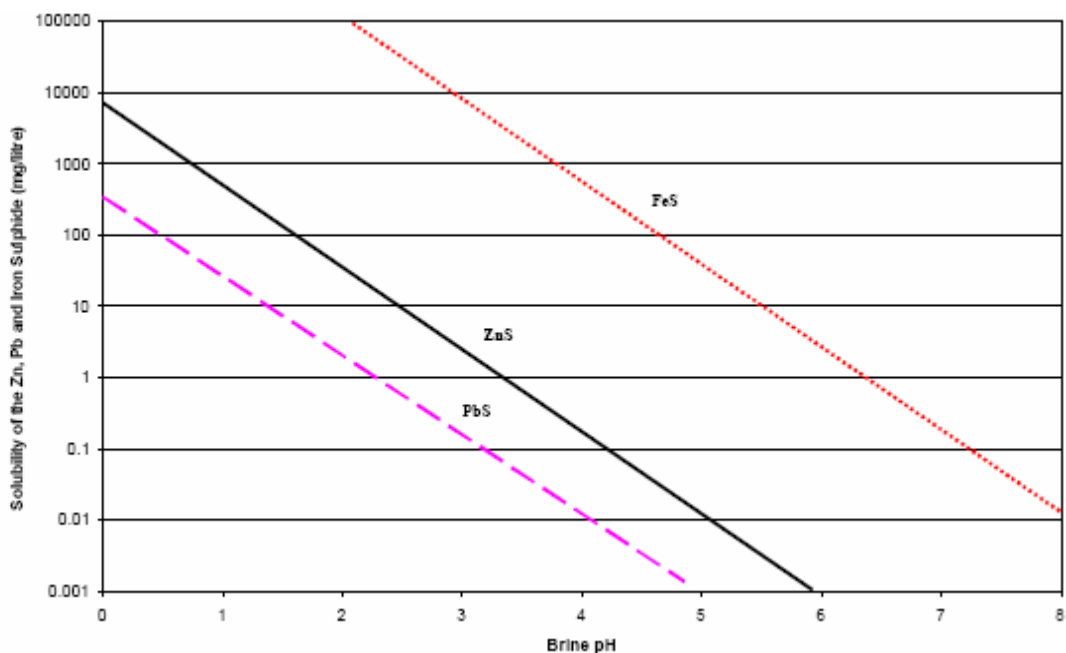


Figure 2.6 Comparison of zinc, lead and iron sulfide solubility in 1M NaCl brine at 25 °C (Collins and Jordan, 2001)

2.6 Oilfield Scale Types

The most common scales encountered in oilfield operations are sulfates such as calcium sulfate (anhydrite, gypsum), barium sulfate (barite), and Strontium sulfate (celestite) and calcium carbonate. Other less common scales have also been reported such as iron oxides, iron sulfides and iron carbonate. Lead and zinc sulfide scale has recently become a concern in a number of North Sea oil and gas fields (Collins and Jordan, 2001). There follows a brief description of each scale.

2.6.1 Calcium Carbonate Scales

Calcium carbonate or calcite scale is frequently encountered in oilfield operations. But the calcite has the greatest stability in oilfield circumstances, so it is the most common form of calcium carbonate encountered in oilfield production operation.

Calcium carbonate crystals are large, but when the scale is found together with impurities in the form of finely divided crystals, then the scale appears uniform. Deposition of CaCO₃ scale results from precipitation of calcium carbonate is as per the following equation:



As it will be seen later calcium carbonate scale can also be formed by combination of calcium and bicarbonate ions, and this reaction is the major cause of calcium carbonate scale deposition in oilfield operations. This is because only a small percentage of the bicarbonate ions dissociated at the pH values found in most injection waters to form H⁺ and CO₃⁻² (Moghadasi *et al.*, 2004b).

In many oilfields, the deposition of calcium carbonate scale on surface and subsurface production equipment creates an operation problem. The formation water in which the carbonate-scale-forming components are initially dissolved becomes supersaturated with calcium carbonate because of the drop in pressure during production. The continuous flow of a supersaturated solution through the production equipment results in the growth of a dense layer of calcium-carbonate crystals (Bezemer and Bauer, 1969).

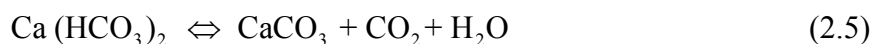
Carbonate scales frequently appear in the wellbore, especially near the wellhead where, because of pressure drop, dissolved CO₂ escaped from produced water and caused water pH as well as the saturation index of carbonate minerals to increase (Zhang and Farquhar, 2001).

In the pre-seawater breakthrough period, calcium carbonate precipitation, caused by the loss of CO₂ from the formation water produced, can be observed. CaCO₃ scaling is not difficult to control by scale inhibitors or by removal with acid.

The water is drained to the surface and suffers from significant pressure drop and temperature variations during the production. The continuous pressure drops

lead to degassing of the carbon dioxide with an increase in pH value of the produced water and precipitation of calcium carbonate (Mackay, 2003; Rousseau *et al.*, 2003).

Carbonate scale formation occurs when connate water or aquifer water passes through the bubble point and carbon dioxide is evolved. As carbon dioxide is evolved, the solubility with respect to carbonate declines rapidly and forms a precipitate with divalent ions, such as iron, and more commonly calcium, as outlined in the following equation (Mackay and Jordan, 2005):



According to Clemmit *et al.*, (1985), calcium carbonate scale is formed by a different mechanism. As few waters contain the actual carbonate ion, the scaling potential arises from decomposition of calcium bicarbonate. This decomposition is due to the pressure reductions (at chokes or separators) releasing carbon dioxide and thus moving the equilibrium (with a pH increase) of the above reaction to the right and producing calcium carbonate. If the quantity of calcium carbonate produced exceeds its solubility in the water, then precipitation can occur.

2.6.2 Calcium Sulfate Scales

Calcium sulfate scale poses a unique problem for the salts under consideration because it occurs with one of three different phases. Calcium sulfate exists in several crystalline forms. These include gypsum ($\text{CaSO}_4 \cdot 1/2\text{H}_2\text{O}$) and anhydrite (CaSO_4).

Gypsum, the most common scale occurs at relatively low temperature. At higher temperature (above 100 °C), the stable phase predicted is anhydrite (CaSO_4). However, hemihydrate has been known to form at 100 to 121 °C, especially in non-turbulent systems and in high ionic strength brines (Moghadasi *et al.*, 2003a).

Calcium sulfate, which is important in desalination geochemistry and petroleum engineering, is complicated by the fact that it can crystallize from aqueous solution in three forms: gypsum ($\text{CaSO}_4 \cdot 2\text{H}_2\text{O}$), hemihydrate ($\text{CaSO}_4 \cdot 1/2\text{H}_2\text{O}$) and anhydrate (CaSO_4). These compounds may be stable depending on temperature and ionic strength and they have decreasing solubilities with increasing temperatures above 40 °C. Vetter *et al.* (1982) have studied the morphology of scale.

Among various types of mineral scales, calcium sulfate is one of major scales in petroleum industry that can cause severe flow assurance and formation damage issues. Many parameters are affecting this problem. Temperature, pressure, fluid concentration, ratio of brine to hydrogen, fluid dynamic and type of porous media are among these parameters (Tahmasebi *et al.*, 2007).

According to Oddo *et al.*, (1991), calcium sulfate scale formation is somewhat dependent on temperature, but is typically precipitated because of a decrease in pressure or an increase in the relative concentrations of calcium or sulfate. CaSO_4 solubility is fairly independent of pH and hence, can readily precipitate in an acid environment.

The case where water injection (seawater, river, aquifer, or produced water) is used for pressure maintenance and sweep, the mixing of incompatible brines can lead to the formation of sulfate scales when the injection water contains sulfate ions (Mackay and Jordan, 2005).



2.6.3 Barium Sulfate Scale

The barium sulfate scaling is a chronic disaster in waterflood projects with incompatible injected and formation waters. This is usually due to precipitation of

BaSO₄ from the mixture of both waters and consequent permeability reduction resulting in well productivity decrease (Bedrikovetsky *et al.*, 2006).

Barium sulfate scale (barite) in oil fields can be precipitated easily on the basis of already available information relating to thermodynamic condition and the kinetics of precipitation (Nancollas and Liu, 1975; Mitchell *et al.*, 1980).

Barium sulfate is the most insoluble scale that can be precipitated from oilfield waters. It forms a hard scale which is extremely difficult to remove. The solubility of barium sulfate is about a thousand times less than of calcium sulfate, at surface conditions.

The solubility of barium sulfate goes up with increasing temperature, pressure and salt content of the brine. Thus prediction of barium sulfate scale is much easier than the others since a pressure, temperature or salt content drop will increase precipitation.

A common case of barium sulfate scale is the mixing of two or more incompatible waters. Seawater is often used during workovers, or for flooding formations which contain an appreciable amount of barium ions. Mixing of these waters represents a risk of subsequent formation and wellbore damage caused by barium sulfate deposition (Connell, 1983).

In the post seawater-breakthrough period, however, there is a much more serious problem of precipitation of barium sulfate from an incompatibility between the formation water and seawater. BaSO₄ scale removal is particularly difficult. Thus, BaSO₄ scale treatment must focus mainly on its prevention through the use of scale-control chemicals. Thus, the severity of the scaling problem is determined both by the scaling rate and the efficiency of the chemical inhibitors (Mazzollni *et al.*, 1992).

In most cases, the scaled-up wells are caused by the formation of sulfate scales of barium and strontium. Due to their relative hardness and low solubility, there are limited processes available for their removal and the preventive measure such as the *squeeze* inhibitor treatment has to be taken. It is therefore important to have a proper understanding of the kinetics of scale formation and its detrimental effect on formation damage under both inhibited and uninhibited environment (Wat *et al.*, 1992).

2.6.4 Strontium Sulfate Scale

Strontium sulfate scale formation has become a growing concern in oil-production systems (Nassivera and Essel, 1979). Until recently, the appearance of strontium in oilfield scales has been primarily in the presence of barium sulfate scale. Almost pure SrSO_4 scale now is observed in several production wells around the world. The scale formation is primarily a result of subsurface commingling of waters, which results in water supersaturated in SrSO_4 .

Strontium sulfate solubilities may play a role in many disciplines of science and engineering. For example, strontium sulfate forms scale in oil and/or geothermal fields which are frequently accompanied by other sulfates of alkaline earth metals.

Strontium sulfate behaves like barium sulfate except the former is more soluble under the same conditions. Most of the field scale barium sulfate deposits contains strontium sulfate too (Essel and Carlberg, 1982; Shen and Corsby, 1983).

2.6.5 Sources of Zinc and Lead and the Mechanism of Sulfide Formation

Zinc sulfide scale is more likely when mixing of incompatible fluids such that of formation waters rich in zinc with H_2S gas in the well caused the deposition of this type of

scales. Several sources of zinc/lead and sulfide ions are possible within produced fluids (Collins and Jordan, 2003).

(1) Potential sources of zinc and lead ions include

- (a) Reaction products of formation minerals (sphalerite zinc sulfide (ZnS) and galena lead sulfide (PbS)) during connate and aquifer water contact over many millions of years could result in partial mineral dissolution (Sverjensky, 1984).
- (b) Reaction of injected water used for pressure support into the aquifer or oil leg can result in the fresh or seawater reacting with minerals within the formation can become enriched in heavy metal ions.
- (c) Zinc ions sourced from heavy brine completion fluids lost into the formation during drilling and well workover operations (zinc bromide). Biggs (1992) (cited in Collins and Jordan, 2003) reported that a loss of 500 bbls of 17.2 ppg zinc bromide completion fluid within a reservoir resulted in significant zinc sulfide scale formation with the presence of 2 ppm of hydrogen sulfide from the reservoir.
- (d) In an oil field operated in the North Sea UK sector, the presence of zinc sulfide on downhole gauges and logging tools was reported within a well where zinc bromide brines had been lost during completion operations. Zinc levels within the produced fluids were in the region of 10 to 50 ppm for several months during initial water breakthrough.

(2) Potential sources of Sulfide Ions Include

- (a) Hydrogen sulfide (H₂S) gas is the most likely source of sulfide ions to allow the formation of lead/zinc sulfide scale. Low concentration (in the tens of ppm levels) of H₂S has been reported in produced gas from wells where lead and zinc sulfide scale problems have been reported.

- (b) Decomposition of drilling compounds and corrosion inhibitor can also produce sulfide ions at high temperature when tested in autoclave equipment but are very unlikely to be the source of sufficient sulfide ions to give scale deposition over many years of production. The most likely source of sulfide ions is from reservoir hydrogen sulfide gas.

2.6.6 Iron Sulfide Scale

Iron sulfide species have been known to cause operational problems in the oil industry. Iron sulfide scale is present in oil and gas producing wells, sour wells and water injectors where the injected water has high sulfate content. The sources of iron are the formation brines (especially in sandstone formations) and the well tubular. Iron produced by corrosion processes can be minimized by employing various corrosion protection techniques (Nasr-El-Din and Al-Humaidan, 2001).

According to Raju *et al.* (2003), the disposal water contains dissolved H₂S, whereas the aquifer water contains dissolved iron. When these two waters are mixed together, H₂S reacts with the iron ions and precipitates iron sulfide species, as shown in Equation (2.7).



2.7 Scale Prevention and Removal

2.7.1 Prevention Scale Formation

The most obvious way of preventing a scale from forming during oil production is to prevent the creation of supersaturation of the brine being handled. This may sometimes be possible by altering the operating conditions of the reservoir, for example by ensuring that the wellbore pressure is sufficient to prevent the

liberation of gas and by injecting water which is compatible with formation water. However, economics usually dictate that the use of inhibitors is preferred.

The formation of mineral scale in production facilities is a relatively common problem in the oil industry. Most scale forms either by pressure and temperature changes that favor salt precipitation from formation waters, or when incompatible waters mix during pressure maintenance or waterflood strategies. Scale prevention is achieved by performing *squeeze* treatments in which chemical scale inhibitors are injected in the producers near wellbore (Romero *et al.*, 2007).

2.7.1.1 Operational Prevention

There are two operational preventions:

(1) **Avoid mixing Incompatible Waters**

The importance of avoiding incompatibility problems should be obvious from the preceding discussion. However, in offshore locations like the North Sea there is no economic method of obtaining compatible water, so sea water must be used.

(2) **PH Control**

Lowering the pH will increase the solubility of carbonate scales (but may cause corrosion problems). This method is not widely used in the oilfield, since accurate pH control is needed. However, it is useful for cooling waters.

2.7.2 Scale Control Chemicals

In oil and gas well operations, water-insoluble scale is formed in tubing, casings, and associated equipment, as well as in the wellbore and the formation itself,

which carry, at least in part, water or brine waters. These waters can contain insoluble calcium, barium, strontium, magnesium, and iron salts.

Scale inhibitors are chemicals which delay, reduce or prevent scale formation when added in small amounts to normally scaling water. Most of modern scale inhibitors used in the oilfield functions by one or both of the following mechanisms (Connell, 1983):

- (1) When scale first begins to form, very tiny crystals precipitate from the water. At this point, the scale inhibitor adsorbs onto the crystal surface thus preventing further growth.
- (2) In some cases, scale inhibitors prevent the scale crystals from adhering to solid surfaces such as piping or vessels.

According to Bezemer and Bauer (1969), the most common classes of inhibitor chemicals are inorganic phosphates, organophosphorous compounds and organic polymers. Polyphosphonocarboxylic acid (PPCA) and Diethylenetriaminepenta (methylenephosphonic acid) (DETPMP) are two common commercial scale inhibitors used in the oil and gas industry. Normally, PPCA is regarded as nucleation inhibitor and DETPMP as a growth inhibitor (Chen *et al.*, 2004).

In the majority of cases, a good scale inhibitor should be effective at 5-15 ppm in clean water. However, if substantial amount of suspended solids are present, higher inhibitor concentrations will be necessary. Moreover, the reason being that the inhibitor will adsorb onto surface of the solids in the water, thereby reducing the amount available to inhibit scale formation.

Scale inhibitors that are periodically pumped down production wells and into the producing formation for short distances around the wellbore have been developed and are widely utilized. The inhibitor contacts the formation and is adsorbed onto the reservoir petrofabric. It is later slowly released into the produced fluids, thereby

inhibiting the formation of sulfate scales for some period of time, usually several months. When the inhibitor concentration levels fall too low to be effective, the well is again squeezed with chemical and the cycle is repeated. This technique is widely known as squeeze inhibition (McElhiney *et al.*, 2001).

The formation of mineral scale (carbonate/sulfate/sulfide) within the near wellbore, production tubing and topside process equipment has presented a challenge to the oil and gas industry for more than 50 years. Chemical methods to control scale have been developed including scale squeeze treatments and continual chemical injection. A key factor in the success of such treatments is the understanding of chemical placement and the effectiveness of the treatments chemicals (Jordan *et al.*, 2006b).

Squeezing is the most common method for scale control downhole. Scale inhibitor, diluted in brine, is displaced into the producing formation where it is retained and then released slowly back into the aqueous phase during normal well production. Squeeze inhibition is effective in a wide variety of situations; however, it has some drawbacks. The squeeze chemical, often a phosphonate or high molecular weight sulphonate, is usually dissolved and diluted in water for transport down the wellbore.

Several challenges must be overcome in order to develop an effective combined scale removal and scale inhibition treatment. The most notable are (Smith *et al.*, 2000):

(1) Cost

The combined treatment has to offer an economic advantage when compared to serial stimulation and inhibition treatments.

(2) Corrosion control

The scale inhibitor must not cause a significant change in the corrosivity of the stimulation system. If the stimulation system requires the use of a corrosion inhibitor then the scale inhibitor must not prevent its function.

(3) System compatibility

The scale inhibitor must be completely compatible with the stimulation system, both live and spent. The combined treatment must also be compatible with formation fluids.

(4) Inhibitor adsorption

The scale inhibitor has to effectively adsorb onto the formation, throughout the potential pH range of the stimulation system (live to spent).

(5) Process compatibility

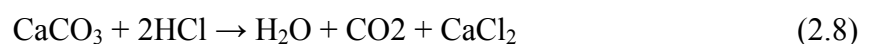
The flow-back after a combined scale removal and inhibition treatment (live or spent) must have no opposed effect on the process system operation.

Several combined scale removal and inhibition systems could be considered in order to meet these challenges. Hydrochloric acid (HCl) may be the most cost effective treatment to remove calcium carbonate, but corrosion control, system compatibility and inhibitor adsorption may all be difficult in a combined treatment. Conversely, scale solvers may offer better corrosion control and scale inhibitor compatibility when spent, but will be higher cost. Organic acids could offer a compromise which allows most of the system requirements to be met.

2.7.3 Scale Removal Methods

2.7.3.1 Calcium Carbonate

Hydrochloric acid is the most effective way of dissolving calcium carbonate under most conditions. Concentrations of 5-15% HCl are normally used (Connell, 1983):



A corrosion inhibitor must be added to the acid to stop it from attacking the pipework and a surfactant is usually added to make the surfaces water wet.

2.7.3.2 Calcium Sulfate

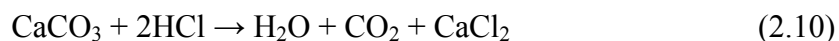
The following may be used to dissolve calcium sulfate (Connell, 1983):

(1) Converters

Inorganic converters are usually carbonates or hydroxides which react with calcium sulfate and convert it to acid soluble calcium carbonate or calcium hydroxide. The conversion treatment is then followed by a hydrochloric acid treatment to dissolve the resulting scale:



Then



(2) Solvents:

Solvents are now available which will completely dissolve gypsum scale.

Other compounds used (to a lesser extent) are EDTA and salt water.

2.7.3.3 Barium Sulfate

One of the most common reasons for production loss is the development of scales inside the production strings, blocking the flow of the reservoir fluid to the surface facilities. Barium sulfate scale is among the toughest scales to remove, whether mechanically or chemically (Guimaraes *et al.*, 2007).

Barium sulfate could only be removed by mechanical means. However, chemicals based on EDTA are now available which have had some success in dissolving barium sulfate.

2.8 Scale Prediction

2.8.1 Laboratory Evaluation

Scale formation can be predicted by laboratory experiments. Several experimental studies have been conducted to determine the scaling potential in different oilfields. The detailed experimental parameters are listed in tables in Appendix A.

Mitchell *et al.* (1980) conducted to investigate experimentally the effect of incompatibility of injected water and formation water in the Forties field. They used a core with six injectors at one end and one outlet at the other end to simulate a production well. The flow rates of injection and formation water were adjusted so that one part of injection water was injected to ten parts of formation water.

They found that the injection pressure remained relatively constant most of the time and then increased rapidly just before the core became completely blocked. They stated that the initial scale deposition occurred around the surfaces of the pores. As more scale was deposited, the pore-throat flow area was reduced.

Read and Ringen (1982) investigated a series of laboratory tests to evaluate the extent of formation damage which could result from scales formed within the porous rock in North Sea oil reservoir. These tests were performed in glassware, bead packs, and synthetic alumina cores. Initially, the formation water and seawater were analyzed. It showed that mixtures of these waters could precipitate both strontium and barium sulfate.

From analyses, the weight of precipitates of these salts was calculated based on solubility products. To confirm these calculations, blends of both waters were mixed in glassware and the total amount of precipitate was determined by filtering and weighing. As a check, the precipitate was also re-dissolved in dilute HCl and the concentrations of calcium, strontium, and barium were determined by atomic absorption analysis.

Nevertheless, for mixing test in porous media, were also conducted in a pack of 4 mm glass beads and in synthetic alumina cores that were 4 inches in length and 3/2 inches in diameter. The mixing test was all conducted at reservoir temperature 70°C, no pressure was applied during a test. The cores were first saturated with formation water, and a base permeability determined. Core flooding was done in varying proportions of seawater and formation water and pressure differential was continuously recorded throughout the flow.

From the experimental results, it was the worst permeability loss occurred with highest amount of precipitation for lower proportion of seawater. The core test in which 10% seawater was used shows a dramatic increase in the differential pressure, as rapid blocking was observed due to scale deposition.

Lindlof and Stoffer (1983) conducted a laboratory study to evaluate possible strontium sulfate and calcium sulfate scaling associated with the injection of seawater into the Arab-D reservoir in Saudi Arabia. The laboratory tests showed no measurable reduction in permeability due to incompatibility effects between Arab-D formation water and seawater when the two waters mix in the pore channels during displacement of one water by the other. They described that mixing of Arab-D water with seawater in various proportions demonstrated that strontium sulfate could be precipitated.

Todd and Yuan (1990) presented the results of laboratory experiments carried out at room temperature to investigate the formation of barium sulfate and strontium sulfate [(Ba, Sr)SO₄] solid solution in multi-pressure-tapped cores. Two brines, one barium-and

strontium-rich and the other sulfate-rich, separately to the front face of a core plug to ensure that the two brines mixed uniformly immediately after entering the core. Pressure differentials were measured and the changing permeability distribution along the core length was calculated. The morphology and chemical analysis of scaling crystals as shown by Scanning Electron Microscopy (SEM) are presented.

Results show a large extent of permeability damage caused by [(Ba, Sr) SO₄] solid solution deposits on rock pore surface. The rock permeability decline and morphology and size of the scaling crystals indicate the influence of the supersaturations of BaSO₄ and SrSO₄ and the concentration ratio of barium to strontium ions.

Bezerra *et al.* (1990) conducted a laboratory study to investigate the deposition of barium and strontium sulfate scales in producing wells of the Namorado field. Two incompatible waters one barium-and strontium-rich formation water and the other sulfate-rich sea water injected into sandstone cores to study scale formation in porous media. Pressure data were used to calculate the permeability of the sandstone as a function of the injected fluids. A significant drop in permeability around 65% was observed after precipitation.

Todd and Yuan (1992) described a laboratory study carried out at 70°C to examine (Ba, Sr) SO₄ solid-solution scale formation in porous media under the influence of flow and in static bulk solutions. Two incompatible waters were injected into a core to study scale formation in porous media, and static scale precipitation tests were performed in glass jars. Synthetic North Sea water and two formations waters were used in elevated temperature experiments to simulate field scale formation. Firstly, the formation water (water M) had medium scale precipitation when mixed with seawater and the other (water ST) had severe scaling tendency.

Results of experiments carried out at the elevated temperatures again demonstrate that substantial scale deposition could occur in a rock core and could cause considerable decline of rock permeability resulting from the mixing of two incompatible waters.

Allaga *et al.* (1992) described two linear flooding experiments of permeability reduction of sandpacks caused by solids generation and migration. Type A experiments investigated the effects that precipitates had on the permeability reduction of unconsolidated sandpacks. The initial permeabilities of the sandpacks were adjusted with a mixture of silica flour and sand. In type B experiments, they measured the ion and solid waves produced while the precipitation/dissolution reactions were occurring in the sandpacks. Two solids, calcium and barium sulfate crystals, were injected into and generated within the sandpacks by chemical reaction.

Furthermore, a precipitate formed when two solutions, one solution rich in sulfate ions and another solution rich in barium or calcium ions, were mixed inside the sandpack. Calcium and barium sulfate precipitates did not plug the sandpacks to the same extent. One experiment with barium sulfate precipitate produced a 60% reduction in initial permeability. Calcium sulfate precipitates consistently plugged all sandpacks, causing a 10% to 20% reduction in the original permeability.

Wat *et al.* (1992) presented results of BaSO₄ formation kinetics in both beaker tests and in highly reproducible sandpacks which simulates the flow in porous medium. Synthetic North Seawater and formation water were mixed inside the sandpack to study scale formation in porous media. For the in-situ scaling experiments, the crystal growth process appeared to be localized. The permeability decline was likely caused by the continuous growth of crystals and not by particle transport and flow blockage. The scale precipitation process in porous medium was likely to be dominated by heterogeneous nucleation with the [Ba⁺⁺] ion concentration in the sandpack effluents consistently less than that of similar beaker tests.

Nevertheless, the scale morphology varies considerably from the point of mixing. Under steady state, the scaling process within the porous medium was contributed by a range of supersaturated mixtures. The point where the incompatible brines first come into contact with each other has the highest supersaturation and with maximum amount of deposit. Furthermore, results of in-situ scaling in highly

reproducible sandpicks have been included to provide information on likely formation damage and comparison of crystal growth under static and dynamic flow environment.

Jordan *et al.* (2000) conducted an experimental work to develop an effective treatment strategy for production wells in North Slope Alaska, specifically those with electrical submersible pumps (ESP's) that suffered significant performance impairment at water cuts of less than 5% because carbonate scale deposited within the ESP's. During the injection at different stages, the formation water is rich in cations (Ba, Sr, and Ca) and the injection water is rich in anions (SO₄) into porous medium.

Furthermore, at very low water cut (<1%), scale formation could cause operational problems with downhole production equipment. It was possible to form not only conventional calcium carbonate scale from produced water, with high bicarbonate and high calcium levels, but also iron carbonate deposited from a combination of iron from formation water and corrosion products.

McElhiney *et al.* (2001) conducted a laboratory study to investigate the problem of in-situ barium sulfate precipitation in West Africa offshore reservoir. Core flooding experiments conducted at frontal velocities of 0.31 m/day in fired Berea sandstone cores to evaluate in-situ barium sulfate precipitation at ambient temperature (~ 70°F) and atmospheric pressure. Synthetic raw seawaters containing low and high sulfate contents were mixed in-situ with formation water containing dissolved barium ions before injection.

Furthermore, the precipitation loss of barium sulfate was observed by the measurement of the effluent profiles of sulfate ion and barium ion. The results indicated that for low sulfate seawater, the barium sulfate scaling potential was reduced, which was also verified by SEM analysis.

Moghadasi *et al.* (2002) presented an experimental and theoretical study of calcium sulfate scale formation and particle movement in the porous media used of packing bed with twelve different sizes of the glass and sand bead and the eight core plug that gathered from the Siri oilfields. Two incompatible waters, Persian Gulf water and Mishrif formation water were injected into a core to study scale formation in porous media.

Moreover, permeability decrease was affected by the following parameters: solid particle concentration, flow rate, and the initial permeability of porous medium. The high rates of permeability damage happened under conditions of high concentration of solid particles, small ratio of solid particle size to the mean diameter as well as low flow rates in low permeability porous media during water injection. One of the important factors in permeability reduction because of the movement of internal solid particles was the sticking factor.

Furthermore, the modeling results provided same information for understanding the mechanisms of permeability alteration resulting from solid particle invasion into a porous medium.

Collins and Jordan (2003) conducted an experimental study to investigate the deposition of zinc sulfide scale that had been found in several fields along the Gulf Coast of the U.S.A. and in fields within the North Sea Basin at high temperature and high salinity. Lead and zinc sulfide scales were very insoluble at typical formation brine pH and salinity. Their solubility increased with increasing brine salinity, temperature and falling pH.

Nevertheless, lead and zinc sulfide scale occurrence have been reported when high salinity brines were produced along with oil and gas within the Gulf of Mexico, onshore U.S.A. and North Sea (both UK and Norwegian sector). The formation of such deposits could result in expensive mitigation and significant differed oil production.

Moghadasi *et al.* (2003b) presented an experimental and theoretical study of permeability reduction of porous media caused by scaling. Each solution system consisted of two salts, one rich in calcium ions and the other rich in sulfate or carbonate ions, which were kept separate until they had entered the porous medium. Since mixing calcium nitrate and sodium sulfate or sodium carbonate results in calcium sulfate or calcium carbonate which crystallizes on the porous medium.

Permeability decline caused by scale formation in the porous medium ranged from less than 30% to more than 90% of the initial permeability, depending on solution composition, initial permeability, temperature, flow rate, and solution injection period. The pattern of permeability decline in a porous medium due to continues scaling was characterized by a concave curve with a steep initial decline, which gradually decreased to a low.

Nevertheless, the initial steepness of those curves generally decreased with increasing distance from the point of mixing of incompatible solutions. Several factors influencing scale formation had been examined. Increasing temperature, supersaturation and flow rate had a detrimental effect on the permeability reduction. Flow rate caused more for calcium carbonate precipitation than calcium sulfate.

Voloshin *et al.* (2003) studied core flooding tests for western Siberian oil fields. They concluded that injected water salinity and the mineralogical composition of formation rock played an important role in the process of scaling in the reservoirs and the wells. During interaction with the rock, the injected water changed its ionic composition, becoming richer in either carbonates or sulfates, or both.

Furthermore, analysis of electric submersible pump deposits showed that carbonates (calcium and magnesium), quartz, chlorite, and gypsum were present in the mineral composition of the scale deposits. While carbonates were among the main components of the deposits, chloride and gypsum were present in negligible quantities in every sample. In some deposits, siderite and iron oxide were present too.

Nasr-El-Din *et al.* (2004) described a laboratory study to utilize high sulfate pit brine and calcium chloride solutions as a means to permeability of water producing zones. Two incompatible waters one contains high concentration calcium ions and other contains high sulfate content were injected into carbonate core from a carbonate reservoir in Saudi Arabia. Compatibility tests indicated immediate precipitation of calcium sulfate when pit water and calcium chloride brines were mixed.

Nevertheless, coreflood testes indicated that maximum core plugging occurred when pit brines were injected into cores saturated with CaCl_2 brines. The degree of core damage depended on the injection rate.

Moghadasi *et al.* (2004a) presented an experimental and theoretical study of permeability reduction of porous media caused by scaling. Two incompatible solutions of calcium and sulfate/carbonate ions were injected into the porous medium, where calcium sulfate or calcium carbonate was generated by chemical reaction.

They concluded permeability decline caused by scale formation in the porous bed ranged from less than 30% to more than 90% of the initial permeability, depending on solution composition, initial permeability, temperature, flow rate, and solution injection period. The pattern of permeability decline in a porous medium due to scaling injection was characterized by a steep initial decline which gradually slowed down to a lower. Several factors influencing scale formation had been examined. Both increasing temperature and flow rate had a detrimental effect on the permeability reduction.

Strachan *et al.* (2004) performed laboratory studies to estimate the suitability of aqueous and non-aqueous scale inhibitors for downhole application in dry and lower water cut wells in the Magnus field. Synthetic brine Magnus formation water and seawater were injected into the porous medium. Corefloods connected to a novel water block remover indicated no formation damage was observed with the polymeric

and phosphonate precipitation inhibitors and those treatment packages were considered to be suitable for pre-emptive squeeze in the BP Magnus field.

Ahmed (2004) presented an experimental and theoretical study of permeability reduction of porous media caused by scaling. Two incompatible solutions containing Ca^{+2} and SO_4^{-2} ions injected into Berea sandstone cores, which were kept separate until entering the porous medium.

The results indicated increased rate of CaSO_4 precipitation at higher temperatures, higher flood velocities, and greater brine supersaturation, whereas pressure had a slight effect on CaSO_4 precipitation. Moreover, the results were utilized to build a general reaction rate equation to predict CaSO_4 precipitation in Berea sandstone for a given temperature, brine supersaturation, and flooding velocity.

Bedrikovetsky *et al.* (2005) conducted a laboratory study to determine chemical reaction rate constant versus flow velocity in porous media for scaling conditions in field N (Brazil). Two incompatible waters, one barium-rich formation water and the other sulfate-rich sea water injected into outcrop RB (Brazil) cores. Two series of steady state testes on simultaneous injection of formation and injection waters with barium sulfate formation have been performed for different velocities in two cores. It was shown that the chemical reaction rate constant is proportional to flow velocity, in the range studied.

2.8.2 Modeling Development

Today scale prevention is the way oilfield operators choose, when touched with scaling problems in oilfield production, as scale prevention is technically and economically more effective than redissolution, once scale has formed. One essential step in scale prevention is scale prediction. Along with laboratory

experiments, scale formation can be predicted by several models to determine the scaling potential in different oilfields.

Vetter *et al.* (1982) presented a model for predicting simultaneous precipitation of barium sulfate, strontium sulfate and calcium sulfate. Water compositions, pressure and temperature were taken into account. They showed the effect of scaling of a less soluble sulfate, such as BaSO_4 , on the precipitation of more soluble salts such as SrSO_4 and CaSO_4 . The scale component has the lowest solubility product (e.g. BaSO_4) that precipitates first because of removal of some sulfate ions from the solution.

Furthermore, the new ionic product required for calculating this precipitation is adjusted for BaSO_4 precipitation. This is followed by the precipitation of the second component having the larger solubility product (e.g. SrSO_4). Finally the last component of this series, CaSO_4 , will precipitate. The entire process is repeated and continuous re-dissolution and precipitation of all scale-forming compounds (BaSO_4 , SrSO_4 and CaSO_4) for each set of thermodynamic conditions at which precipitation can occur.

Bertero *et al.* (1988) presented a numerical model which couples a reservoir-fluid-flow/thermal-equilibrium simulator with a chemical-equilibrium computer code. The reservoir simulator, called AGIPS, is a finite-difference numerical model which calculates the evolution in time of the amount of scale formed in any point of the reservoir and inside the wells when changes occur in the temperature of the injected water and when the injection water mixes with reservoir brine.

Nevertheless, the model calculates temperature and pressure profiles in the reservoir, together with their evolution in time, taking into account the permeability reduction caused by scale formation. For validation of their model, mixtures with different proportions of injection and reservoir water (taken from North African oil fields) were prepared and kept in a pressure vessel at reservoir conditions.

The Results were presented for the chemical-equilibrium code validation by matching experimental data on scale formation in mixtures of incompatible waters. An example is also given of AGIPS use in simulating a five-spot waterflood where incompatible water is injected.

Yuan and Todd (1991) developed a model for predicting sulfate scaling problems due to commingling of chemically incompatible waters as well as by temperature and pressure changes. This model is based on the Pitzer equation and has proved to be successful in calculating sulfate solubilities over wide ranges of solution compositions and temperature. The model is capable of predicting the scaling tendencies of barium, strontium and calcium sulfates at various water compositions, temperature, and pressures covering oil field conditions.

The model also predicts competitive simultaneous co-precipitation of BaSO_4 , SrSO_4 , and CaSO_4 , where sulfate is a common ion, reflecting the precipitation of more than one sulfate mineral. Moreover, this model was used in evaluating the sulfate scaling potentials resulting from mixing North Sea injection water with Forties formation water. The predicted scaling precipitation was substantiated by field observations.

Yeboah *et al.* (1993) developed Oilfield Scale Prediction Model (OSPMoD) which predicts the potential and deposition profile based on extensive thermodynamic and kinetic data. The first major step of the model is to use the input data (produced water analysis and thermo-chemical data) to determine the thermodynamic scaling potential. If scale is predicted to form, the next step is to use kinetic and well data to determine the scale deposition profile from bottomhole to the surface. Thus, it computes the deposition profile as a function of position and time if a well is predicted to scale.

In addition to the highly informative and attractive graphic display of results, the model provides extensive tabulation of the results including calculation of densities, activity coefficients, solubilities, supersaturations, solubility product

constants, equilibrium composition (including pH, partial pressure of CO₂ and HCO₃) saturation indices, concentration, velocity, amount and type of scale and available cross-sectional area at different positions and times.

Thomas *et al.* (1995) developed an expert system for prediction and analysis of the damage potential in the oilfield during production and injection due to interactions between the fluids and the solid phase. These interactions are because of hydro-mechanical processes and/or changes in physiochemical conditions of the fluid (pH, temperature, ionic strength) and cause a reduction in the permeability of the reservoir rocks and technical equipment. The expert system FROCKI (Fluid-Rock-Interactions) was written in LISP as an object-oriented computer language to manage all these problems of oil fields.

Moghadasi *et al.* (2003a) developed a model which was based on experimental data and empirical correlations that perfectly matched Iranian oilfield conditions where water injection was performed for reservoir pressure maintenance. The first step of the model is to use the water analysis and physical conditions (temperature and pressure) to determine the scaling potential. If scale is expected to form, the next step is to use kinetic and well data to compute the scale deposition.

Furthermore, this model can be applied to predict scaling deposition because of commingling of chemically incompatible waters within the system. The model predicted the effect of temperature, pressure, and pH on scale formation. It was found that CaCO₃ scale formation increased with increase in temperature, a decrease in pressure and an increase in pH. The precision of the results was found to be affected only by the occurrence of water sampling and water analyzing.

Rousseau *et al.* (2003) applied a model to find quick correlations between physical measurements and the predicted risk of scaling in Angolan reservoirs which are dolomitic with temperatures ranging from 150 to 164 °C with a nearly constant pressure (320 bar). The model took into account the cumulated effects of water flow in connection with pressure and temperature variations, and changes in dynamic

water composition because of the mixing. Here, the kinetic module of the SCALE2000 software was used to explain the scaling phenomenon.

Mackay (2003) developed a model for scale deposition, which was an extension of his work on mixing of injected, connate, and aquifer brines in water flooding and its relevance to oilfield scaling. In this model, the location of maximum scale deposition and the resulting brine compositions at the production wells are calculated for a range of sensitivities, including reservoir geometry (1D, 2D aerial and vertical, and 3D), well geometry and the reaction rate.

Moreover, limitations to his modeling work were lack of kinetic reaction rates, mixing zone, and impact on permeability. Mixing of brines in the wellbore was not discussed as well, although there was obviously a relationship between in-situ deposition and the availability of scaling ions that may damage the tubing.

2.9 Summary

From the survey of the literature, most of the flooding experiments contain normal salinity (normal concentration of calcium and strontium) and normal concentration of barium and they were conducted with different media like bead packs, sandpacks, and alumina cores, and were run at either low or particular temperatures and pressures.

This research was conducted as an experimental study, containing high salinity (high concentration of calcium and strontium) and high concentration of barium, to investigate permeability reduction by deposition of scale formation in sandstone cores.

CHAPTER 3

METHODOLOGY

3.1 Introduction

This chapter outlines the experimental research work to be done in order to achieve the objectives of this study. Materials used, design of the experimental equipment, set up and experimental procedure are all described in the following sections.

3.2 Materials Used

The materials used in this study were:

3.2.1 Porous Medium

In all flooding experiments, sandstone cores from Malaysia with 3 inch length and of diameter 1 inch with average porosity of 32% and of initial permeability varied from 12.30 to 13.87 md were used. No oil was present in the cores. All the cores were cleaned using methanol in Soxhlet extractor and dried in a Memmert Universal Oven at 100 °C for overnight before use. Table 3.1 lists the physical properties of all core samples used in this study.

Table 3.1: Physical properties of sandstone cores used in this study

Core of run #	Length (inch)	Diameter (inch)	Pore volume (cm)	Porosity (%)	Absolute permeability (md)
1	3	1	4.46	29.81	12.76
2	3	1	5.20	34.75	13.46
3	3	1	4.39	29.34	13.52
4	3	1	5.67	37.89	12.40
5	3	1	5.57	37.23	13.34
6	3	1	4.69	31.35	12.30
7	3	1	5.47	36.56	12.85
8	3	1	5.10	34.09	12.70
9	3	1	4.95	33.08	12.36
10	3	1	5.79	38.70	13.84
11	3	1	5.46	36.49	13.60
12	3	1	4.56	30.48	13.70
13	3	1	4.37	29.21	12.53
14	3	1	5.36	35.82	13.55
15	3	1	5.64	37.69	12.41
16	3	1	4.80	32.08	12.96
17	3	1	5.51	36.83	12.83
18	3	1	4.96	33.15	12.45
19	3	1	5.49	36.69	12.98
20	3	1	6.22	41.57	12.85
21	3	1	5.39	36.02	12.47
22	3	1	4.65	31.08	12.55
23	3	1	5.40	36.09	13.57
24	3	1	4.75	31.75	12.43
25	3	1	4.51	30.14	13.87
26	3	1	4.72	31.55	13.63
27	3	1	4.43	29.61	13.73
28	3	1	6.91	46.18	12.87
29	3	1	6.13	40.97	12.72
30	3	1	4.12	27.54	12.38
31	3	1	4.38	29.27	12.42
32	3	1	5.53	36.96	13.36
33	3	1	4.58	30.61	12.32
34	3	1	4.98	33.28	12.78
35	3	1	5.37	35.89	13.48
36	3	1	4.02	26.87	13.54

3.2.2 Brines

The ionic compositions of synthetic formation water and water injection (Barton and Angsi seawaters) are given in Tables 3.2 and 3.3. Note that the formation water contained calcium, strontium, and barium ions, and the seawater contained sulfate ions. It was clear that the mixing of these waters could lead to calcium, strontium, and barium sulfate precipitation.

Seven salts used for the preparation of synthetic formation water and water injections were given in table 3.3. The description of these salts is as follow:

- (1) Sodium Chloride grade (AR) NaCl (M.Wt. = 58.44 g/mol, 99.8% purity) supplied by QReC™.
- (2) Potassium Sulfate K₂SO₄ (M.Wt. = 174.25 g/mol, 99% purity) supplied by BHD chemicals Ltd Pool England.
- (3) Magnesium Chloride MgCl₂.6H₂O (M.Wt. = 203.30 g/mol, 98% purity) supplied by R&M Chemicals.
- (4) Calcium Chloride (dihydrate) grade (AR) CaCl₂.2H₂O (M.Wt. = 147.02 g/mol, 78% purity) supplied by QReC™.
- (5) Sodium Bicarbonate NaHCO₃ (M.Wt. = 84.01 g/mol, 99.5% purity) supplied by GCE Laboratory Chemicals.
- (6) Strontium Chloride (6-hydrate) SrCl₂.6H₂O (M.Wt. = 266.62 g/mol, 99% purity) supplied by GCE Laboratory Chemicals.
- (7) Barium Chloride (dihydrate) grade (AR) BaCl₂.2H₂O (M.Wt. = 244.28 g/mol, 99% purity) supplied by QReC™.

Table 3.2: The ionic compositions of synthetic formation and injection waters

Ionic	Normal salinity formation water (ppm)	High salinity formation water (ppm)	Normal barium formation water (ppm)	High barium formation water (ppm)	Barton seawater (ppm)	Angsi seawater (ppm)
Sodium	52,132	52,132	42,707	42,707	9,749	10,804.50
potassium	1,967	1,967	1,972	1,972	340	375.05
Magnesium	4,260	4,260	102	102	1,060	1,295.25
Calcium	7,000	30,000	780	780	384	429.20
Strontium	500	1,100	370	370	5.4	6.577
Barium	10	10	250	2,200	<0.2	-
Chloride	99,653	146,385	66,706	67,713	17,218	19,307.45
Sulfate	108	108	5	5	2,960	2,750
Bicarbonate	350	350	2,140	2,140	136	158.80

Table 3.3: Compounds of synthetic formation and injection waters

Compound	Normal salinity formation water (ppm)	High salinity formation water (ppm)	Normal barium formation water (ppm)	High barium formation water (ppm)	Average between Barton and Angsi seawaters (ppm)
Sodium Chloride	132,000	132,000	106,500	106,500	26,100
Potassium Sulfate	-	-	-	-	5,180
Magnesium Chloride	35,625	35,625	853	853	9,846
Calcium Chloride	25,677	110,045	-	-	-
Sodium Bicarbonate	482	482	-	-	-
Strontium Chloride	1,521	3,347	-	-	-
Barium Chloride	-	-	445	3,914	-

3.3 Equipment Set-up

A schematic diagram and photograph of the experimental set-up used in this study were shown in Figures 3.1 and 3.2 respectively. It comprised:

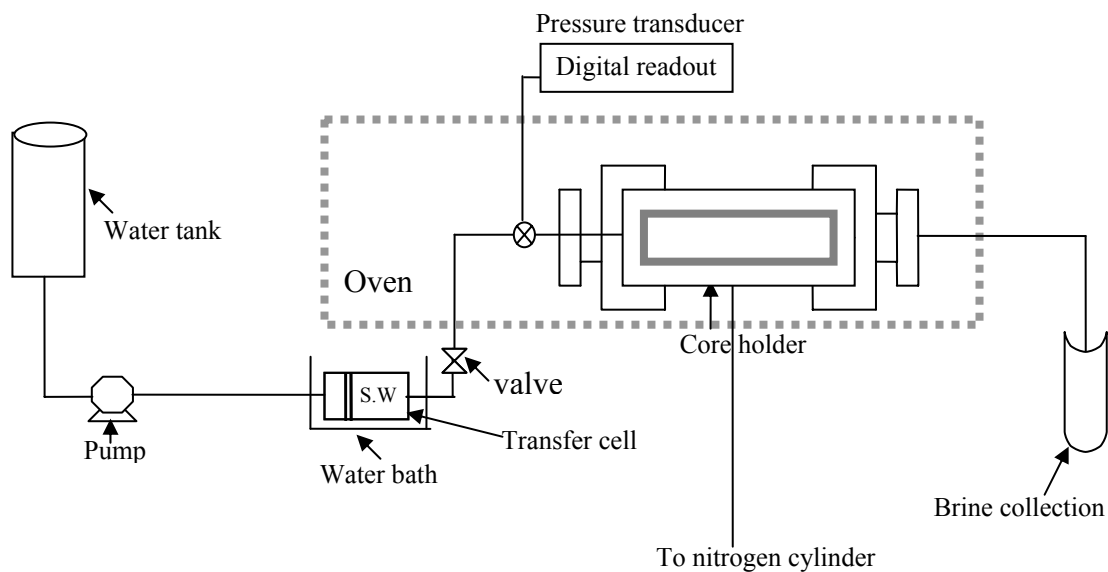


Figure 3.1 Schematic of the coreflooding apparatus



Figure 3.2 Photograph of the coreflooding apparatus

3.3.1 Core Holder

A Hassler type, stainless steel core holder designed for consolidated core samples, 3 inch length and 1 inch diameter, was used. The holder was manufactured by TEMCO, Inc., USA and could withstand pressures upto 10,000 psia. Photograph of core holder is shown in Figure 3.3.

The core sample is housed inside rubber sleeve. An end plug made of stainless steel is inserted into end of the sleeve and is pressed against the core sample by a retaining screw. End plug have circular grooves to ensure fluid injection into and production from the entire cross-section of the core. The outlet plug has one production port at the center.

The annular space between the sleeve and the core holder body is filled with a confining fluid and is pressurized up to the desired pressure. This pressure prevents fluid by-pass around the core and ensures good sealing between the ferrules and sleeve. The confining pressure was applied using cylinder of nitrogen gas.



Figure 3.3 Core holder

3.3.2 Fluid Injection Pump

Double-piston plunger pump (Figure 3.4) manufactured by Lushyong Machinery Industry Limited, with 1.5 horse power motor, maximum design pressure of 35 bars and approximate flow rate of 20 L/min was used to inject the brines during flooding at different pressures.



Figure 3.4 Double- piston plunger pump

3.3.3 Transfer Cell

Stainless steel transfer cell (Figure 3.5) manufactured by TEMCO, Inc., USA which can withstand pressures up to 10,000 psia was used to store and pump the injected brine to the core holder. The cell with a capacity of 1000 ml has a free-floating piston, which separates the pump fluid (distilled water) from the injection brine. The pump fluid was pumped into a transfer cell to displace the brine into the core.



Figure 3.5 Stainless steel transfer cell

3.3.4 Oven

During all flooding runs, the core holder was placed inside a temperature controlled oven is shown in Figure 3.6.



Figure 3.6 A temperature controlled oven

3.3.5 Pressure Transducer

The differential pressure across the core during flooding runs was measured by using a pressure transducer (model E-913 033-B29) manufactured by Lushyong Machinery Industry Limited, with a digital display, as shown in Figure 3.7.



Figure 3.7 Pressure transducer with a digital display

3.3.6 Laboratory Thermal Equipment (Water Bath)

During all flooding runs, the transfer cell was placed inside a temperature controlled bath, as shown in Figure 3.8 and manufactured by TEMCO, Inc., USA.



Figure 3.8 A temperature controlled water bath

3.3.7 Vacuum Pump

Two stage high vacuum pump (Figure 3.9) manufactured by TEMCO, Inc., USA was used for air evacuation during core saturation.



Figure 3.9 Vacuum pump

3.3.8 A Core Cutter Purchased

A core cutter purchased from Norton, USA, was used to cut the sandstone cores, as shown in Figure 3.10.



Figure 3.10 Sandstones cutting equipment

3.3.9 Soxhlet Extractor

Before each run, the core sample was cleaned for five hours by methanol in Soxhlet extractor, as shown in Figure 3.11. It consists of round bottle, sample holder, and condenser.



Figure 3.11 Soxhlet extractor

3.3.10 Memmert Universal Oven

Before each run, the core sample was dried for overnight in a temperature controlled oven at 100°C as shown in Figure 3.12.



Figure 3.12 Memmert universal oven

3.3.11 Viscometer

Brookfield viscometer (model PV III head unit, USA) equipped with a circulated temperature water bath was used for measuring injection brines viscosities at various temperatures is shown in Figure 3.13.



Figure 3.13 Brookfield viscometer with a circulated temperature water bath

3.3.12 Auxiliary Equipment and Tools

Many other pieces of equipment and tools were used during this study. These include pressure gauges, thermocouples, stainless steel fittings and tubings, valves, filters, water tanks, nitrogen cylinder, weighing balance, conical and round bottom flasks of different capacities, and plastic bottles for sampling.

3.4 Experimental Procedure

The general purpose of the laboratory study was to investigate permeability reduction by deposition of scale formation in a porous medium and knowledge of solubility of scale formation and how its solubilities were affected by changes in salinity and temperature.

3.4.1 Beaker Test

The intent of this study was to determine solubility of common oil field scales from mixing synthetic brines (formation water and sea water) at high salinity (high concentration of calcium and strontium), high concentration of barium, various temperatures (40 to 90 °C) and 1 atm.

The experimental procedures used in the determination of solubility of common oil field scales from mixing synthetic brines (formation water and sea water) were:

- (1) For each experiment of common oil field scales, 100 mL of each filtered opposite waters were poured simultaneously into a beaker.

- (2) The synthetic brines were heated on hot plate, as shown in Figure 3.14, and the solution was stirred by magnetic stirrer and after that the solution was filtered through 0.45- μm filter paper.
- (3) After filtration, 5 ml of the filtrate was taken into a 50 ml volumetric flask and was diluted with distilled water to make up 50 ml of solution. This instantaneous dilution of CaCO_3 , CaSO_4 , SrSO_4 , and BaSO_4 containing brines was performed in order to prevent CaCO_3 , CaSO_4 , SrSO_4 , or BaSO_4 precipitation between filtering and analytical determination of the Ca, Ba, and Sr concentration.
- (4) The calcium, barium, and strontium determinations were calibrated by measuring five standard solutions. Standard solutions were prepared from CaCl_2 , BaCl_2 , and SrCl_2 solutions.
- (5) Calcium, barium, and strontium concentrations in the diluted filtrates were determined by Atomic Absorption Spectrometry. After multiplying with the dilution factor, the exact concentrations of calcium, barium, and strontium were computed.



Figure 3.14 Hot plate

3.4.2 Core Test

The test rig was designed to investigate the effect of temperatures, differential pressure and at different concentrations of calcium, strontium, and barium ions on the scaling tendency of brines.

3.4.2.1 Core Saturation

Equipment of core saturation used in this study was shown in Figure 3.15 and comprised a core-holder, vacuum pump, hand pump, pressure gauge and water tank. The procedures of core saturation are as follow:

- (1) Before each run, the core sample was dried in a Memmert Universal Oven at 100 °C for overnight. The core sample was prepared for installation in the core-holder.
- (2) A vacuum was drawn on the core sample for 4 to 5 hours to remove all air from the core. The core was saturated with formation water at room temperature.
- (3) The formation water was then injected by hand pump into the core-holder to saturate the core until the pressure reach 2500 psig. The system was left overnight to ensure 100% saturation.



Figure 3.15 Equipments of core saturation

3.4.2.2 Porosity Measurement

The porosity of a core sample was measured in conjunction with the saturation step described above. Porosities are determined from the volumes of the brines and the dimensions of cores. Porosities of all the cores used in this study were listed in Table 3.1.

3.4.2.3 Initial Permeability Measurement

After porosity measurement, the core holder with the saturated core sample was connected to the flooding apparatus (Figure 3.1). The annulus between the rubber sleeve and the core holder body was then filled with a confining fluid (nitrogen gas). The confining pressure was then adjusted to be approximately double inlet pressure.

The initial permeability was measured by flooding the core with formation water. Variable differential pressure was used and the corresponding flow rates were recorded to calculate initial permeability using Darcy's law. Table 3.1 lists the initial

permeabilities of the cores used in this study. From the initial (k_i) and damaged (k_d) permeabilities calculation, damage ratio can be determined.

Darcy's law:

$$k = Q\mu L / \Delta P A \quad (3.1)$$

where,

- k = permeability (Darcy)
- μ = liquid viscosity (cp)
- Q = flow rate (cc/sec)
- L = length of core (cm)
- ΔP = differential pressure across core holder (atm)
- A = cross-sectional area of core (cm²)

The damage ratio (DR) given by:

$$DR = \frac{k_d}{k_i} = \frac{\text{rock permeability after damage}}{\text{original rock permeability}} \quad (3.2)$$

3.4.2.4 Flooding Experiment

The procedure of flooding experiment is as given below:

- (1) The system consisting of the core holder assembly with the saturated core sample placed inside the oven and transfer cell containing sea water was then placed inside the water bath and heated to the desired temperature of the run. The required confining pressure was then adjusted to be approximately at double inlet pressure.
- (2) A flooding run was started by setting plunger pump at different pressures. Thus, the seawater was injected into the core and mixed with formation water

inside the porous media. The inlet pressure was measured by pressure transducer while the outlet pressure was atmospheric pressure.

- (3) During each run, the flow rate across the core was recorded continuously and the permeability of core was calculated using Darcy's linear-flow equation before and after scale deposition.
- (4) The core sample was removed at the end of flooding then dried and cut into sections for Scanning Electron Microscopy (SEM).

3.4.2.5 Scanning Electron Microscopy (SEM)

Scanning Electron Microscopy (SEM) was used to examine the cores before and after scale deposition. For selected runs, the core sample was removed at the end of flooding and broken into sections. The front of the cores was then examined by SEM to reveal the nature of scale formation crystals.

CHAPTER 4

RESULTS AND DISCUSSION

In this chapter, effects of temperature, concentration of brine, and differential pressure on permeability reduction by deposition of scale formation in a porous medium and knowledge of solubility of scale formation and how its solubilities are affected by changes in salinity and temperature were investigated. The experimental results have been graphically presented, analyzed, and discussed. A total of 36 runs were performed. The detailed experimental data were presented in Appendices B and C.

4.1 Beaker Test

The calcium, barium, and strontium concentrations in the diluted filtrates were determined using atomic absorption spectrometry. The solubilities of CaCO_3 , CaSO_4 , BaSO_4 , and SrSO_4 at various temperatures of this study were calculated and are given in Tables 4.1 - 4.4. Graphical presentations are given in Figures 4.1 - 4.4.

The expected trend in this temperature range is a decrease of CaSO_4 , SrSO_4 solubilities, and BaSO_4 solubility increases with increasing temperature. The solubility of CaSO_4 and SrSO_4 decrease with increasing temperature because of dissociation of CaSO_4 and SrSO_4 which are exothermic reaction. But this phenomenon is different as compared to that of BaSO_4 . Solubility of BaSO_4 increases with increasing temperature due to its endothermic reaction. A graphical presentation of the experimental results (Figures 4.1 - 4.4) illustrates this trend in these experiments. The sulfate ion content

in the sea water brine was reacted with barium ions content in the formation water instantaneously but it was a reaction of both calcium and strontium ions during heating. The more precipitation of CaCO_3 , CaSO_4 , SrSO_4 , and BaSO_4 results from the presence of a large concentration of calcium, strontium, and barium ions as compare to less precipitation at normal concentration of calcium, strontium, and barium ions.

Calcium carbonate scale can be formed by combination of calcium and bicarbonate ions, and this reaction is the major cause of calcium carbonate scale deposition in oilfield operations. This is because only a small percentage of the bicarbonate ions dissociated at the pH values found in most injection waters to form H^+ and CO_3^{-2} (Moghadasi *et al.*, 2004b).

Solubility of CaCO_3 is greatly influenced by the carbon dioxide content of the water and temperature increases. CaCO_3 becomes less soluble as temperature increases. During heating CO_2 comes out of solution and precipitation of calcium carbonate. Supersaturation was the most important reason behind mineral precipitation. Increased supersaturation would result in a more rapid rate of scale precipitation.

The experimental results confirm the general trend in solubility dependencies for common oil field scales with temperatures is obvious and is similar to that observed in the earlier work (Jacques and Bourland 1983; Lindlof and Stoffer 1983; Oddo *et al.*, 1991; Moghadasi *et al.*, 2003a; Mackay, 2003; Rousseau *et al.*, 2003 and Mackay and Jordan, 2005).

Table 4.1: Solubility of CaCO₃ at various temperatures

Temperature (°C)	Solubility of CaCO ₃ at high salinity (Ca = 30,000 ppm) (ppm)	Solubility of CaCO ₃ at normal salinity (Ca = 7,000 ppm) (ppm)
40	24780.02	6254.82
50	23301.12	5849.36
60	22698.00	4267.51
70	22502.50	3895.17
80	22045.31	3648.23
90	21712.06	3341.46

Table 4.2: Solubility of CaSO₄ at various temperatures

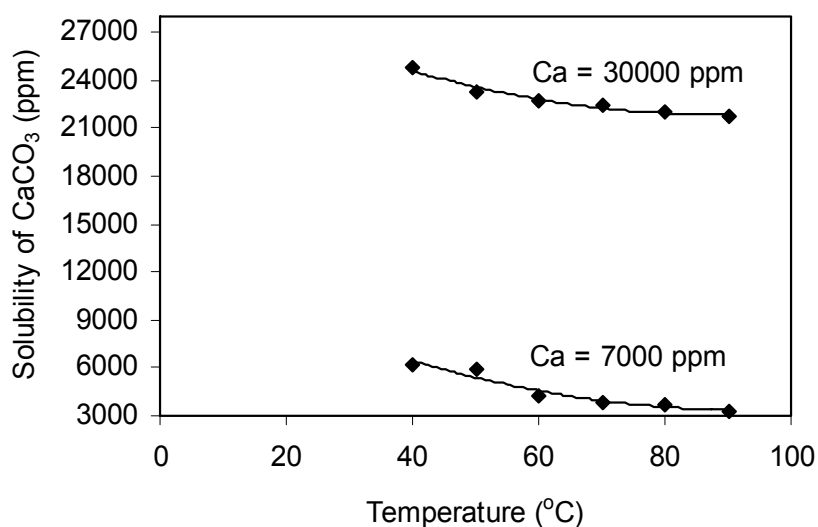
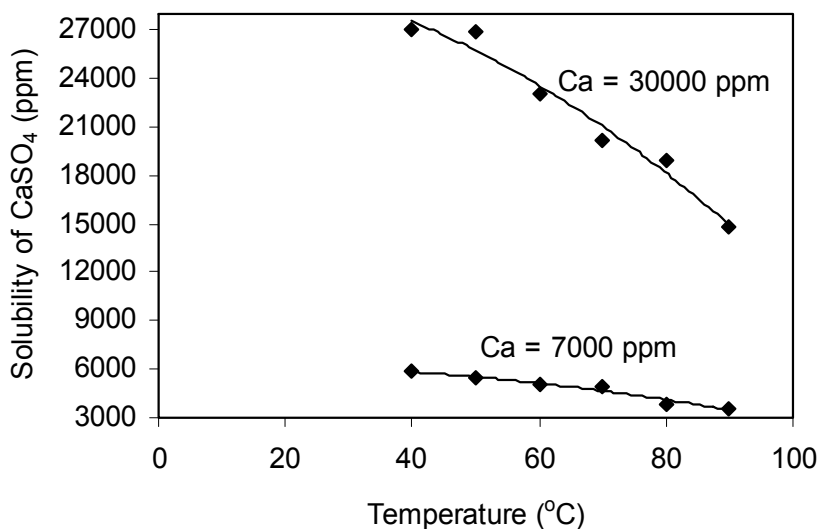
Temperature (°C)	Solubility of CaSO ₄ at high salinity (Ca = 30,000 ppm) (ppm)	Solubility of CaSO ₄ at normal salinity (Ca = 7,000 ppm) (ppm)
40	27033.32	5890.71
50	26918.48	5410.35
60	23118.47	5096.25
70	20154.34	4951.25
80	18923.25	3837.50
90	14771.73	3565.14

Table 4.3: Solubility of SrSO₄ at various temperatures

Temperature (°C)	Solubility of SrSO ₄ at high salinity (Sr = 1100 ppm) (ppm)	Solubility of SrSO ₄ at normal salinity (Sr = 500 ppm) (ppm)
40	913.25	369.45
50	850.65	363.08
60	705.12	351.23
70	680.32	293.25
80	620.33	260.70
90	430.12	241.40

Table 4.4: Solubility of BaSO₄ at various temperatures

Temperature (°C)	Solubility of BaSO ₄ at high (Ba =2200 ppm) (ppm)	Solubility of BaSO ₄ at normal (Ba =250 ppm) (ppm)
40	810.96	128.50
50	900.87	137.25
60	1300.02	169.13
70	1530.63	175.64
80	1620.50	181.30
90	1740.13	192.88

**Figure 4.1** Solubility of CaCO₃ is largely dependent on temperature**Figure 4.2** CaSO₄ solubility is dependent on temperature

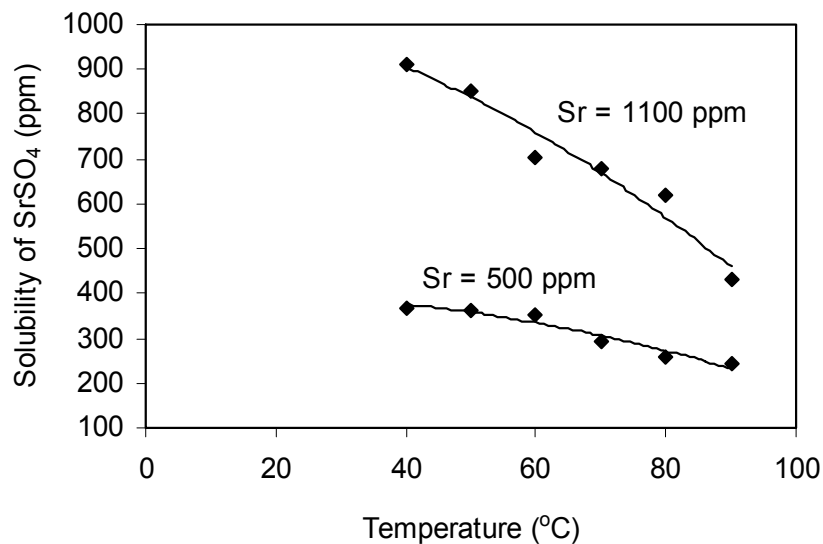


Figure 4.3 SrSO₄ solubility is dependent on temperature

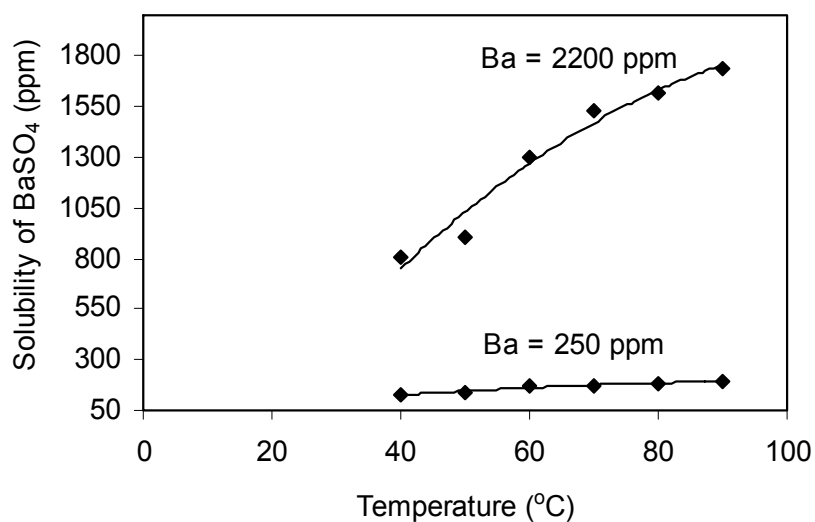


Figure 4.4 BaSO₄ solubility is dependent on temperature

4.2 Core Test

The main objective of this part of the investigation is to study permeability reduction caused by common oil field scales deposition in porous media.

The coreflood experiments were designed to investigate the effect of temperature (50 - 80 °C), differential pressure (100 - 200 psig), and different

concentrations of calcium, strontium, and barium ions (Table 3.2) on the scaling tendency of brines.

During each run, the flow rate across the core was recorded continuously and the permeability of core was calculated using Darcy's linear-flow equation. This decrease in flow rate only occurred during the experiments when supersaturated brine was flowing through the cores. This confirms that the decrease is due to precipitation of the calcium, strontium, and barium sulfates in the core with the consequent reduction in its permeability and porosity. In the following, the results for CaSO_4 , SrSO_4 , and BaSO_4 experiments are discussed individually.

4.2.1 Calcium and Strontium Sulfates Experiments

In these experiments, the seawater was mixed with formation water within the sandstone cores at temperatures (50 – 80 °C), differential pressure (100 - 200 psig), and different concentrations (7000 - 30000 ppm of Ca^{++} and 500 - 1100 ppm of Sr^{++}) of this study are given in tables (appendix C).

Typical results for flow rate and permeability reduction obtained were plotted versus time and pore volumes of injected brine in Figures (4.5 - 4.25 and Appendix E). In the following, extend of permeability damage, permeability decline trend, and the results for various temperatures, concentrations, and differential pressure are discussed individually.

4.2.1.1 Extend of Permeability Damage

Extend of permeability loss caused by CaSO_4 and SrSO_4 scaling in the rock pores varied in different situations. Figure 4.5 shows the permeability change of a less damaged core at temperature (50 °C) and differential pressure (100 psig); Figure

4.6 shows that of a severely damaged core after CaSO_4 and SrSO_4 scaling at temperature ($80\text{ }^\circ\text{C}$) and differential pressure (200 psig).

Nevertheless, about 4% - 14% permeability loss is observed in Figure (4.5), but about 15% - 23% permeability reduction could occur in a heavily scaled core, as Figure 4.6 indicates. The reduction in permeability might be caused due to crystals blocking the pore throats as shown in the SEM view of Figure 4.49. The amount of precipitation varied within the sandstone cores. The scale formation decreased as it moves away from the formation water inlet part.

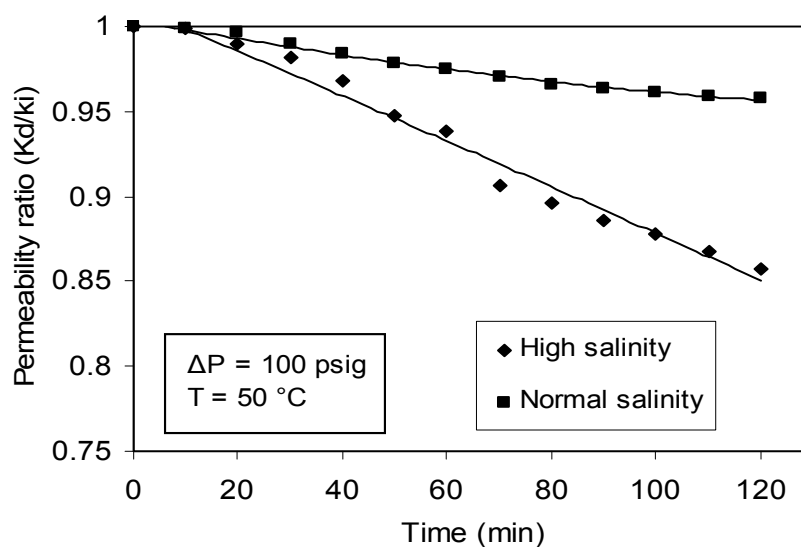


Figure 4.5 Variation of permeability ratio as a function of time showing the effect of concentration at 100 psig and $50\text{ }^\circ\text{C}$

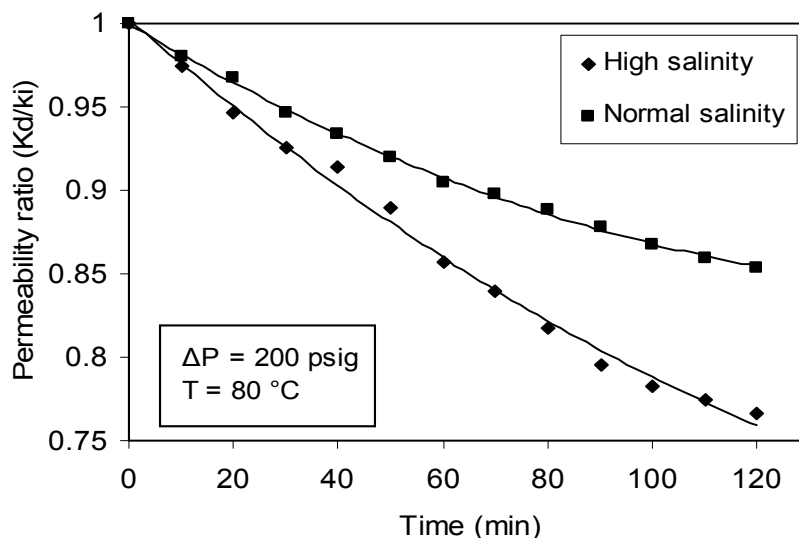


Figure 4.6 Variation of permeability ratio as a function of time showing the effect of concentration at 200 psig and 80 °C

4.2.1.2 Decline Trend of Permeability Ratio

Figures 4.7 - 4.18 show the permeability decline trend changes with brine-injection time. During the initial flow period, the permeability declined sharply soon after the two waters mixed in the pores. The permeability decline then slowed and gradually leveled out after the permeability decreased greatly. This phenomenon was observed in all the core tests in which the scaling damage was severe. The same trend was reported by Todd and Yuan (1992), Moghadasi *et al.* (2002), Moghadasi *et al.* (2003b), Moghadasi *et al.* (2004a) and Ahmed (2004).

4.2.1.3 Effect of Temperature

Temperature has a significant influence on solubility and crystal growth of CaSO_4 and SrSO_4 is very important. To study its effect on the permeability reduction, a set of tests were performed, where differential pressure and concentration of calcium and strontium ions were kept constant and temperature was varied.

Figures 4.7 - 4.12 and E.1 - 6 (Appendix E) show variation of flow rate and permeability reduction with time at different temperatures. These figures show that at higher temperatures the permeability declines more rapidly. This is because the rate of precipitation increases with temperature. The increase in temperature also causes a raise in supersaturation, because the solubility of CaSO_4 and SrSO_4 decrease with temperature. This must have led to an increase of rate of precipitation and consequently a faster permeability decline.

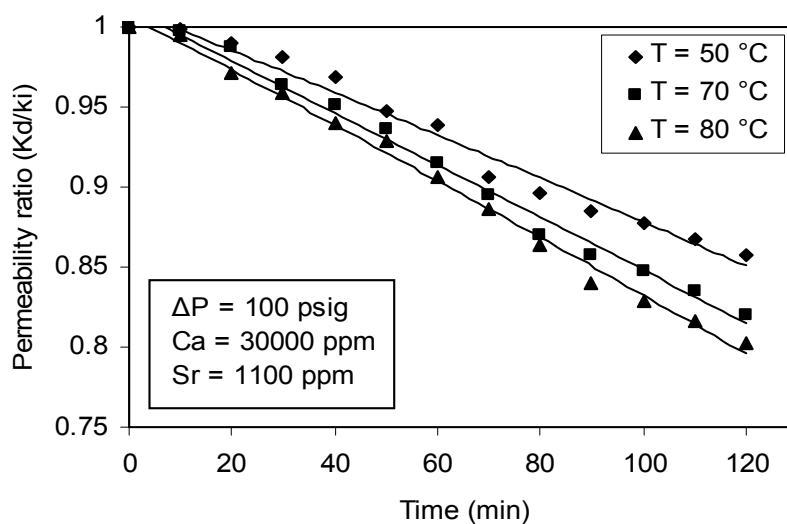


Figure 4.7 Variation of permeability ratio as a function of time showing the effect of temperature at 100 psig

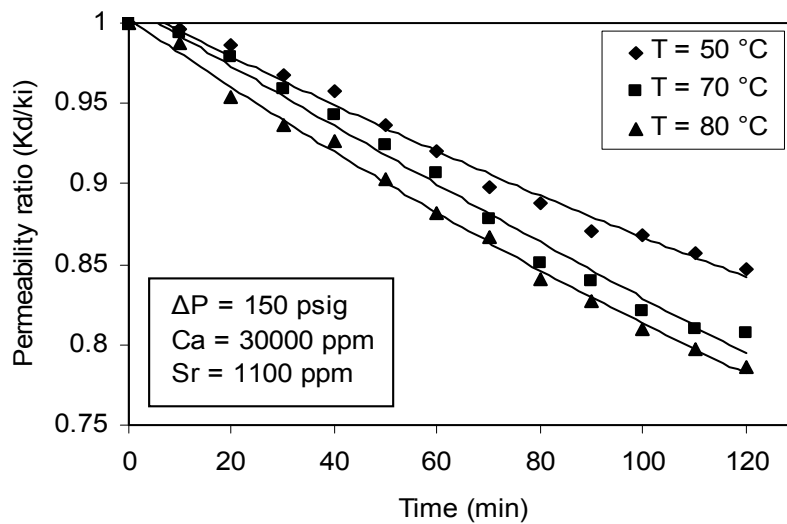


Figure 4.8 Variation of permeability ratio as a function of time showing the effect of temperature at 150 psig

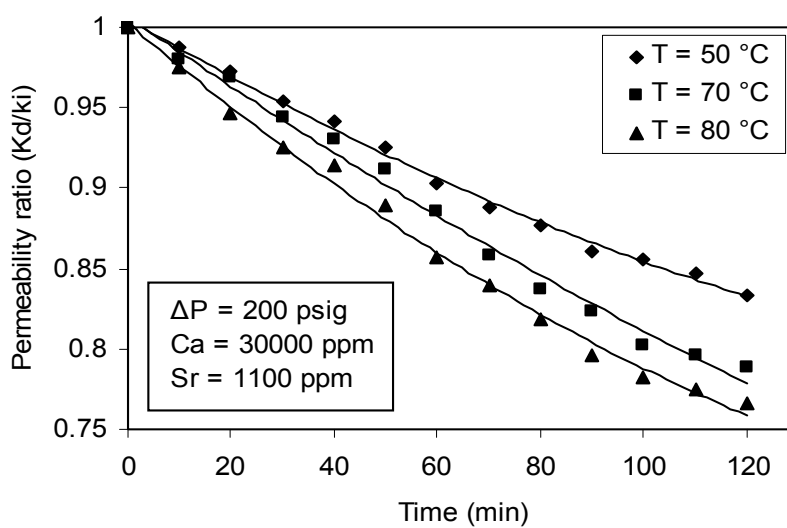


Figure 4.9 Variation of permeability ratio as a function of time showing the effect of temperature at 200 psig

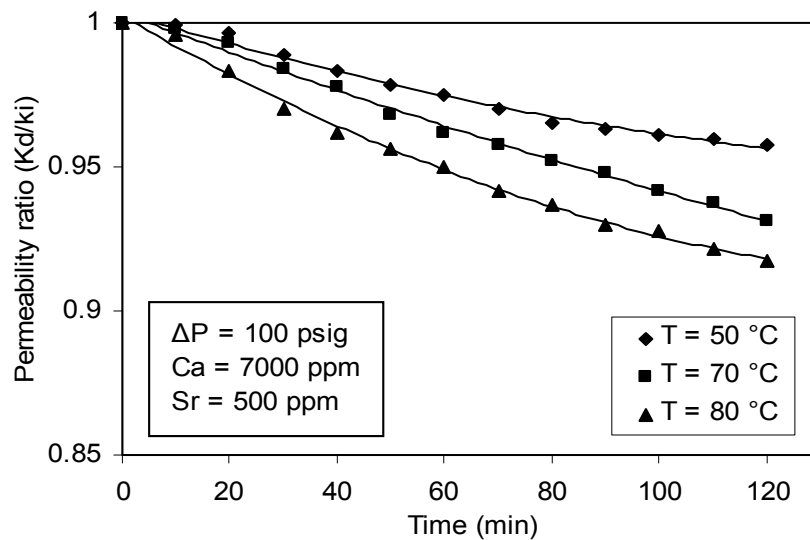


Figure 4.10 Variation of permeability ratio as a function of time showing the effect of temperature at 100 psig

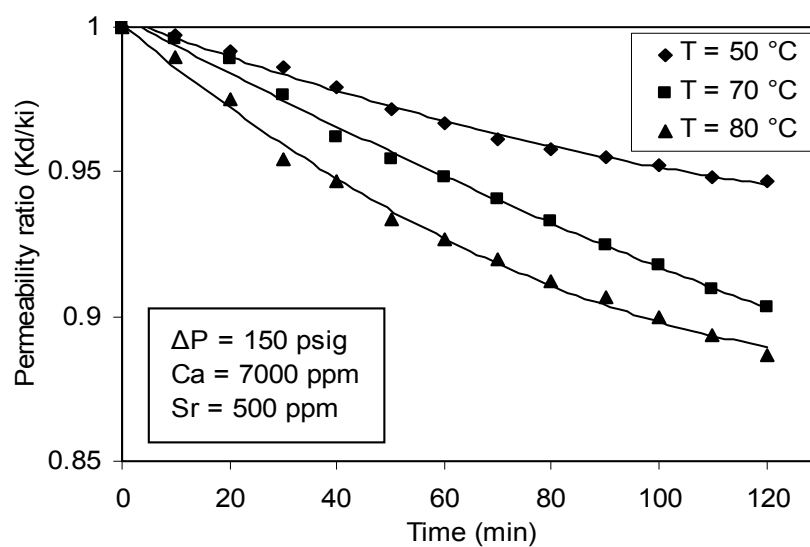


Figure 4.11 Variation of permeability ratio as a function of time showing the effect of temperature at 150 psig

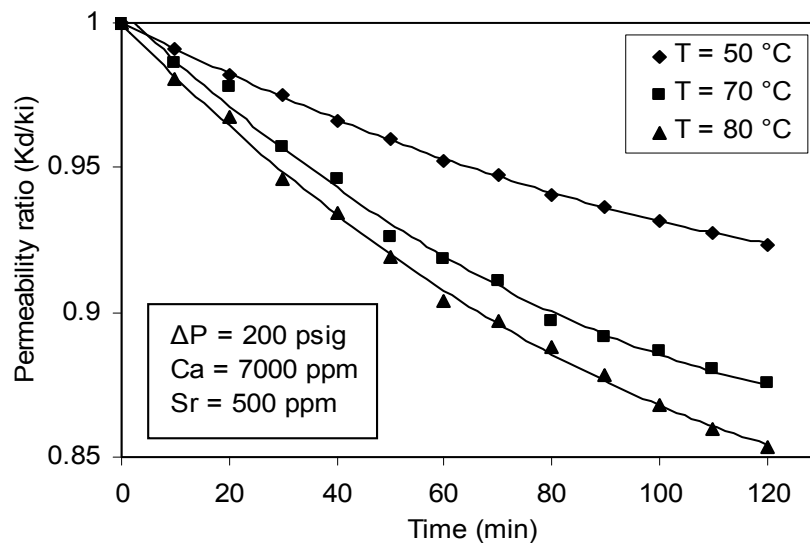


Figure 4.12 Variation of permeability ratio as a function of time showing the effect of temperature at 200 psig

4.2.1.4 Effect of Differential Pressure

To investigate the effect of differential pressure on flow rate and permeability reduction a number of tests were carried out. In these experiments, the concentration of brine and temperature were kept constant and differential pressures are varied from 100 to 200 psig.

The variation of flow rate and permeability reduction with time at different differential pressures are shown in Figures 4.13 - 4.18 and E.7 - 12 (Appendix E). From these figures, the permeability decline of porous medium is evident, even at such low differential pressures.

The results illustrate that at low differential pressure, scale formation has already as significant effect on the permeability decline as shown in Figures 4.13 and 4.16 for high and normal salinity respectively. As, the differential pressure was increased, the rate of permeability decline becomes more rapid.

Moreover, at higher differential pressure more sulfate ions will pass through the porous medium in a given interval of time. The supersaturation at the porous medium will therefore increase the rate of precipitation. This increased precipitation rate will produce a larger permeability decline as shown in Figures 4.15 and 4.18 for high and normal salinity respectively. These results agreed with result by reported by Moghadasi *et al.*, (2002), Moghadasi *et al.*, (2003b) and Moghadasi *et al.*, (2004a).

Furthermore, the overall permeability of porous medium at high salinity decreased to between 14% to 23% of initial permeability and normal salinity between 4% - 15% of initial permeability depending on the differential pressure used.

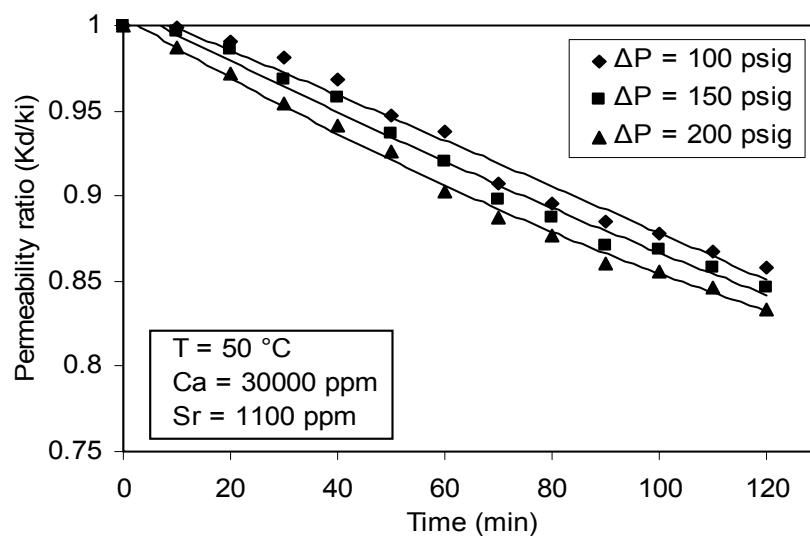


Figure 4.13 Variation of permeability ratio as a function of time showing the effect of differential pressure at 50 °C

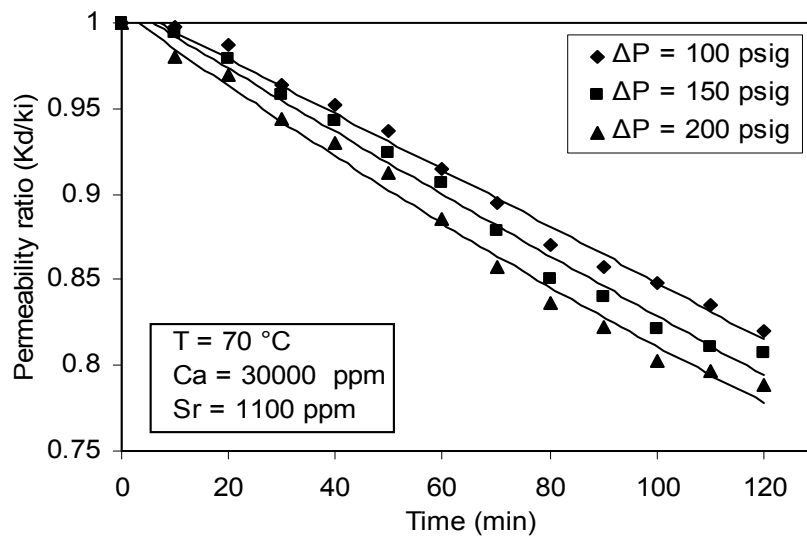


Figure 4.14 Variation of permeability ratio as a function of time showing the effect of differential pressure at 70 °C

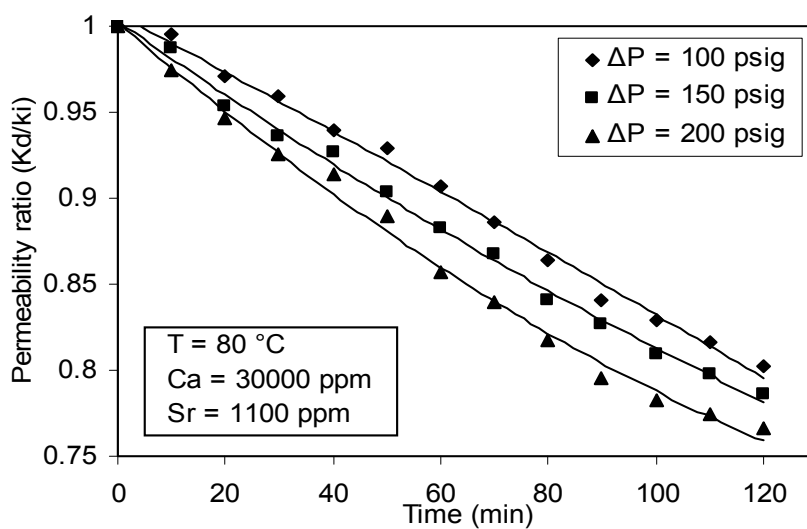


Figure 4.15 Variation of permeability ratio as a function of time showing the effect of differential pressure at 80 °C

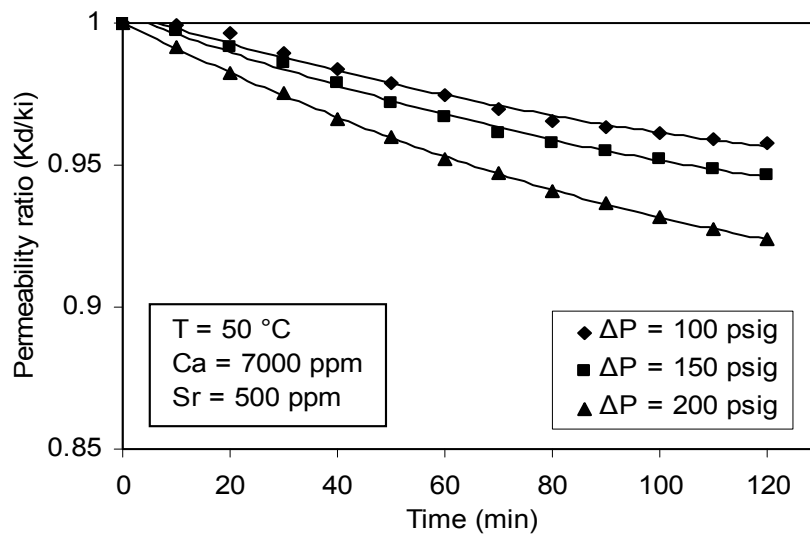


Figure 4.16 Variation of permeability ratio as a function of time showing the effect of differential pressure at 50 °C

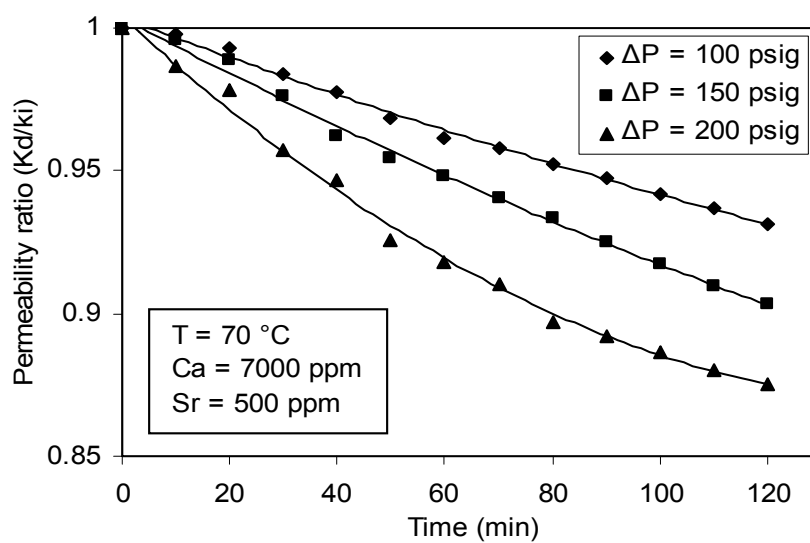


Figure 4.17 Variation of permeability ratio as a function of time showing the effect of differential pressure at 70 °C

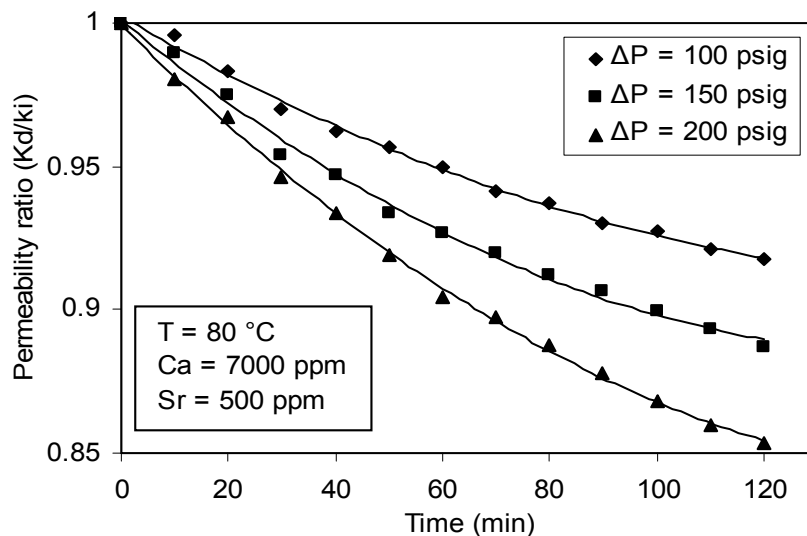


Figure 4.18 Variation of permeability ratio as a function of time showing the effect of differential pressure at 80 °C

4.2.1.5 Effect of Concentration

A number of tests were carried out to study the effect of brine concentration on permeability reduction. These tests were carried out at differential pressure from 100 to 200 psig and temperatures of 50, 70 and 80 °C with two different brine concentrations (high and normal salinity, see Table 3.2).

Figures 4.19 to 4.25 and E. 33 - 41 (Appendix E) show the variation in permeability decline with time and pore volumes of injected brine for different concentrations of calcium and strontium. When the concentration of brine (i.e. supersaturation) is increasing, plugging and hence permeability loss occurs more rapidly. The permeability decline due to high concentration of calcium and strontium ions is greater than for normal concentration of calcium and strontium ions, for given experimental conditions.

This observation is in good agreement with observations reported in the earlier work (Read and Ringen, 1982; Todd and Yuan, 1990; Todd and Yuan, 1992;

Moghadasi *et al.*, 2002, Moghadasi *et al.*, 2003b; Moghadasi *et al.*, 2004a; Ahmed, 2004).

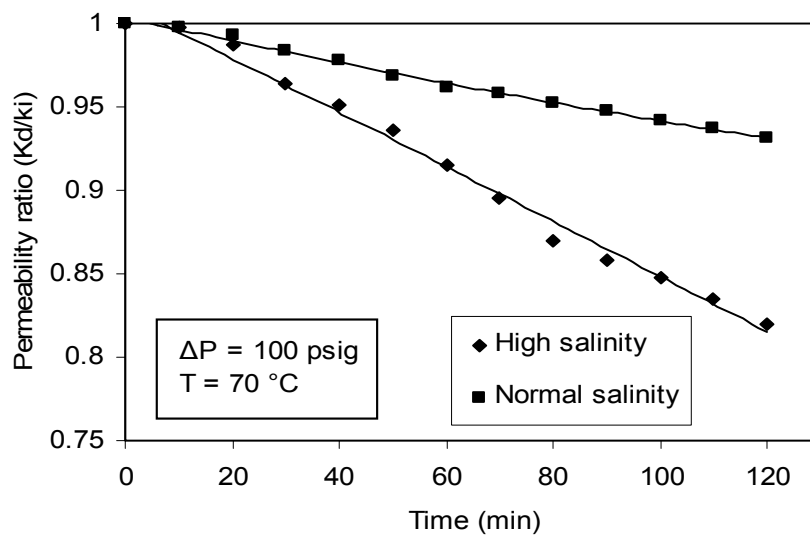


Figure 4.19 Variation of permeability ratio as a function of time showing the effect of concentration at 100 psig and 70 °C

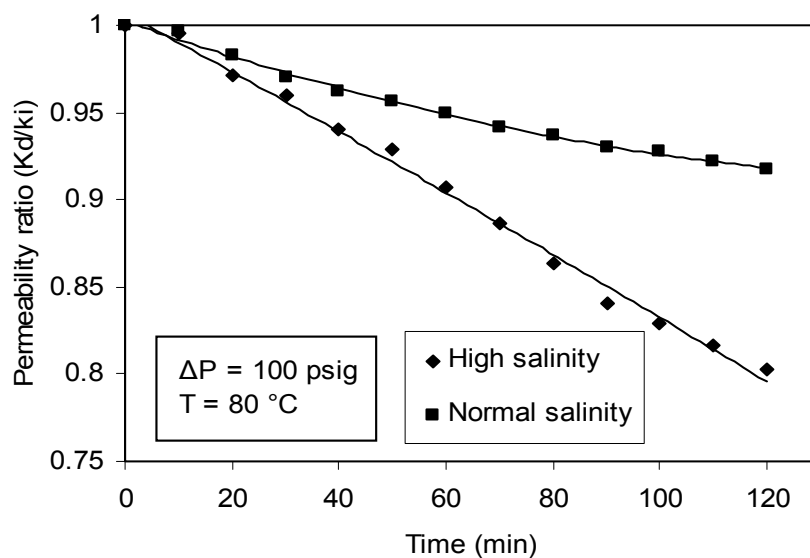


Figure 4.20 Variation of permeability ratio as a function of time showing the effect of concentration at 100 psig and 80 °C

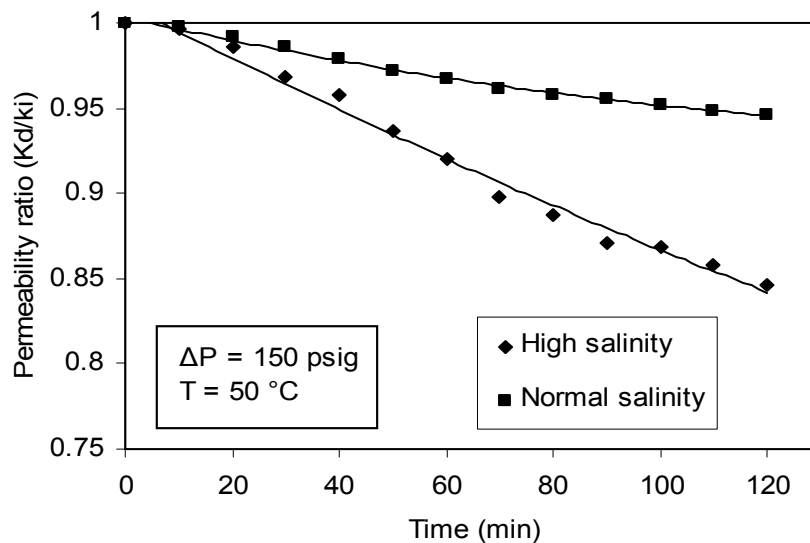


Figure 4.21 Variation of permeability ratio as a function of time showing the effect of concentration 150 psig and 50 °C

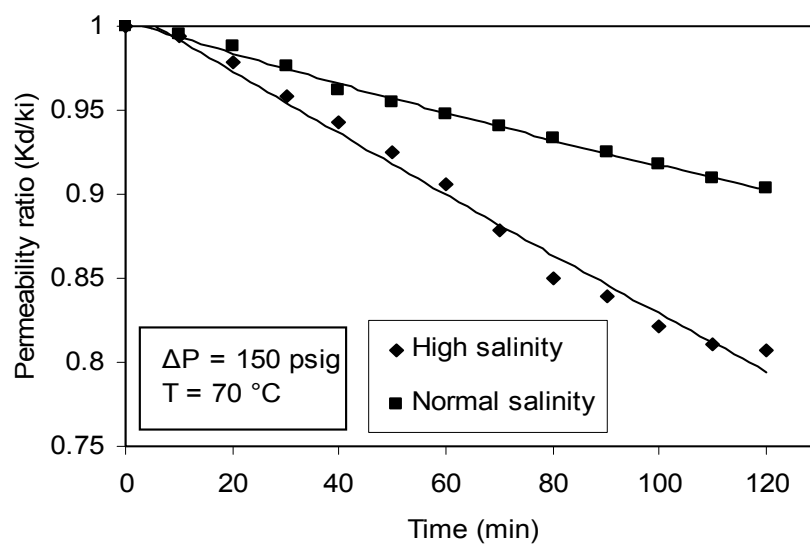


Figure 4.22 Variation of permeability ratio as a function of time showing the effect of concentration 150 psig and 70 °C

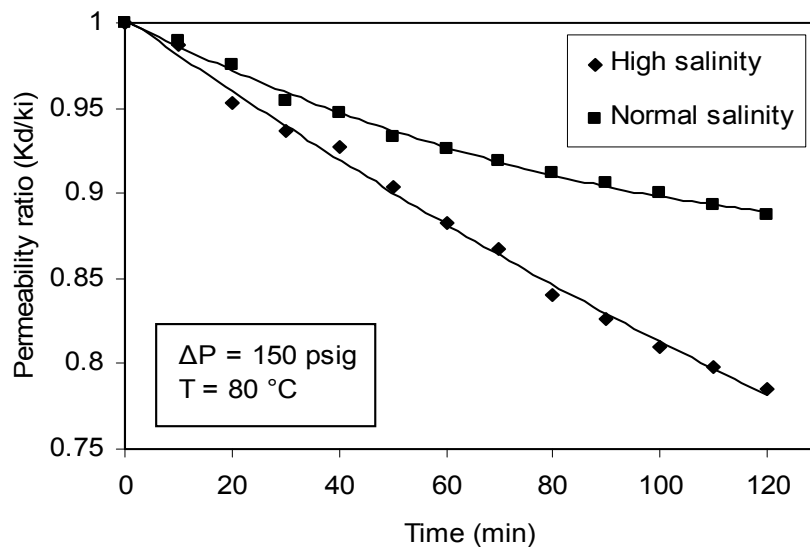


Figure 4.23 Variation of permeability ratio as a function of time showing the effect of concentration 150 psig and 80 °C

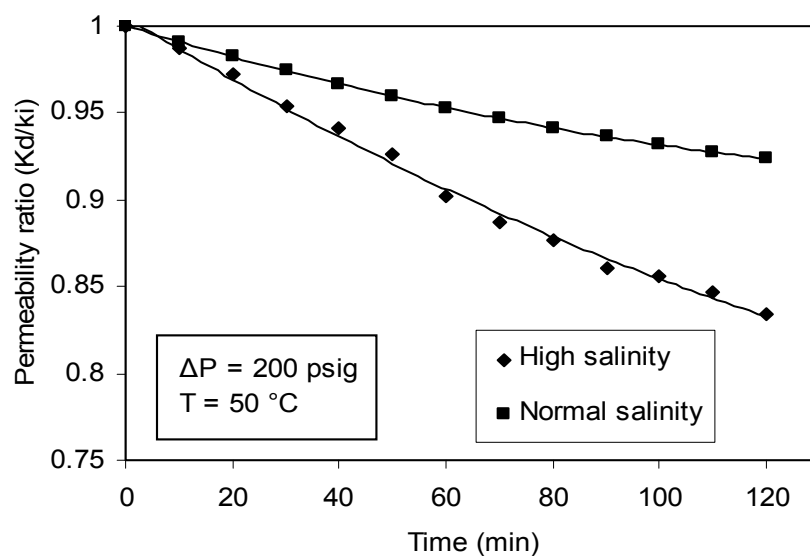


Figure 4.24 Variation of permeability ratio as a function of time showing the effect of concentration 200 psig and 50 °C

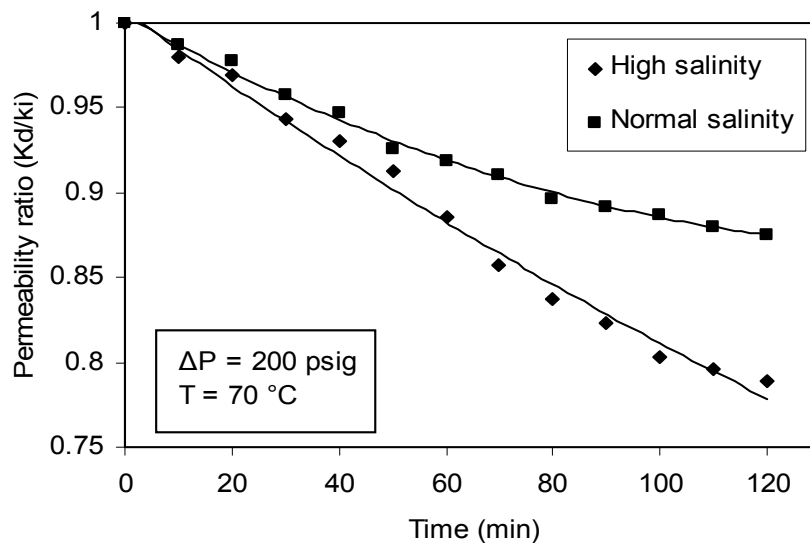


Figure 4.25 Variation of permeability ratio as a function of time showing the effect of concentration 200 psig and 70 °C

4.2.2 Barium Sulfate Experiments

The experimental procedure for scale formation with barium sulfate was exactly the same as the procedure used for calcium and strontium sulfates experiments.

A series of experiments was designed to investigate the effect of operating parameters such as differential pressure (100 - 200 psig); temperature (50 – 80 °C) and concentration (250 - 2200 ppm of Ba⁺⁺) on barium sulfate scale formation as given in tables (Appendix B).

The flow rate was measured in each run for time periods. Figures 4.26 to 4.46 and D.1 - 42 (Appendix D) show variation of the flow rate and permeability decline as a function of time and pore volumes of injected brine. In the following, extend of permeability damage, permeability decline trend and the results for various temperatures, concentrations and differential pressure are discussed individually:

4.2.2.1 Extend of Permeability Damage

Extend of permeability loss caused by BaSO_4 scaling in the rock pores varied in different situations. Figure 4.26 shows the permeability change of a less damaged core at temperature ($80\text{ }^\circ\text{C}$) and differential pressure (100 psig); Figure 4.27 shows that of a severely damaged core after BaSO_4 scaling at temperature ($50\text{ }^\circ\text{C}$) and differential pressure (200 psig). About 5% - 12% permeability loss was observed in Figure 4.26, but about 9%-19% initial permeability reduction occurred in a heavily scaled core, as shown in Figure 4.27.

Moreover, the reduction in permeability is possibly caused by crystals blocking the pore throats as shown by the SEM (Figure 4.48). The amount of precipitation varied within the sandstone cores, there being more scale near the formation water inlets and least scale was observed furthest from the inlet parts.

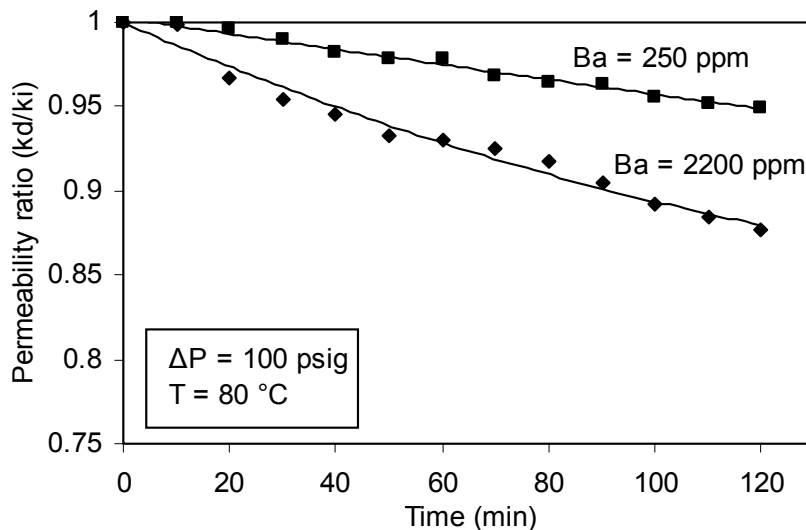


Figure 4.26 Variation of permeability ratio as a function of time showing the effect of concentration at 100 psig and $80\text{ }^\circ\text{C}$

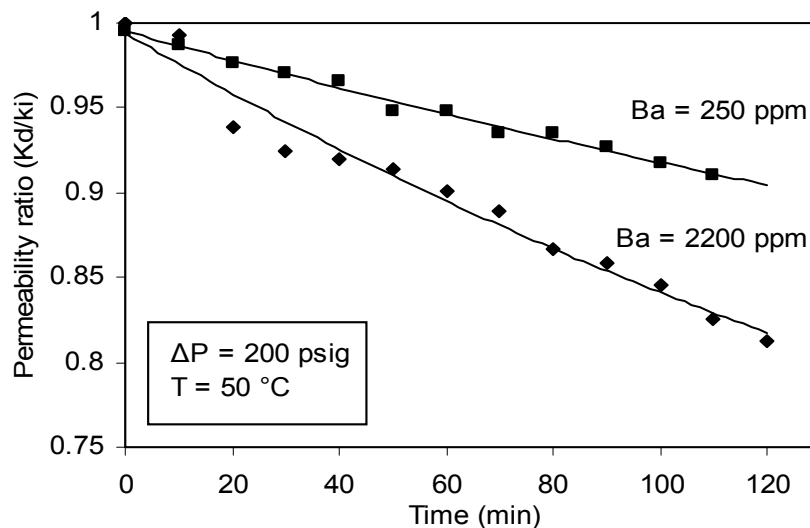


Figure 4.27 Variation of permeability ratio as a function of time showing the effect of concentration at 200 psig and 50 °C

4.2.2.2 Decline Trend of Permeability Ratio

The overall core permeability with brine- injection time curves from all core tests had concave shapes and shown in Figures 4.28 to 4.39. Even the final extent of permeability reduction was small. Such permeability declined trends indicates that the initial stage of scale formation resulted in fast permeability damage and that the damage rate was significantly reduced after a certain period of scale deposition. This phenomenon was observed in all the core tests in which the scaling damage was severe. The same trend was reported by Todd and Yuan (1990) and Todd and Yuan (1992).

4.2.2.3 Effect of Temperature

The influence of temperature on the solubility and crystal growth of barium sulfate is very important. To study its effect on the permeability reduction, a number of experimental runs were carried out. In these experiments, the concentration of

brine and differential pressure were kept constant and temperatures were varied from 50 to 80 °C.

Figures 4.28 to 4.33 and D.22 - 27 (Appendix D) show the variation of permeability reduction with time and pore volumes of injected brine at different temperatures. These figures show that the effect of temperature on permeability reduction. As temperature rises, the rate of nucleation and crystal growth and plugging are decreased. Consequently in lower temperature, the rate of permeability ratio reduction becomes faster.

Comparing the findings from the scale formation study at 50 °C in Figure 4.27 with those obtained from 80 °C experiments in Figure 4.26 reveals some aspects of the effect of temperatures. The permeability decline is less rapid at higher temperature, since the rate of precipitation decrease with temperature.

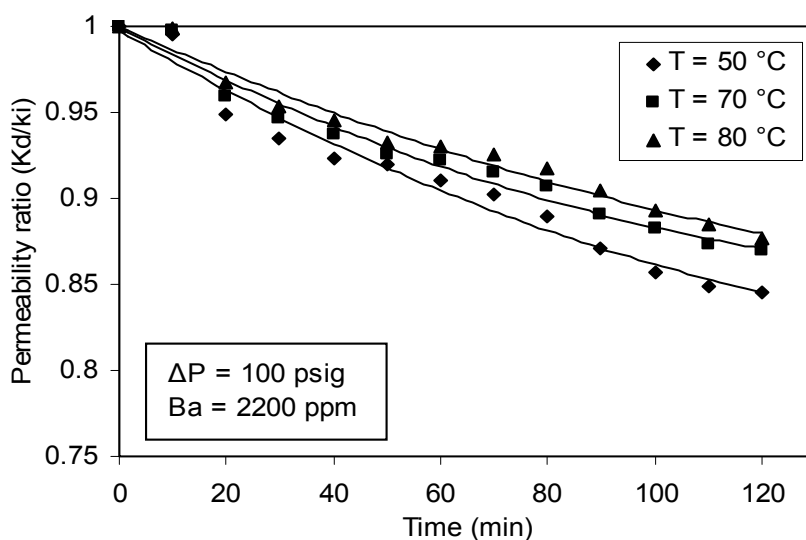


Figure 4.28 Variation of permeability ratio as a function of time showing the effect of temperature at 100 psig

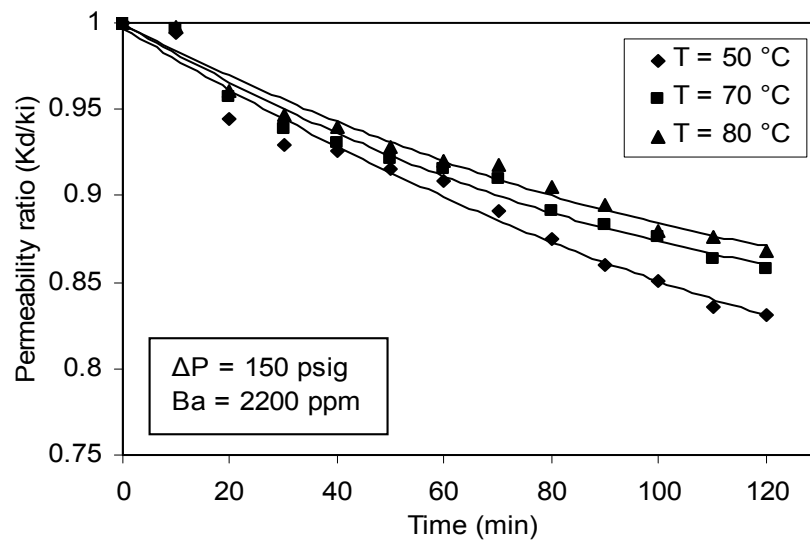


Figure 4.29 Variation of permeability ratio as a function of time showing the effect of temperature at 150 psig

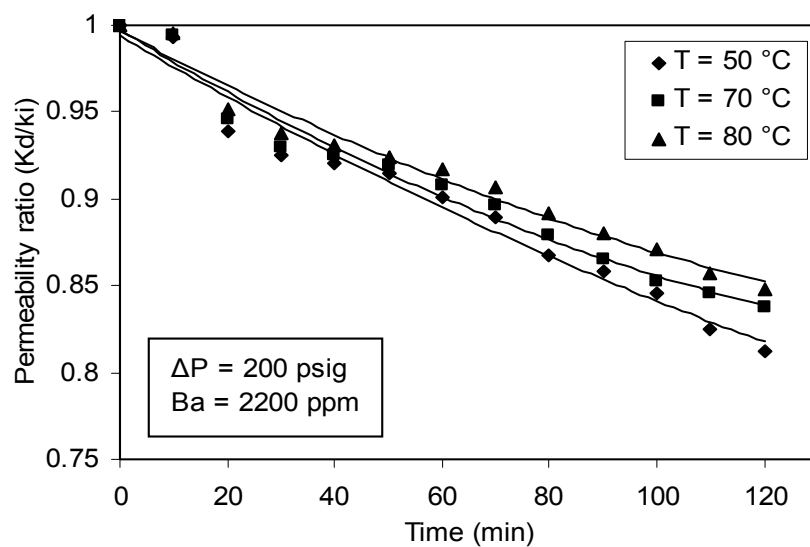


Figure 4.30 Variation of permeability ratio as a function of time showing the effect of temperature at 200 psig

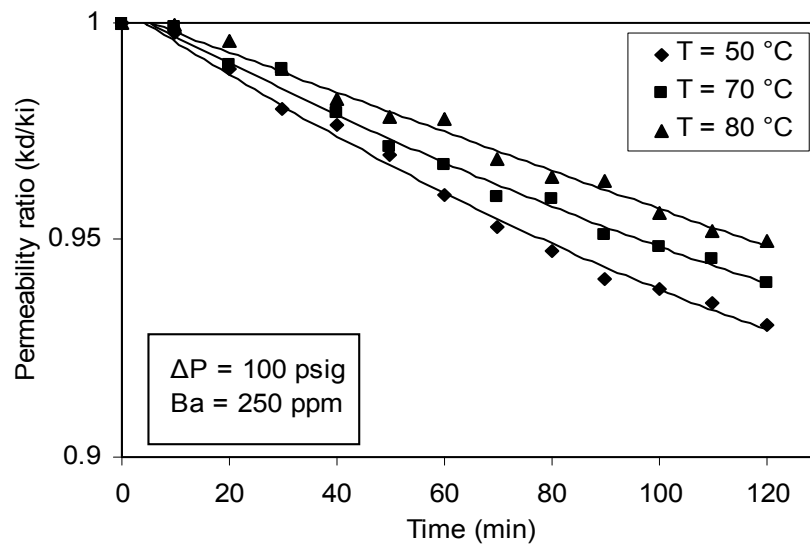


Figure 4.31 Variation of permeability ratio as a function of time showing the effect of temperature at 100 psig

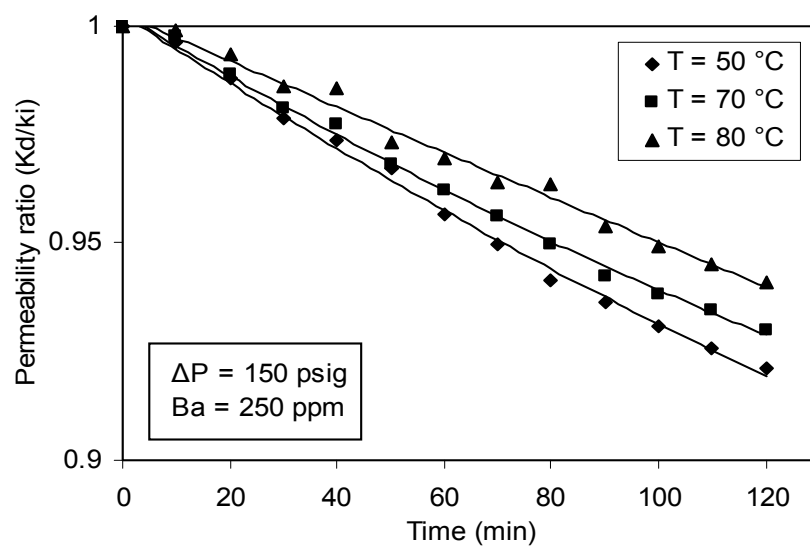


Figure 4.32 Variation of permeability ratio as a function of time showing the effect of temperature at 150 psig

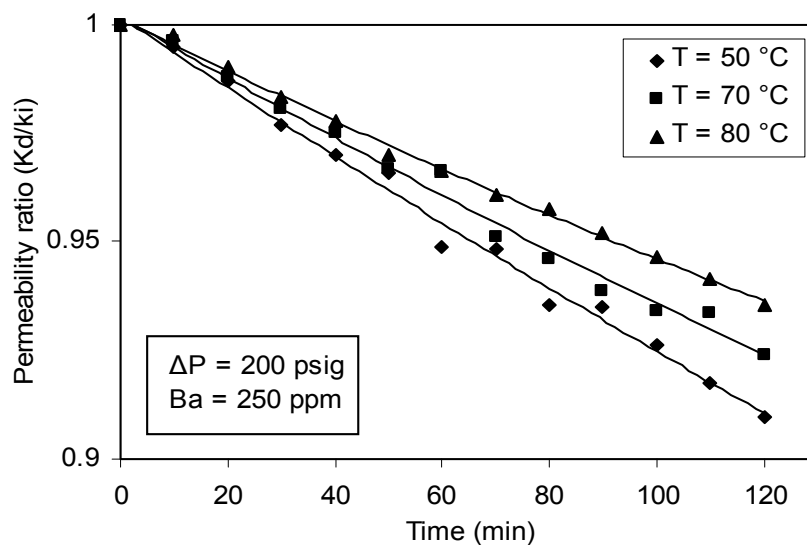


Figure 4.33 Variation of permeability ratio as a function of time showing the effect of temperature at 200 psig

4.2.2.4 Effect of Differential Pressure

To investigate the effect of injection differential pressure on flow rate and permeability reduction, number of experimental runs were performed, in which the concentration of barium ion and temperature were kept constant while the injection differential pressure was varied in each test.

The variations of flow rate and permeability ratio as a function of time at different differential pressures are shown in Figures 4.34 to 4.39 and D.7-12 (Appendix D). From these figures, the rates of permeability decreased sharply as the differential pressure increased. The reason for this behavior may be due to the fact that rate of plugging increases as differential pressure increases.

From the Figures 4.34 to 4.39 and D.7-12 (Appendix D), scale formation has a significant effect on decrease in permeability even at such low differential pressure. As, the differential pressure was increased, the rate of permeability declined more rapidly. At higher differential pressures, more sulfate ions passed through the porous medium in a given interval of time, hence providing more material for deposition.

This shows that by increases of differential pressure, the value of supersaturation increased; consequently the rate of precipitation, crystal growth and plugging is rapidly raised and sharply decrease in permeability ratio. This observation is in good agreement with observations reported in previous studies (Todd and Yuan, 1990; Todd and Yuan, 1992).

In these experiments, the overall permeability of porous medium at high barium decreased to between 12% to 19% of initial permeability and normal barium between 5% - 9% of initial permeability depending on the differential pressure used.

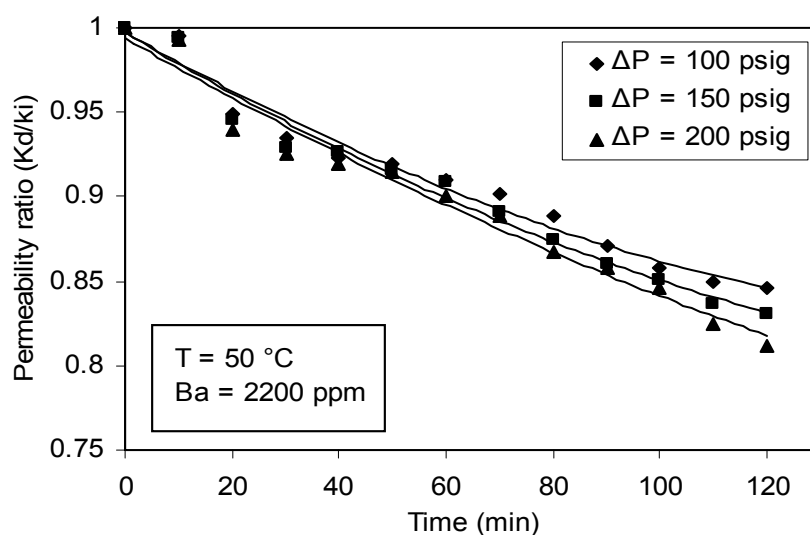


Figure 4.34 Variation of permeability ratio as a function of time showing the effect of differential pressure at 50 °C

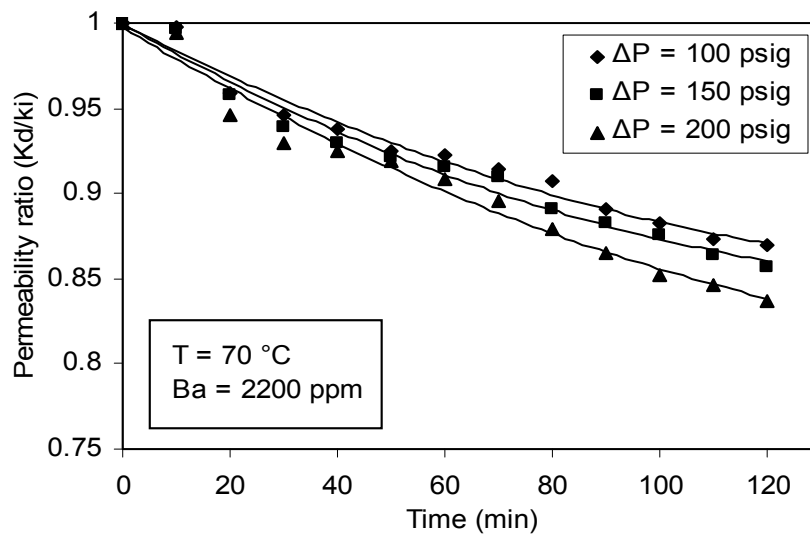


Figure 4.35 Variation of permeability ratio as a function of time showing the effect of differential pressure at 70 °C

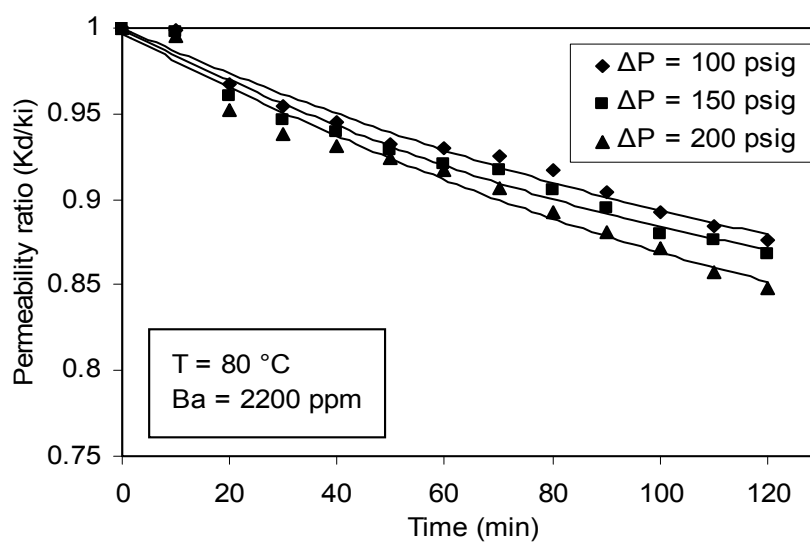


Figure 4.36 Variation of permeability ratio as a function of time showing the effect of differential pressure at 80 °C

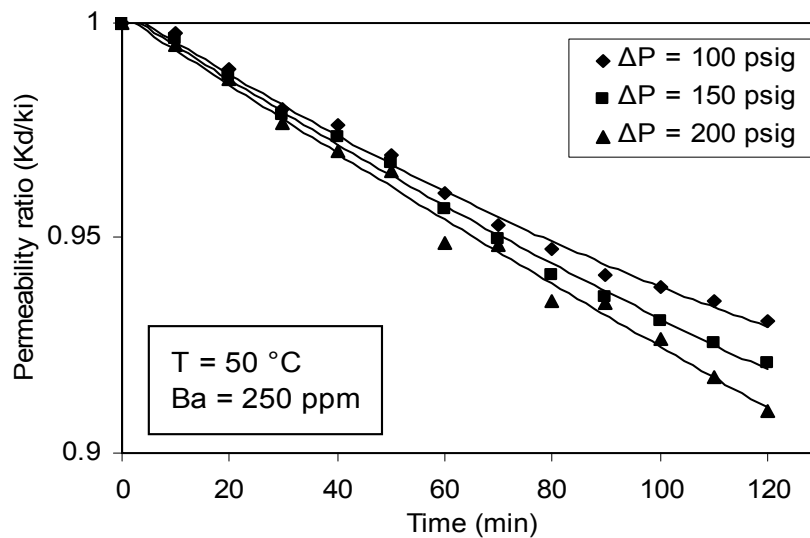


Figure 4.37 Variation of permeability ratio as a function of time showing the effect of differential pressure at $50\text{ }^\circ\text{C}$

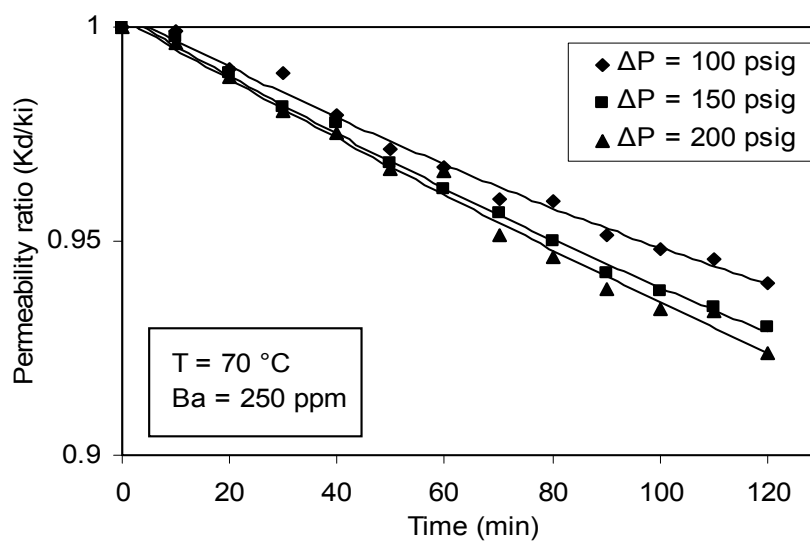


Figure 4.38 Variation of permeability ratio as a function of time showing the effect of differential pressure at $70\text{ }^\circ\text{C}$

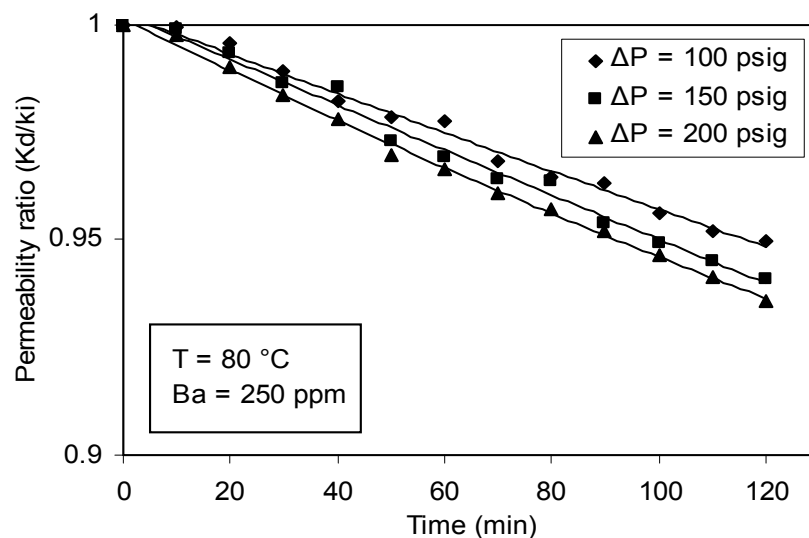


Figure 4.39 Variation of permeability ratio as a function of time showing the effect of differential pressure at 80 °C

4.2.2.5 Effect of Concentration

To investigate the effect of brine concentration on permeability reduction and flow rate a number of tests were considered, in which the differential pressure and temperature was remained constant with two different brine concentrations (high and normal barium, see Table 3.2).

Figures 4.40 to 4.50 and D.34 - 44 (Appendix D) show the variation in permeability decline with time and pore volumes of injected brine for different concentrations of barium. These figures show that the effect of concentration on permeability ratio reduction. A concentration is increased the supersaturation of brine raises and the rate of nucleation and crystal growth raised. Therefore by increasing of concentration, the rate of reaction, nucleation, crystal growth and plugging are increased.

Moreover, the permeability decline due to high concentration of barium ions is greater than for normal concentration of barium ions, for given experimental conditions. This observation is in good agreement with observations reported in the

earlier work (Read and Ringen, 1982; Mitchell *et al.*, 1980; Todd and Yuan, 1990; Todd and Yuan, 1992; Wat *et al.*, 1992).

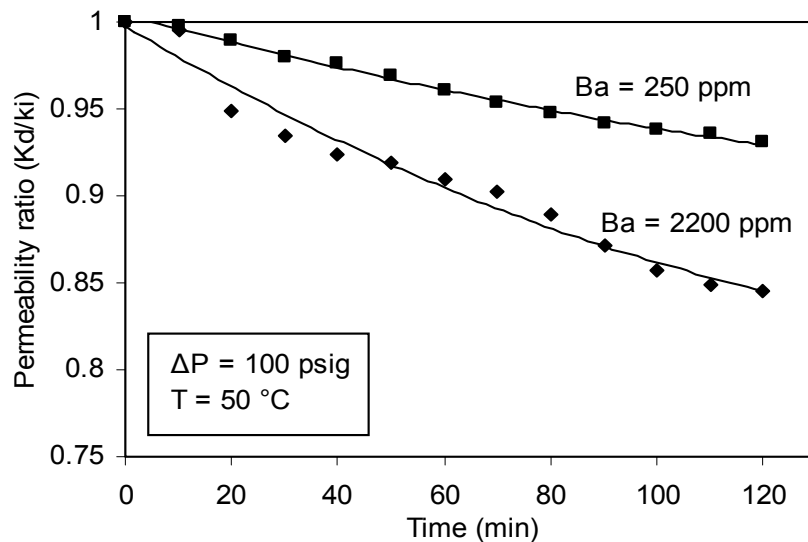


Figure 4.40 Variation of permeability ratio as a function of time showing the effect of concentration at 100 psig and 50 °C

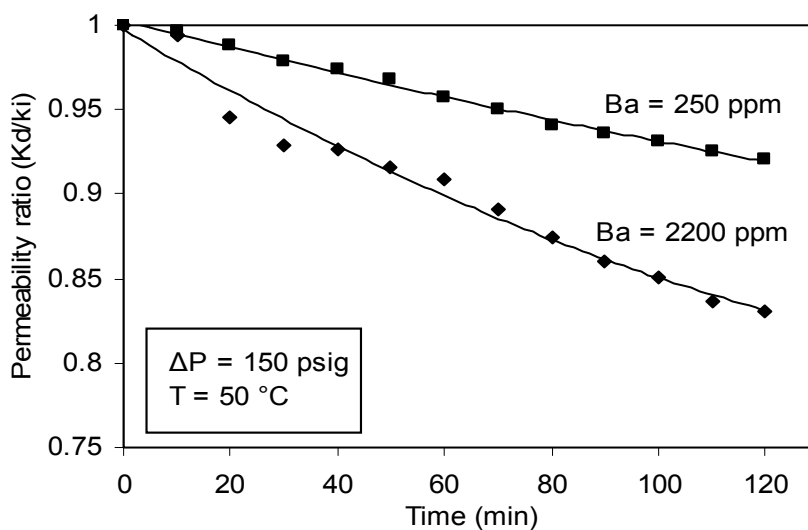


Figure 4.41 Variation of permeability ratio as a function of time showing the effect of concentration at 150 psig and 50 °C

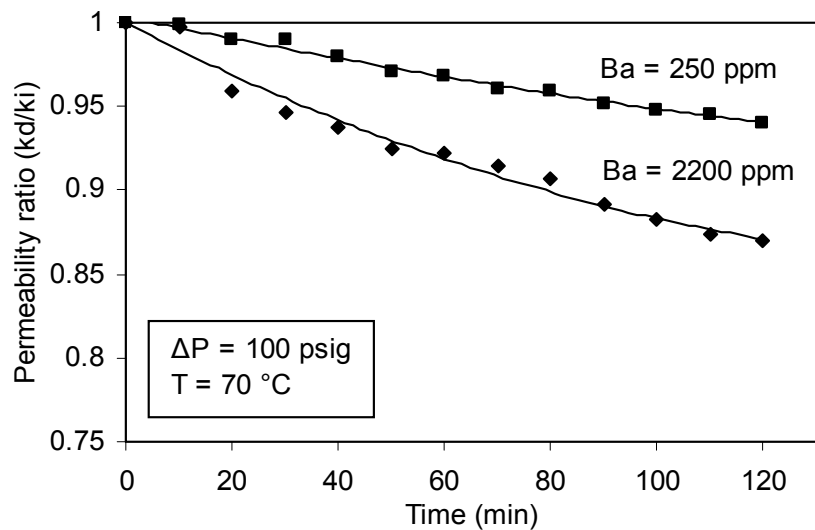


Figure 4.42 Variation of permeability ratio as a function of time showing the effect of concentration at 100 psig and 70 °C

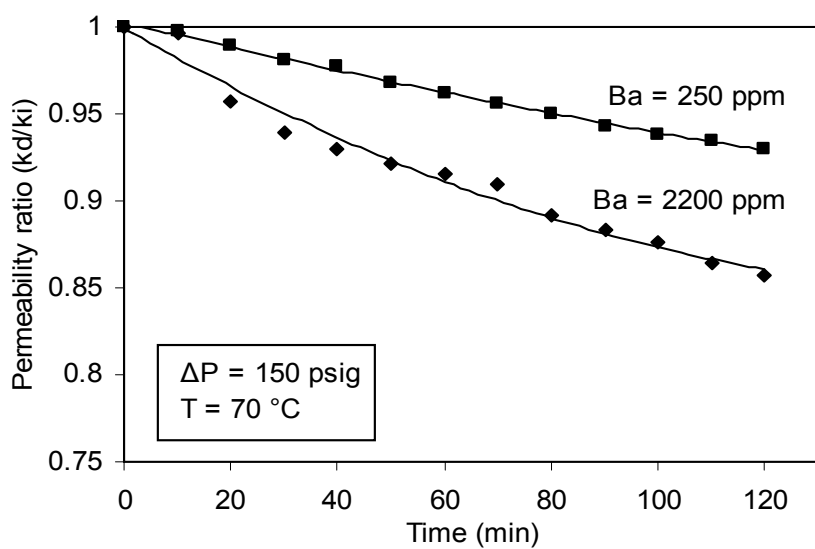


Figure 4.43 Variation of permeability ratio as a function of time showing the effect of concentration at 150 psig and 70 °C

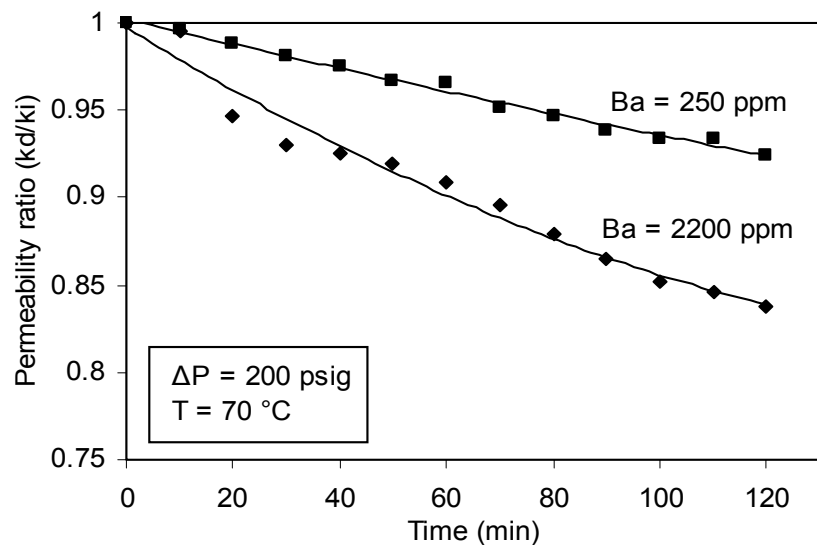


Figure 4.44 Variation of permeability ratio as a function of time showing the effect of concentration at 200 psig and 70 °C

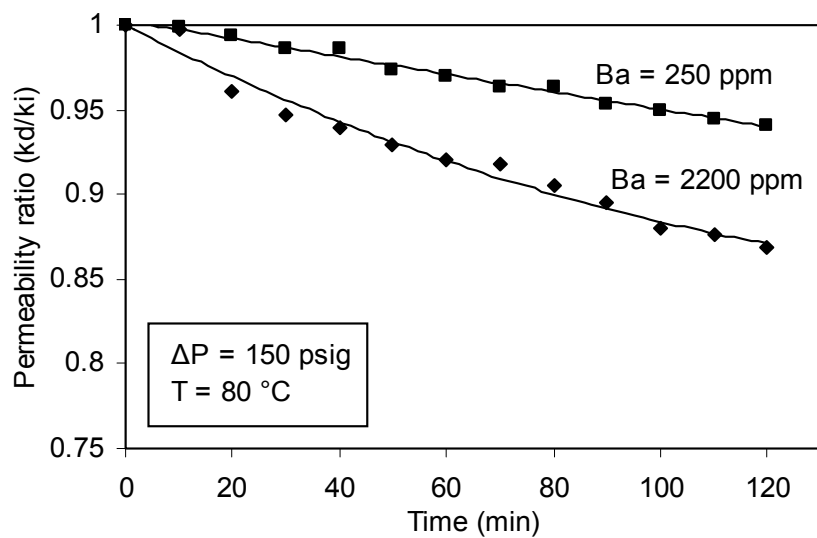


Figure 4.45 Variation of permeability ratio as a function of time showing the effect of concentration at 150 psig and 80 °C

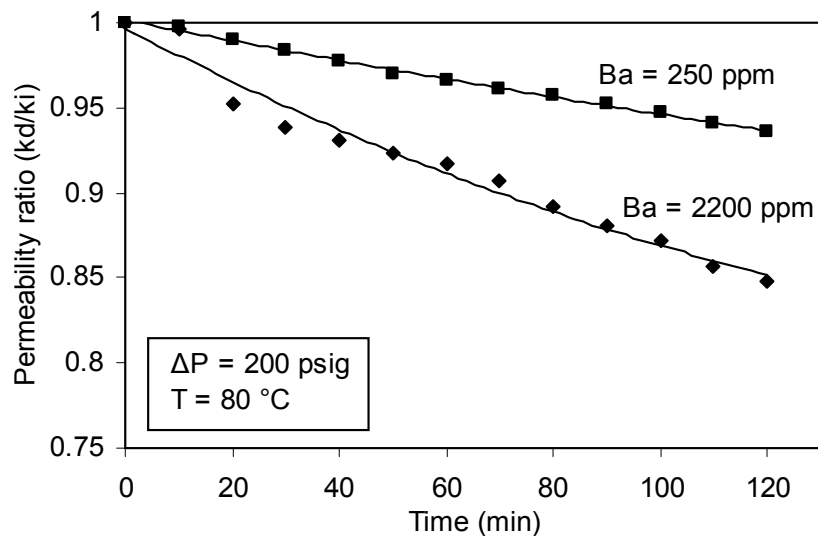


Figure 4.46 Variation of permeability ratio as a function of time showing the effect of concentration at 200 psig and 80 °C

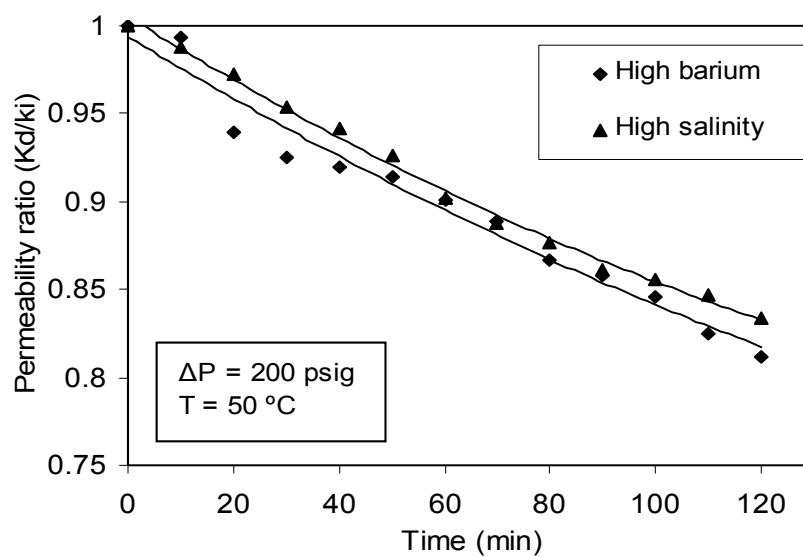


Figure 4.47 Variation of permeability ratio as a function of time showing the effect of concentration at 200 psig and 50 °C

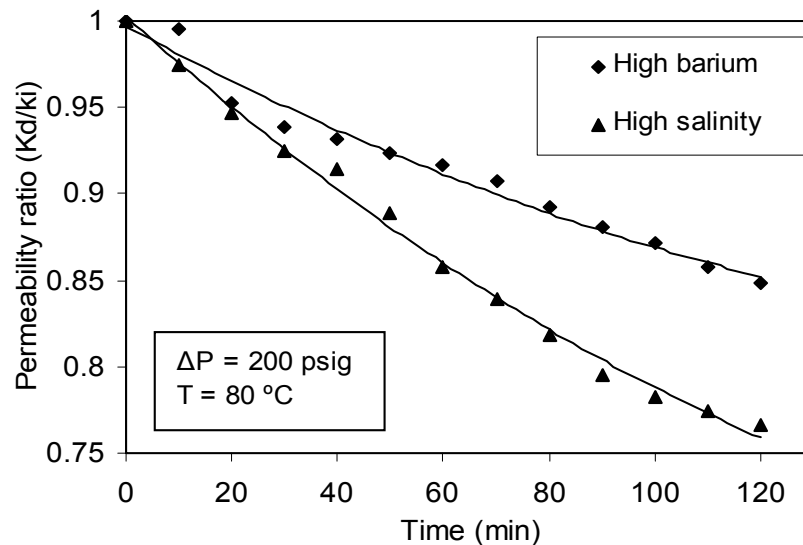


Figure 4.48 Variation of permeability ratio as a function of time showing the effect of concentration at 200 psig and 80 °C

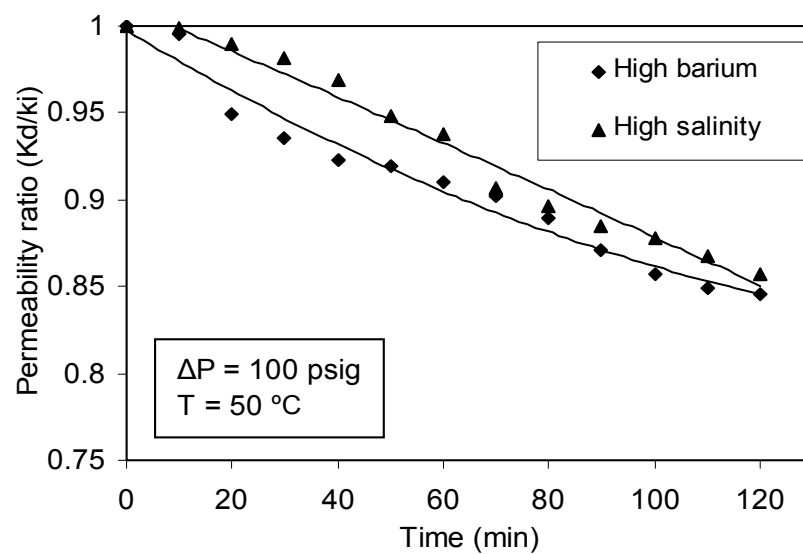


Figure 4.49 Variation of permeability ratio as a function of time showing the effect of concentration at 100 psig and 50 °C

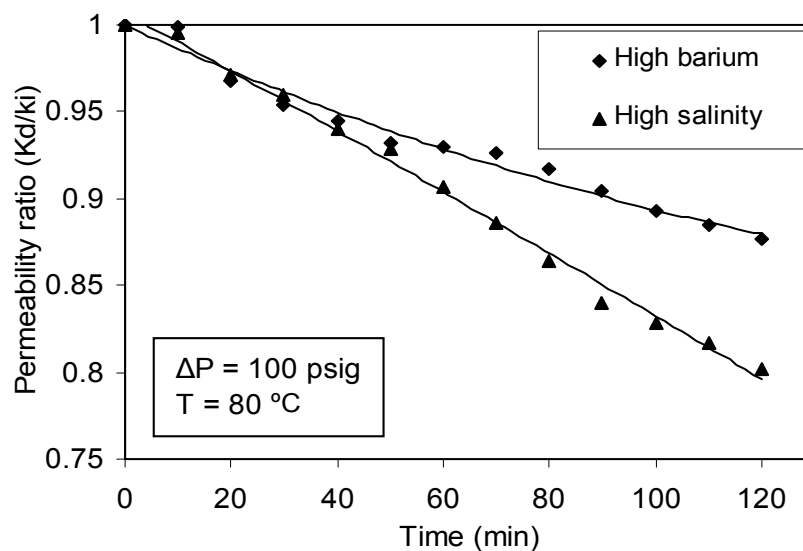


Figure 4.50 Variation of permeability ratio as a function of time showing the effect of concentration at 100 psig and 80 °C

4.3 Scanning Electron Microscopy Analysis

The scaled core samples were examined by SEM to observe the particle size and morphology of the precipitates. The formation of CaSO_4 , SrSO_4 , and BaSO_4 during flow of injection and formation waters in porous media have been observed by Scanning Electron Microscopy (SEM) micrographs which shows CaSO_4 , SrSO_4 , and BaSO_4 crystals formation in porous space.

Figures 4.51 and 4.52 show SEM image of the CaSO_4 , SrSO_4 , and BaSO_4 scaling crystals in rock pores precipitated from mixed seawater with formation water inside the cores. Comparison of BaSO_4 with CaSO_4 and SrSO_4 formed in porous media did not show significant differences in crystal external morphology. The differences line in the irregularity of crystals formed in rock pores and the crystal size variations from one location to another in a core. The average size of BaSO_4 crystals precipitated from mixed brines was about 2.5 μm larger than the average size of CaSO_4 and SrSO_4 crystals is about 1.8 μm .

In all core tests, the abundance of scale reduced significantly from the front of the core to the rear indicating that scale formation in porous media was rapid with the observation that the flow rate decreased soon after two incompatible waters were mixed into a core. The observations of scaling sites from previous tests (Todd and Yuan, 1990; Todd and Yuan, 1992; Ahmed, 2004) were confirmed by this test results.

In general, Figures 4.51 and 4.52 indicate that the front sections of a core suffered considerable greater scaling damage. The reason the scaling decreased downstream of a core is clear: most of the scaling ions had deposited within the front sections as soon as they were mixed and left few ions to precipitate from the flow stream in the rear sections. Figure 4.53 shows an SEM image of an unscaled core samples.

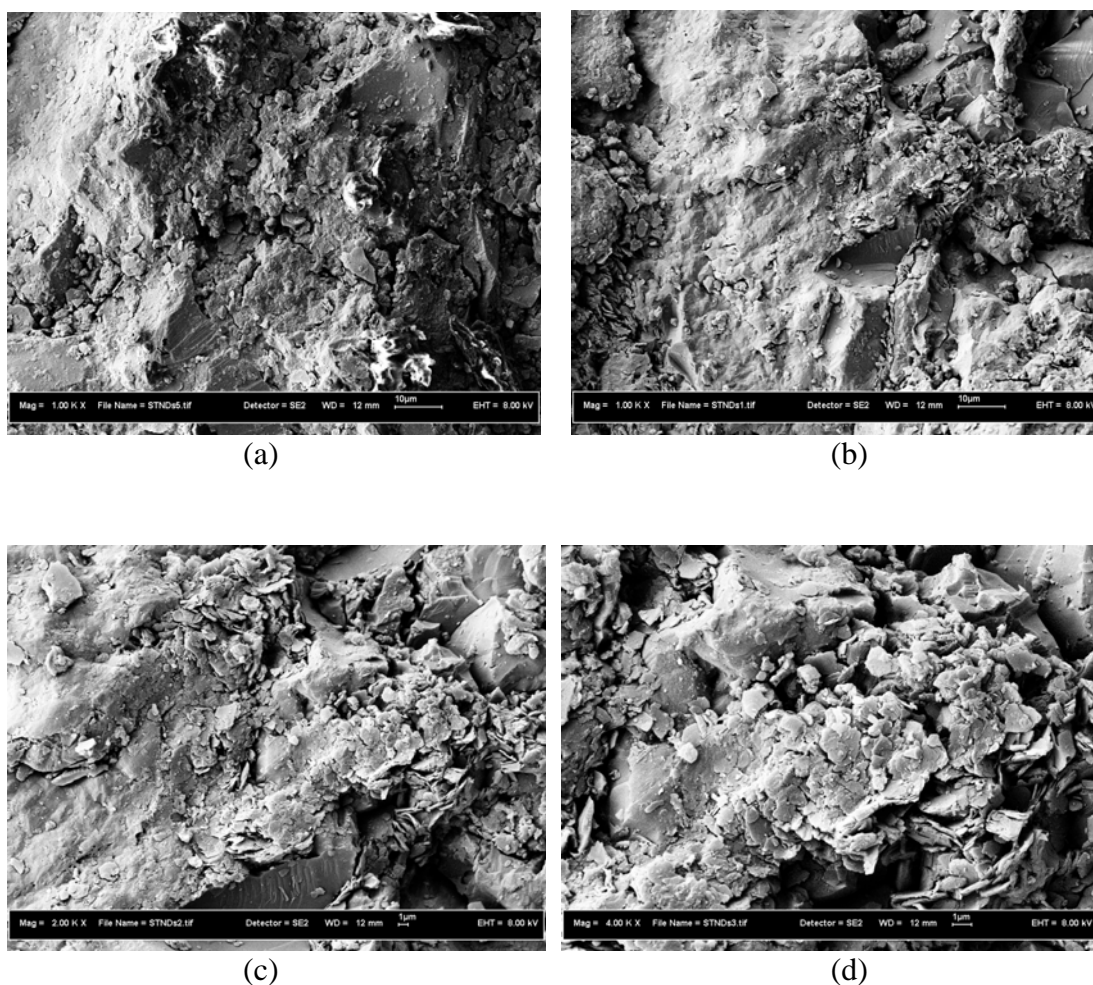


Figure 4.51 SEM image of an unscaled sandstone cores

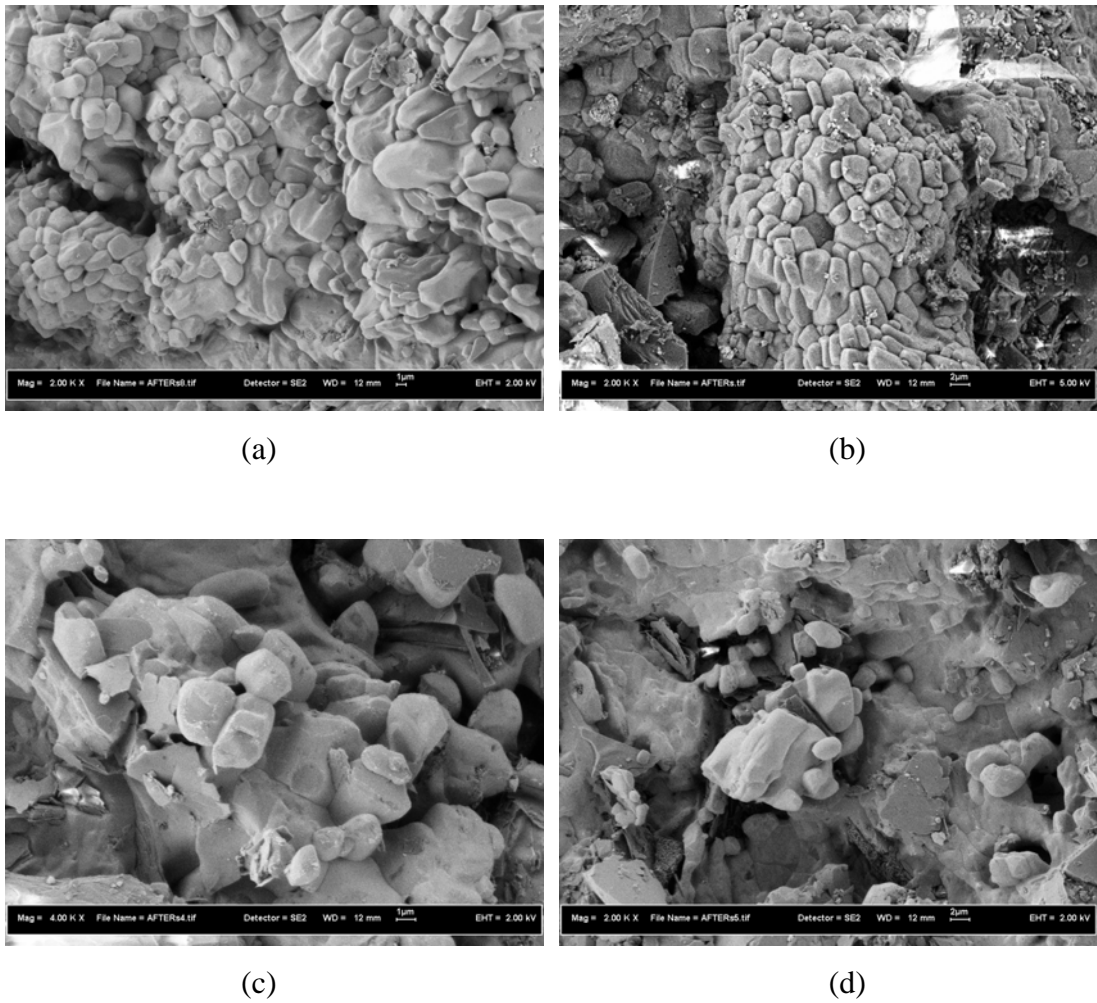


Figure 4.52 SEM image of BaSO₄ scale in sandstone core at 200 psig and 50 °C

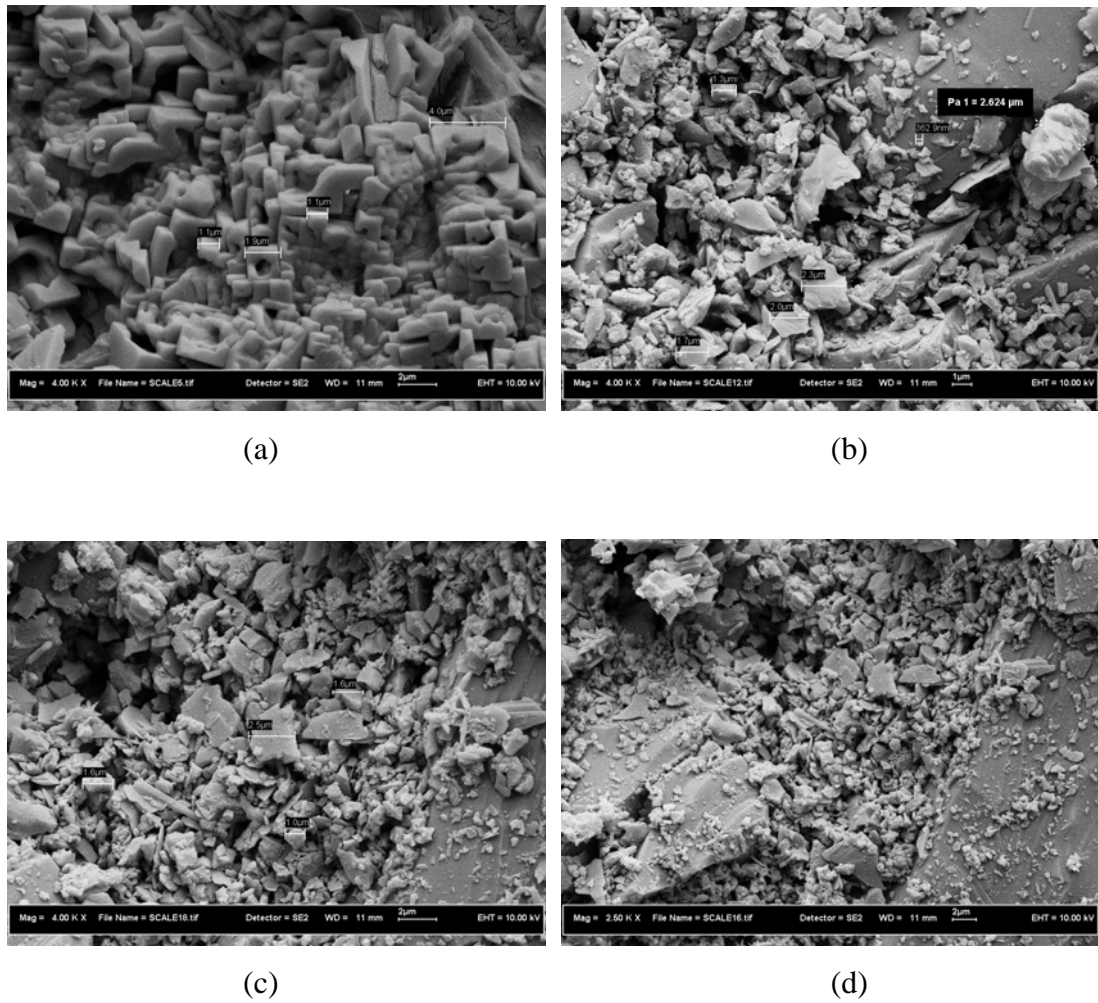


Figure 4.53 SEM image of CaSO₄ and SrSO₄scales in sandstone core at 200 psig and 80 °C

CHAPTER 5

CONCLUSIONS AND RECOMMENDATIONS

5.1 Conclusions

The work carried out in this study focused on the effect of temperature, concentration of brine, and differential pressure on permeability reduction by deposition of scale formation in a porous medium and the solubility of scales formed and how their solubilities were affected by changes in salinity and temperature.

Coreflood tests with injected and formation waters at various sets of conditions such as temperature, differential pressure and concentration gave the following conclusions.

- (1) The experimental results confirm the general trend in solubility dependencies for common oil field scales, determined at various temperatures. A temperature rise from 40 to 90 °C causes an increase in BaSO₄ solubility and a decrease of CaCO₃, CaSO₄, and SrSO₄ solubilities.
- (2) Laboratory coreflooding has demonstrated that *in-situ* precipitation of calcium, strontium and barium sulfates occurs when synthetic seawater containing sulfate is mixed *in-situ* with formation water that contains a significant amount of dissolved calcium, strontium, and barium ions.

- (3) This scale is expected to form when pressure maintenance by seawater injection into the aquifer is started. More severe scaling by this material is to be expected when seawater breakthrough into production wells.
- (4) Permeability decline caused by CaSO_4 , SrSO_4 , and BaSO_4 scale formation in the porous media ranged from 4% to 23% of the initial permeability, depending on brine composition, initial permeability, temperature, differential pressure, and brine injection period.
- (5) The worst permeability loss occurred in the porous media from 15% to 23% of the initial permeability at temperature (80 °C) and differential pressure (200 psig) for CaSO_4 and SrSO_4 experiments and from 9% to 19% of the initial permeability at temperature (50 °C) and differential pressure (200 psig) for BaSO_4 experiments.
- (6) CaSO_4 , SrSO_4 , and BaSO_4 precipitates did not plug the sandstone cores to the same extent. The experiments with CaSO_4 and SrSO_4 precipitates produced a 4% to 23% reduction in initial permeability. The experiments with BaSO_4 precipitate produced a 5% to 19% reduction in initial permeability.
- (7) The pattern of permeability decline in a porous medium due to scaling injection was characterized by a concave curve with a steep initial decline which gradually slowed down to a lower. The initial steepness of these curves generally decreased with increasing distance from the point of mixing of the incompatible brines. The concave shape of the permeability-time curves was common to the majority of the porous medium flow tests.
- (8) Several factors influencing scale formation had been examined. Increasing temperature, concentration of brine (i.e. supersaturation), and differential pressure had a detrimental effect on the permeability reduction.
- (9) At higher temperatures, CaSO_4 and SrSO_4 scale is increased because the solubilities of CaSO_4 and SrSO_4 decrease with temperature. This must have increased the rate of precipitation and consequently the permeability decline.

- (10) The permeability decline due to high concentration of calcium, strontium, and barium ions is greater than for normal concentration of calcium, strontium and barium ions, for given experimental conditions.
- (11) The formation of CaSO_4 , SrSO_4 , and BaSO_4 during flow of injection and formation waters in porous media have been observed by Scanning Electron Microscopy (SEM) micrographs show CaSO_4 , SrSO_4 , and BaSO_4 crystals formation in porous space.

5.2 Recommendations

Based on the results and conclusions obtained from this study, the following suggestions for future work in the same area are recommended:

- (1) Instead of synthetic brines, real oil field brines can be employed in the study by mixing field disposal water and seawater.
- (2) Scale build-up can be monitored by placing a multipressure tapped core holder in a temperature oven and measuring the pressure drop along the core during flooding.
- (3) The concentrations of calcium, barium, and strontium in effluent sample during coreflood experiments can be determined and much improved using an in-line ion analyzer or some other analytical devices.
- (4) The effect of residual oil saturation on the precipitation reaction can be investigated.

REFERENCES

- Ahmed, J. S. (2004). *Laboratory Study on Precipitation of Calcium Sulphate in Berea Sand Stone Cores*. King Fahd University of Petroleum & Minerals: M.E. Thesis.
- Allaga, A. D., Wu, G., Sharama, M. M. and Lake, W. L. (1992). Barium and Calcium Sulfate Precipitation and Migration inside Sandpacks. *SPE Formation Evaluation*. SPE19765:79 – 86.
- Andersen, I. K., Halvorsen, E., Saelensminde, T. and Ostbye, O. N. (2000). Water Management in a Closed Loop - Problems and Solutions at Brage Field. *The SPE European Petroleum Conference*. October 24-25. Paris, France: SPE 65162, 1 – 12.
- Asghari, K. and Kharrat, R. (1995). Alteration of Permeability by Fine Particle Movement-A Water Injectivity Problem. *The SPE International Symposium on Oilfield Chemistry*. February 14 – 17. San Antonio, Texas: SPE 29006, 655- 665.
- Bagci, S., Kok, M.V. and Turksoy, U. (2000). Determination of Formation Damage in Limestone Reservoirs and its Effect on Production. *Journal of Petroleum Science and Engineering*. 28: 1–12
- Bayona, G.H. (1993). A Review of Well Injectivity Performance in Saudi Arabia's Ghawar Field Seawater Injection Program. *The SPE Middle East Oil Technical Conference and Exhibition*. April 3-6. Bahrain: SPE 25531, 201 – 214.
- Bedrikovetsky, G. P. Moraes, P. G., Monteriro, R., Lopes, P. R., Rosario, F. F. and Bezerra, C. M. (2005). Characterization of Sulphate Scaling Formation

- Damage from Laboratory Measurements (To Predict Well-Productivity Decline). *The SPE fifth International Symposium on Oilfield Chemistry*. February 2 – 4. Texas, USA: SPE 93121, 1 – 14.
- Bedrikovetsky, G. P., Mackay, E., Monteriro, P. R., Gladstone, M. P. and Rosario, F. F. (2006). Laboratory and Field Prediction of Sulfate Scaling Damage. *The 2006 SPE International Oilfield Scale Symposium*. May 30 –1 June. Aberdeen, UK: SPE 100611, 1 – 18.
- Bertero, L., Chierici, L. G., Gottardi, G., Mesini, E. and Mormino, G. (1988). Chemical Equilibrium Models: Their Use in Simulating the Injection of Incompatible Waters. *SPE Reservoir Engineering*. February 1988, 288 – 294.
- Bezemer, C. and Bauer, A. K. (1969). Prevention of Carbonate Scale Deposition: A Well-Packing Technique with Controlled Volubility Phosphates. *Journal of Petroleum Technology*. April 1969, 505 – 514.
- Bezerra, M. C. M., Khali, N. C. and Rosario, F. F. (1990). Barium and Strontium Sulfate Scale Formation due to Incompatible Water in the Namorado Field, Campos Basin, Brazil. *The SPE latten American production engineering conference*. October 14 – 18. Rio Janetro: SPE 21109, 1 – 5.
- Brown, F. D. A., Merrett, J. S. and Putnam, S. J. (1991). Coil-Tubing milling/ Underreaming of Barium Sulphate Scale and Scale Control in the Forties Field. *The Offshore Europe Conference*. September 3 – 6. Aberdeen: SPE 23106, 1 – 17.
- Carlberg, L.B. and Matthews, R. R. (1973). Solubility of Calcium Sulfate in Brine. *The Oilfield Chemistry Symposium of the Society of Petroleum Engineers of AIME*. May 24-25. Denver, Colo: SPE 4353, 1-10.
- Chen, T., Neville, A. and Yuan, M. (2004). Effect of PPCA and DETPMP Inhibitor Blends on CaCO₃ Scale Formation. *The 6th International Symposium on Oilfield Scale*. May 26 – 27. Aberdeen, UK: SPE 87442, 1 –7.

- Clemmit, F. A., Ballance, C. D. and Hunton, G. A. (1985). The Dissolution of Scales in Oilfield Systems. *The Offshore Europe 85 Conference in conjunction with the Society of Petroleum Engineers of AIME*. September 10 – 13. Aberdeen: SPE 14010, 1 –32.
- Collins, R. I. and Jordan, M. M. (2001). Occurrence, Prediction and Prevention of Zinc Sulfide Scale within Gulf Coast and North Sea High Temperature/High Salinity Production Wells. *The SPE Third International Symposium on Oilfield Scale*. January 30 – 31. Aberdeen, UK: SPE 68317, 1 – 17.
- Collins, R. I. and Jordan, M. M. (2003). Occurrence, Prediction and Prevention of Zinc Sulfide Scale within Gulf Coast and North Sea High-Temperature and High-Salinity fields. *SPE Production and Facilities*, August 2003. 200 – 209.
- Collins, R. I. (2005). Predicting the Location of Barium Sulfate Scale Formation in Production Systems. *The SPE International Symposium on Oilfield Scale*. May 11 – 12. Aberdeen, UK: SPE 94366, 1 – 6.
- Collins, R. I., Duncum, D.S., Jordan, M. M. and Feasey, D. N. (2006). The Development of a Revolutionary Scale-Control Product for the Control of Near-Well Bore Sulfate Scale within Production Wells by the Treatment of Injection Seawater. *The 2006 SPE Oilfield Scale Symposium*. 31 May- 1 June. Aberdeen, UK: SPE 100357, 1 – 20.
- Connell, D. (1983). *Prediction and Treatment of Scale in North Sea Fields*. Heriot-watt university : M.E. Thesis
- Crowe, W. C. (1986). Precipitation of Hydrated Silica from Spent Hydrofluoric Acid. *Journal of Petroleum Technology*. November 1986, 1234 – 1240.
- El-Hattab, I. M. (1982). GUPCO'S Experience in Treating Gulf of Suez Seawater for Waterflooding the El Morgan Oil Field. *Journal of Petroleum Technology*. July 1982, 1449 – 1460.

- Essel, J. A. and Carlberg, L. B. (1982). Strontium Sulfate Scale Control by Inhibitor Squeeze Treatment in the Fatech Field. *Journal of Petroleum Technology*. June 1982, 1302 – 1306.
- Guimaraes, Z., Franca, B. A., Duque, H. L, Souza, D. B. R., Porto, M., Neves, D. and Peixoto, C. (2007). Case Histories of Barium Sulfate Scale Removal in Offshore Wells, Brazil, Using a New Engineered Combination of Coiled-Tubing Tools. *The 2007 SPE/ICOTA Coiled Tubing and Well Intervention Conference and Exhibition*. March 20 – 21. Texas, USA: SPE 107063, 1 – 8.
- Jacques, F. D. and Bourland, I. B. (1983). A Study Solubility of Strontium Sulfate. *Society of Petroleum Engineers Journal*. April 1983, 292 – 300.
- Jordan, M. M. and Mackay, J. E. (2005). Integrated Field Development for Effective Scale Control Throughout the Water Cycle in Deep Water Subsea Fields. *The SPE Europec/EAGE Annual Conference*. June 13 – 16. Madrid, Spain: SPE 94052, 1 –9.
- Jordan, M. M., Collins, R. I. and Mackay, J. E. (2006a). Low-Sulfate Seawater Injection for Barium Sulfate Scale Control: A life-of-Field Solution to a Complex Challenge. *The 2006 SPE International Symposium and Exhibition on Formation Damage Control*. February 15 – 17. Lafayette, LA: SPE 98096, 1 – 23.
- Jordan, M. M., Johnston, J. C. and Robb, M. (2006b). Evaluation Methods for Suspended Solids and Produced Water as an Acid in Determining Effectiveness of Scale Control Both Downhole and Topside. *SPE Production and operations*. February 2006, 7 – 18.
- Jordan, M. M., Graff, J. C. and Cooper, N. K. (2000). Development and Deployment of a Scale Squeeze Enhancer and Oil-Soluble Scale Inhibitor To Avoid Deferred Oil Production Losses During Squeezing Low-Water Cut Wells, North Slope, Alaska. *The 2000 SPE International Symposium on Formation Damage Control*. February 23 – 24. Lafayette, Louisiana: SPE 58725, 1 – 18.

- Khatib, I. Z. (1994). Prediction of Formation Damage Due to Suspended Solids: Modeling Approach of Filter Cake Buildup in Injectors. *The SPE 89th Annual Technical Conference and Exhibition*. September 25 – 28. New Orleans, USA: SPE 28488, 263 – 273.
- Khelil, C., Harouaka, A. and Delhoume, A. (1979). Water Injection in Algeria-Problems and Solutions. *The Middle East Oil Technical Conference of the Society of Petroleum Engineers*. March 25-29. Manama, Bahrain: SPE 7762, 97 – 106.
- Krueger, F. R. (1986). An Overview of Formation Damage and Well Productivity in Oilfield Operations. *Journal of Petroleum Technology*. February 1986, 131 – 152.
- Leone, A., J. and Scott, M., E. (1988). Characterization and Control of Formation Damage during Water Flooding Of a High-Clay-Content Reservoir. *SPE Reservoir Engineering* . November 1988, 1279 – 1286.
- Lindlof, C. J. and Stoffer, G. K. (1983). A case study of sea water injection incompatibility. *Journal of Petroleum Technology*, July 1983 1256 – 1262.
- Mackay, J. E. (2003). Modeling In-Situ Scale Deposition: The Impact of Reservoir and Well Geometries and Kinetic Reaction Rates. *SPE Production and Facilities*. February 2003, 45 – 56.
- Mackay, J. E. (2005). Scale Inhibitor Application in Injection Wells to Protect Against Damage to Production Wells: when does it work?. *The SPE European Formation Damage Conference*. May 25 – 27. Scheveningen, Netherlands: SPE 95022, 1 –9.
- Mackay, J. E. and Jordan, M. M. (2005). Impact of Brine Flow and Mixing in the Reservoir on Scale Control Risk Assessment and Subsurface Treatment Options: Case Histories. *Journal of Energy Resources Technology*. 127: 201 – 213.

- Mackay, J. E., Collins, R. I. and Jordan, M. M. (2003). PWRI: scale Formation Risk Assessment and Management. *The SPE 5th International Symposium on Oilfield Scale*. January 29 – 30. Aberdeen, UK: SPE 80385, 1 – 18.
- Mazzollni, I. E., Betero, L. and Truefltt, S. C. (1992). Scale Prediction and Laboratory Evaluation of BaSO₄ Scale inhibitors for Seawater Flood in a High-Barium Environment. *SPE Production Engineering*. SPE 20894, 186 – 192.
- McElhiney, E. J., Sydansk, D. R., Benzel, M. W. and Davidson, B. K. (2001). Determination of in-situ precipitation of barium sulfate during coreflooding. *The SPE third International Symposium on Oilfield scale*. January 30–31. Aberdeen, UK: SPE 68309, 1 – 11.
- Mitchell, W. R., Grist, M. D. and Boyle, J. M. (1980). Chemical Treatments Associated With North Sea Projects. *Journal of Petroleum Technology*: SPE 7880, 904 – 912.
- Moghadasi, J., Jamialahmadi, M., Muller-Steinhagen, H., Sharif, A., Ghalambor, A., Izadpanah, R. M. and Motaie, E. (2003a). Scale Formation in Iranian Oil Reservoir and Production Equipment during Water Injection. *The 5th International Oilfield Scale Symposium and Exhibition*. January 29 – 30. Aberdeen, UK: SPE 80406, 1 – 14.
- Moghadasi, J., Jamialahmadi, M., Muller-Steinhagen, H. and Sharif, A. (2003b). Scale Formation in Oil Reservoir and Production Equipment during Water Injection (Kinetics of CaCO₄ and CaCO₃ Crystal Growth and Effect on Formation Damage). *The SPE European Formation Damage Conference*. May 13 – 14. Hague, Netherlands: SPE 82233, 1 –12.
- Moghadasi, J., Jamialahmadi, M., Muller-Steinhagen, H., Sharif, A., Izadpanah, R. M., Motaie, E. and Barati, R. (2002). Formation Damage in Iranian Oil Fields. *The SPE International Symposium and Exhibition on Formation Damage control*. February 20 – 21. Lafayette, Louisiana: SPE 73781, 1 – 9.

- Moghadasi, J., Muller-Steinhagen, H., Jamialahmadi, M. and Sharif, A (2004a). Model study on the kinetics of oil field formation damage due to salt precipitation from injection. *Journal of Petroleum Science and Engineering*. 43: 201– 217.
- Moghadasi, J., Jamialahmadi, M., Muller-Steinhagen, H., Sharif, A. (2004b). Formation Damage Due to Scale Formation in Porous Media Resulting From Water Injection. *The SPE International Symposium and Exhibition on Formation Damage control*. February 18-20. Lafayette, Louisiana: SPE 86524, 1 – 11.
- Nancollas, H. G. and Liu, T. S. (1975). Crystal Growth and Dissolution of Barium Sulfate. *Society of Petroleum Engineers Journal*. December 1975, 509 – 516.
- Nasr-El-Din, A. H. (2003). New Mechanisms of Formation Damage: Lab Studies and Case Histories. *The SPE European Formation Damage Conference*. May 13 – 14. Hague, Netherlands: SPE 82253, 1 –12.
- Nasr-El-Din, A. H. and Al-Humaidan, Y. A. (2001). Iron Sulfide Scale: Formation, Removal and Prevention. *The 2001 SPE International Symposium on Oilfield Scale*. January 30 – 31. Aberdeen, UK: SPE 68315, 1 – 13.
- Nasr-El-Din, A. H. Raju, U. K., Hilab, V. V. and Esmail J. O. (2004). Injection of Incompatible Water as a Means of Water Shut-Off. *The 6th SPE International Symposium on Oilfield Scale*. May 26- 27. Aberdeen, UK: SPE 87455, 1 – 13.
- Nassivera, M. and Essel, A. (1979). Fateh field sea water injection – Water Treatment, Corrosion, And scale control. *The Middle East Oil Technical Conference of the Society of petroleum Engineers*. March 25 – 29. Manama, Bahrain: SPE 7765, 133 – 138.
- Oddo, E. J. and Tomson, B. M. (1994). Why Scale Forms and How to Predict It. *SPE Production and Facilities*. February 1994, 47 – 54.

- Oddo, E. J., Smith, P. J. and Tomason, B. M. (1991). Analysis of and Solutions to the CaCO_3 and CaSO_4 Scaling Problems Encountered in Wells Offshore Indonesia. *The 66th Annual Technical Conference and Exhibition of the Society of Petroleum Engineering*. October 6 – 9. Dallas, TX: SPE 22782, 1 – 10.
- Paulo, J., Mackay, J. E., Menzies, N. and Poynton, N. (2001). Implications of Brine Mixing in the Reservoir for Scale Management in the Alba Field. *The 2001 SPE International Symposium on Oilfield scale*. January 30 – 31. Aberdeen, UK: SPE 68310, 1 – 13.
- Raju, U. K., Nasr-El-Din, A. H. and Al-Shafai, A. T. (2003). A Feasibility Study of Mixing Disposal Water with Aquifer Water for Downhole Injection. *The SPE 13th Middle East Oil Show and Conference*. April 5 – 8. Bahrain: SPE 81449, 1 – 9.
- Read, A. P. and Ringen, K. J. (1982). The Use of Laboratory Tests to Evaluate Scaling Problems during Water Injection. *The SPE Sixth International Symposium on Oilfield and Geothermal Chemistry*. January 25 – 27. Dallas, Texas: SPE 10593, 7 – 17.
- Romero, C., Bazin, B., Zaitoun, A. and Leal-Calderon, F. (2007). Behavior of a Scale Inhibitor Water-in-Oil Emulsion in Porous Media. *SPE Production and Operations*. May 2007, 191 – 201.
- Rousseau, G., Hurtevent, C., Azaroual, M., Kervevan, C. and Durance, V. M. (2003). Application of a Thermo-Kinetic Model to the Prediction of Scale in Angola Block 3 Field. *The 5th International Oilfield Scale Symposium*. January 29 – 30. Aberdeen, UK: SPE 80387, 1 – 8.
- Salman, M. Al-Hashem, A. and Carew, J. (1999). Prediction of Scaling for the Seawater Injection System at the Northern Kuwaiti Oil Fields. *The 1999 SPE Middle East Oil Show*. February 20 – 23. Bahrain: SPE 53268, 1 – 5.

- Shen, J. and Corsby, C.C. (1983). Insight into Strontium and Calcium Sulfate Scaling Mechanisms in a Wet Producer. *Journal of Petroleum Technology*. SPE 10597, 1249 – 1255.
- Shuler, J. P., Freitas, A. E. and Bowker, A. K. (1991). Selection and Application of BaSO₄ Scale Inhibitors for a CO₂ Flood, Rangely Weber Sand Unit, Colorado. *Society of Petroleum Engineers*. SPE 18973, 1 – 8.
- Smith, P.S., Clement Jr. C.C., and Mendoza Rojas, A. (2000). Combined Scale Removal and Scale Inhibition Treatments. *The 2000 second International Symposium on Oilfield Scale*. January 26 – 27. Aberdeen, UK: SPE 60222, 1 –6.
- Stalker, R., Collins, R. I. and Graham, M. G. (2003). The Impact of Chemical Incompabilities in Commingled Fluids on the Efficiency of a Produced Water Reinjection System: A North Sea Example. *The SPE International Symposium on Oilfield chemistry*. February 5 –7. Houston, Texas: SPE 80257, 1 –13.
- Strachan, J. C., Heath, M.S., White, K., Williams, G., Strong, A. and Bell, K. (2004). Experience With Pre-Emptive Squeeze Treatments on BM Magnus with Aqueous Based Scale Inhibitors. *The sixth International Symposium on Oilfield Scale*. May 26 – 27. Aberdeen, UK: SPE 87462, 1 – 13.
- Sverjensky, A. D. (1984). Oilfield Brines As Ore-Forming Solutions. *Economic Geology and the Bulletin of Society of Economic Geologists*. 79(1): 23 – 37.
- Tahmasebi, A. H., Kharrat, R. and Masoudi, R. (2007). Prediction of Permeability Reduction Rate Due To Calcium Sulfate Scale Formation in Porous Media. *The 15th SPE Middle East Oil and Gas Show and Conference*. March 11 – 14. Bahrain: SPE 105105, 1 –6.
- Thomas, G. L., Albertsen, M., Perdeger, A., Knoke, K. H.H., Horstmann, W. B. and Schenk, D. (1995). Chemical Characterization of Fluids and Their Modeling With Respect to Their Damage Potential in Injection on Production Processes

- Using an Expert System. *The SPE International Symposium on Oilfield Chemistry*. February 14 – 17. San Antonio, U.S.A.: SPE 28981, 1 – 10.
- Todd, C. A. and Yuan, D. M. (1990). Barium and Strontium Sulfate Solid-Solution Formation in Relation to North Sea Scaling Problems. *SPE Production Engineering*. August 1990, 279 – 285.
- Todd, C. A. and Yuan, D. M. (1992). Barium and Strontium Sulfate Solid-Solution Scale Formation at Elevated Temperatures. *SPE Production Engineering*. SPE 19762: 85 – 92.
- Vetter, J. O., Farone, A. W., Veith, E. and Lankford, S. (1987). Calcium Carbonate Scale Considerations: A Practical Approach. *The SPE production Technology Symposium*. November 16 – 17. Lubbock, Texas: SPE 17009, 1 – 14.
- Vetter, J. O., Kandarpa, V. and Harouaka, A. (1982). Prediction of Scale Problems Due To Injection of Incompatible Waters. *Journal of Petroleum Technology*. February 1982, 273 – 284.
- Voloshin, I. A., Ragulin, V. V., Tyabayeva, E. N., Diakonov, I. I. and Mackay, J. E. (2003). Scaling Problems in Western Siberia. *The SPE fifth International Symposium on Oilfield scale*. January 29 – 30. Aberdeen, UK: SPE 80407, 1 – 8.
- Wat, S. M. R., Sorbie, S. K., Todd, C. A., Chen, P. and Jiang, P. (1992). Kinetics of BaSO₄ Crystal Growth and Effect in Formation Damage. *The SPE International Symposium on Formation Damage control*. February 25 – 27. Lafayette, Louisiana: SPE 23814, 429 – 437.
- Yeboah, D. Y., Somuah, K. S. and Saeed, R. M. (1993). Anew and Reliable Model for Predicting Oilfield Scale Formation. *The SPE International Symposium on Oilfield Chemistry*. March 2 – 5. New Orleans, U.S.A.: SPE 25166, 1 – 10.
- Yuan, D. M. and Todd, C. A. (1991). Prediction of Sulfate Scaling Tendency in Oilfield Operations. *SPE production Engineering*. SPE 18484: 63 – 72.

Zhang, Y. and Farquhar, R. (2001). Laboratory Determination of Calcium Carbonate Scaling Rates for Oilfield Wellbore Environments. *The 2001 SPE International Symposium on Oilfield Scale*. January 30 – 31. Aberdeen, UK: SPE 68329, 1 –7.

APPENDICES

APPENDIX A

SUMMARY OF PREVIOUS EXPERIMENTAL WORKS

No.	Study	Rock	Scale	concentration		Temp.	Press.	Flow rate
1	Mitchell et al., (1980)	Sand pack	barium sulfate and calcium carbonate	Sea water (ppm) See table A.2	Formation water (ppm) See table A.1	20 - 90 °C	4 - 40 psig	1:10
2	Read and Ringen, (1982)	Glass beads and in synthetic alumina cores	barium, strontium, calcium, sulfates and calcium carbonate	Sea water (ppm) See table A.2	Formation water (ppm) See table A.1	20 - 70 °C	1 - 22 Psig	2 ml / min
3	Lindlof and Stoffer, (1983)	Arab - D core (Saudi Arabia)	Strontium and calcium sulfates	Sea water (ppm) See table A.2	Formation water (ppm) See table A.1	-	-	-
4	Bezerra et al.,(1990)	Sand stone Out crop (Brazil)	barium, and strontium sulfates	Sea water (ppm) See table A.2	Formation water (ppm) See table A.1	80 °C	-	0.5 - 1.0 ml/min
5	Allaga et al., (1992)	Sand pack	calcium and barium sulfates	ion	(ppm)	-	-	0.2 ml / min
				Ca	280 - 20000			
				Ba	1332 - 2746			
6	Todd and Yuan, (1992)	Sand stone Clashach	barium, and strontium sulfates	Sea water (ppm) See table A.2	Formation water (ppm) See table A.1	20- 70 °C	1 - 2 Psig	7.5 ml / min

(Continued)

No.	Study	Rock	Scale	concentration		Temp.	Press.	Flow rate
7	Wat et al., (1992)	Sand pack	Barium sulfate	Sea water (ppm) See table A.2	Formation water (ppm) See table A.1	-	-	0.5 ml/min
8	McElhiney et al., (2001)	Berea Sand stone	barium, strontium and calcium sulfates	Sea water (ppm) See table A.2	Formation water (ppm) See table A.1	21 °C	14.7 Psig	-
9	Moghadasi <i>et al.</i> (2002)	Sand pack and Glass beads	barium, strontium and calcium sulfates	Sea water (ppm) See table A.2	Formation water (ppm) See table A.1	25 – 80 °C	1 – 145 psig	1- 200 ml/min
10	Moghadasi <i>et al.</i> (2003b)	Sand pack and Glass beads	calcium and sulfate/ carbonate ions	ion	(ppm)	50 – 80 °C	17.7 psig	25 – 100 ml/min
				Ca	1770 - 13000			
				SO ₄	2600 – 7800			
				CO ₃	800 – 1060			
11	AHMED, J. S. (2004)	Berea Sand stone	calcium sulfate	ion	(ppm)	45 – 95 °C	100 -3000 psig	0.12 – 15 ml/min
				Ca	2180 - 4175			
				SO ₄	1200 - 2400			
12	Strachan et al. (2004)	BP Magnus core material	Barium and strontium, sulfate	Sea water (ppm) See table A.2	Formation water (ppm) See table A.1	116 °C	1500 psig	1 ml/min
13	Moghadasi <i>et al.</i> (2004a)	Sand pack and Glass beads	calcium and sulfate/ carbonate ions	ion	(ppm)	50 – 80 °C	17.7 psig	25 – 100 ml/min
				Ca	1770 - 13000			
				SO ₄	2600 – 7800			
				CO ₃	800 – 1600			
14	Bedrikovetsky et al., (2005)	Out crop RB (Brazil)	Barium sulfate	Sea water (ppm) See table A.2	Formation water (ppm) See table A.1	-	-	-
15	Current Study 2006	Sandstone (Malaysia)	Calcium, strontium and barium sulfates	Sea water (ppm) See table 3.2	Formation water (ppm) See table 3.2	50 – 80 °C	100 - 200 psig	-

Table A.1: Ions of Formation Water

Study	Mitchell et al., (1980)	Read and Ringen, (1982)	Lindlof and Stoffer, (1983)		Bezerra et al. (1990)	Todd and Yuan, (1992)		Wat et al., (1992)	McElhiney et al., (2001)		Moghadasi et al. (2002)	Strachan et al. (2004)	Bedrikovetsky et al., (2005)
			Low-salinity Arab-D	High-salinity Arab-D		M (North sea)	ST (North sea)		West African FW				
Place	Forties (North sea)	(North sea)	Low-salinity Arab-D	High-salinity Arab-D	Namorado field (Brazil)	M (North sea)	ST (North sea)	(North sea)	West African FW		Mishrif in Iranian	Magnus FW (North sea)	Field N (Brazil)
Ca	3110	1100	13574	29760	2760	2809	779	2800	4000	4000	7920	250	-
Ba	250	210	8	10	229	252	2180	250	240	0	18	220	229
Sr	660	230	557	1035	415	574	369	575	230	230	610	45	-
SO ₄	0	<1	404	108	14	11	5	-	16	16	340	0	-
HCO ₃	360	250	369	351	837	496	2140	-	-	-	244	1100	-
Na	30200	15200	29680	51187	33500	29370	41900	29400	37719	37719	43700	11065	38249
K	430	380	-	-	554	372	1700	370	46	46	-	210	-
Mg	480	110	1575	4264	374	504	102	500	873	873	2010	40	-
Cl	53000	28000	73861	143285	59100	52360	68000	52647	68083	67959	86900	17350	59098

Table A.2: Ions of Sea Water

Study	Mitchell et al., (1980)	Read and Ringen, (1982)	Lindlof and Stoffer, (1983)	Bezerra et al. (1990)	Todd and Yuan, (1992)	Wat et al., (1992)	McElhiney et al., (2001)		Moghadasi et al. (2002)	Strachan et al. (2004)	Bedrikovetsky et al., (2005)
Place	North sea	North sea	Arabian Gulf	Campos Basin (Brazil)	North sea	North sea	West African FW		Persian Gulf water	North sea	(Brazil)
Ca	403	450	652	504	428	428	435	108	267	400	-
Ba	0	0	0	1	0	-	0	0	0.09	0	-
Sr	0	9	11	9	8	-	0	0	3.4	8	-
SO ₄	2480	2300	4450	2834	2960	2950	2860	36	3350	2960	2834
HCO ₃	135	170	119	150	124	-	-	-	166	155	-
Na	11000	12100	18043	11500	10890	10890	11424	10665	11750	11470	15169
K	340	-	-	226	460	460	400	190	-	395	-
Mg	1320	1130	2159	1390	1368	1368	1370	475	2996	1340	-
Cl	19800	20950	31808	21300	19700	19766	20635	18170	23000	20510	21299

APPENDIX B

EXPERIMENTAL DATA AND RESULTS OF BARIUM SULFATE

Table B.1: Density and viscosity of formation water at room temperature

	Normal salinity formation water	High salinity formation water	Normal barium formation water	High barium formation water	Sea water
Density (gm/ml)	1.11	1.15	1.07	1.10	1.01
Viscosity (cp)	1.70	1.83	1.53	1.61	-

Table B.2: Viscosity of sea water

Temperature (°C)	Viscosity of sea water (cp)
50	1.37
70	1.06
80	0.95

Table B.3: Experimental data of core flood at high barium: Run # 1

Injected Time (min)	No. of PV's injected	Q (cc/min)	T (°C)	ΔP (psig)	D (in)	L (in)	K_d (md)	K_i (md)	k_d/k_i
10	2.24	10.01	50	100	1	3	12.70	12.76	0.9955
20	4.39	9.60	50	100	1	3	12.11	12.76	0.9490
30	6.51	9.46	50	100	1	3	11.93	12.76	0.9350
40	8.60	9.34	50	100	1	3	11.78	12.76	0.9233
50	10.68	9.30	50	100	1	3	11.73	12.76	0.9192
60	12.74	9.20	50	100	1	3	11.61	12.76	0.9101
70	14.78	9.12	50	100	1	3	11.51	12.76	0.9018
80	16.02	9.00	50	100	1	3	11.34	12.76	0.8890
90	18.77	8.81	50	100	1	3	11.12	12.76	0.8714
100	20.71	8.67	50	100	1	3	10.94	12.76	0.8575
110	22.64	8.59	50	100	1	3	10.84	12.76	0.8493
120	24.56	8.55	50	100	1	3	10.79	12.76	0.8454

Table B.4: Experimental data of core flood at high barium: Run # 2

Injected Time (min)	No. of PV's injected	Q (cc/min)	T (°C)	ΔP (psig)	D (in)	L (in)	K_d (md)	K_i (md)	k_d/k_i
10	3.06	15.91	50	150	1	3	13.38	13.46	0.9943
20	5.97	15.12	50	150	1	3	12.72	13.46	0.9450
30	8.83	14.87	50	150	1	3	12.51	13.46	0.9295
40	11.68	14.81	50	150	1	3	12.46	13.46	0.9260
50	14.5	14.66	50	150	1	3	12.33	13.46	0.9160
60	17.30	14.54	50	150	1	3	12.23	13.46	0.9090
70	20.04	14.27	50	150	1	3	12.00	13.46	0.8910
80	22.73	14.00	50	150	1	3	11.78	13.46	0.8750
90	25.38	13.77	50	150	1	3	11.58	13.46	0.8600
100	28.00	13.61	50	150	1	3	11.45	13.46	0.8510
110	30.58	13.39	50	150	1	3	11.26	13.46	0.8362
120	33.14	13.30	50	150	1	3	11.19	13.46	0.8310

Table B.5: Experimental data of core flood at high barium: Run # 3

Injected Time (min)	No. of PV's injected	Q (cc/min)	T (°C)	ΔP (psig)	D (in)	L (in)	K_d (md)	K_i (md)	k_d/k_i
10	4.85	21.29	50	200	1	3	13.43	13.52	0.9934
20	9.43	20.13	50	200	1	3	12.70	13.52	0.9390
30	13.95	19.83	50	200	1	3	12.51	13.52	0.9250
40	18.44	19.72	50	200	1	3	12.44	13.52	0.9200
50	22.90	19.60	50	200	1	3	12.36	13.52	0.9142
60	27.30	19.31	50	200	1	3	12.18	13.52	0.9010
70	31.64	19.05	50	200	1	3	12.02	13.52	0.8892
80	35.87	18.58	50	200	1	3	11.72	13.52	0.8671
90	40.06	18.40	50	200	1	3	11.61	13.52	0.8584
100	44.19	18.14	50	200	1	3	11.44	13.52	0.8461
110	48.22	17.69	50	200	1	3	11.16	13.52	0.8252
120	52.19	17.41	50	200	1	3	10.98	13.52	0.8120

Table B.6: Experimental data of core flood at high barium: Run # 4

Injected Time (min)	No. of PV's injected	Q (cc/min)	T (°C)	ΔP (psig)	D (in)	L (in)	K_d (md)	K_i (md)	k_d/k_i
10	2.23	12.67	70	100	1	3	12.37	12.40	0.9975
20	4.38	12.19	70	100	1	3	11.90	12.40	0.9595
30	6.50	12.02	70	100	1	3	11.73	12.40	0.9462
40	8.60	11.91	70	100	1	3	11.62	12.40	0.9374
50	10.67	11.75	70	100	1	3	11.47	12.40	0.9253
60	12.74	11.72	70	100	1	3	11.44	12.40	0.9223
70	14.79	11.62	70	100	1	3	11.34	12.40	0.9146
80	16.82	11.53	70	100	1	3	11.25	12.40	0.9072
90	18.82	11.32	70	100	1	3	11.05	12.40	0.8912
100	20.80	11.21	70	100	1	3	10.94	12.40	0.8823
110	22.76	11.10	70	100	1	3	10.83	12.40	0.8731
120	24.71	11.04	70	100	1	3	10.78	12.40	0.8694

Table B.7: Experimental data of core flood at high barium: Run # 5

Injected Time (min)	No. of PV's injected	Q (cc/min)	T (°C)	ΔP (psig)	D (in)	L (in)	K_d (md)	K_i (md)	k_d/k_i
10	3.67	20.42	70	150	1	3	13.29	13.34	0.9964
20	7.19	19.62	70	150	1	3	12.77	13.34	0.9572
30	10.66	19.34	70	150	1	3	12.52	13.34	0.9387
40	14.08	19.06	70	150	1	3	12.40	13.34	0.9301
50	17.47	18.89	70	150	1	3	12.29	13.34	0.9212
60	20.84	18.76	70	150	1	3	12.21	13.34	0.9154
70	24.19	18.64	70	150	1	3	12.13	13.34	0.9094
80	27.47	18.27	70	150	1	3	11.89	13.34	0.8913
90	30.72	18.10	70	150	1	3	11.78	13.34	0.8832
100	33.94	17.95	70	150	1	3	11.68	13.34	0.8756
110	37.12	17.70	70	150	1	3	11.52	13.34	0.8639
120	40.28	17.58	70	150	1	3	11.44	13.34	0.8572

Table B.8: Experimental data of core flood at high barium: Run # 6

Injected Time (min)	No. of PV's injected	Q (cc/min)	T (°C)	ΔP (psig)	D (in)	L (in)	K_d (md)	K_i (md)	k_d/k_i
10	5.34	25.06	70	200	1	3	12.23	12.30	0.9947
20	10.43	23.85	70	200	1	3	11.64	12.30	0.9463
30	15.43	23.44	70	200	1	3	11.44	12.30	0.9301
40	20.40	23.32	70	200	1	3	11.38	12.30	0.9253
50	25.34	23.17	70	200	1	3	11.31	12.30	0.9193
60	30.22	22.89	70	200	1	3	11.17	12.30	0.9082
70	35.03	22.58	70	200	1	3	11.02	12.30	0.8960
80	39.76	22.17	70	200	1	3	10.82	12.30	0.8794
90	44.41	21.80	70	200	1	3	10.64	12.30	0.8647
100	48.99	21.47	70	200	1	3	10.48	12.30	0.8523
110	53.53	21.31	70	200	1	3	10.40	12.30	0.8457
120	58.03	21.10	70	200	1	3	10.30	12.30	0.8374

Table B.9: Experimental data of core flood at high barium: Run # 7

Injected Time (min)	No. of PV's injected	Q (cc/min)	T (°C)	ΔP (psig)	D (in)	L (in)	K_d (md)	K_i (md)	k_d/k_i
10	2.68	14.66	80	100	1	3	12.83	12.85	0.9985
20	5.28	14.21	80	100	1	3	12.43	12.85	0.9675
30	7.84	14.01	80	100	1	3	12.26	12.85	0.9539
40	10.38	13.87	80	100	1	3	12.14	12.85	0.9450
50	12.88	13.69	80	100	1	3	11.98	12.85	0.9323
60	15.38	13.66	80	100	1	3	11.95	12.85	0.9298
70	17.87	13.60	80	100	1	3	11.90	12.85	0.9257
80	20.33	13.47	80	100	1	3	11.79	12.85	0.9175
90	22.76	13.28	80	100	1	3	11.62	12.85	0.9042
100	25.16	13.11	80	100	1	3	11.47	12.85	0.8925
110	27.53	12.99	80	100	1	3	11.37	12.85	0.8845
120	29.88	12.87	80	100	1	3	11.26	12.85	0.8763

Table B.10: Experimental data of core flood at high barium: Run # 8

Injected Time (min)	No. of PV's injected	Q (cc/min)	T (°C)	ΔP (psig)	D (in)	L (in)	K_d (md)	K_i (md)	k_d/k_i
10	4.25	21.70	80	150	1	3	12.66	12.70	0.9972
20	8.35	20.91	80	150	1	3	12.20	12.70	0.9603
30	12.39	20.61	80	150	1	3	12.02	12.70	0.9465
40	16.40	20.45	80	150	1	3	11.93	12.70	0.9394
50	20.36	20.21	80	150	1	3	11.79	12.70	0.9287
60	24.29	20.04	80	150	1	3	11.69	12.70	0.9205
70	28.21	19.97	80	150	1	3	11.65	12.70	0.9173
80	32.07	19.71	80	150	1	3	11.50	12.70	0.9052
90	35.89	19.49	80	150	1	3	11.37	12.70	0.8949
100	39.65	19.17	80	150	1	3	11.18	12.70	0.8802
110	43.39	19.08	80	150	1	3	11.13	12.70	0.8767
120	47.10	18.91	80	150	1	3	11.03	12.70	0.8683

Table B.11: Experimental data of core flood at high barium: Run # 9

Injected Time (min)	No. of PV's injected	Q (cc/min)	T (°C)	ΔP (psig)	D (in)	L (in)	K_d (md)	K_i (md)	k_d/k_i
10	5.68	28.14	80	200	1	3	12.31	12.36	0.9957
20	11.11	26.90	80	200	1	3	11.77	12.36	0.9521
30	16.46	26.49	80	200	1	3	11.59	12.36	0.9381
40	21.78	26.31	80	200	1	3	11.51	12.36	0.9312
50	27.05	26.10	80	200	1	3	11.42	12.36	0.9236
60	32.28	25.90	80	200	1	3	11.33	12.36	0.9170
70	37.46	25.62	80	200	1	3	11.21	12.36	0.9069
80	42.55	25.21	80	200	1	3	11.03	12.36	0.8921
90	47.57	24.87	80	200	1	3	10.88	12.36	0.8804
100	52.54	24.62	80	200	1	3	10.77	12.36	0.8713
110	57.43	24.20	80	200	1	3	10.59	12.36	0.8572
120	62.27	23.95	80	200	1	3	10.48	12.36	0.8483

Table B.12: Experimental data of core flood at normal barium: Run # 10

Injected Time (min)	No. of PV's injected	Q (cc/min)	T (°C)	ΔP (psig)	D (in)	L (in)	K_d (md)	K_i (md)	k_d/k_i
10	1.89	10.92	50	100	1	3	13.81	13.84	0.9978
20	3.76	10.85	50	100	1	3	13.69	13.84	0.9892
30	5.62	10.75	50	100	1	3	13.56	13.84	0.9801
40	7.47	10.71	50	100	1	3	13.51	13.84	0.9765
50	9.31	10.64	50	100	1	3	13.42	13.84	0.9694
60	11.13	10.53	50	100	1	3	13.29	13.84	0.9603
70	12.94	10.46	50	100	1	3	13.19	13.84	0.9532
80	14.73	10.39	50	100	1	3	13.11	13.84	0.9476
90	16.51	10.33	50	100	1	3	13.03	13.84	0.9412
100	18.29	10.30	50	100	1	3	12.99	13.84	0.9385
110	20.06	10.26	50	100	1	3	12.94	13.84	0.9353
120	21.82	10.21	50	100	1	3	12.88	13.84	0.9305

Table B.13: Experimental data of core flood at normal barium: Run # 11

Injected Time (min)	No. of PV's injected	Q (cc/min)	T (°C)	ΔP (psig)	D (in)	L (in)	K_d (md)	K_i (md)	k_d/k_i
10	2.95	16.11	50	150	1	3	13.55	13.60	0.9961
20	5.88	15.98	50	150	1	3	13.44	13.60	0.9879
30	8.78	15.83	50	150	1	3	13.31	13.60	0.9788
40	11.66	15.74	50	150	1	3	13.24	13.60	0.9736
50	14.53	15.65	50	150	1	3	13.16	13.60	0.9675
60	17.36	15.47	50	150	1	3	13.01	13.60	0.9569
70	20.17	15.36	50	150	1	3	12.92	13.60	0.9497
80	22.96	15.22	50	150	1	3	12.80	13.60	0.9413
90	25.73	15.15	50	150	1	3	12.74	13.60	0.9364
100	28.49	15.05	50	150	1	3	12.66	13.60	0.9309
110	31.24	14.99	50	150	1	3	12.59	13.60	0.9256
120	33.97	14.90	50	150	1	3	12.53	13.60	0.9211

Table B.14: Experimental data of core flood at normal barium: Run # 12

Injected Time (min)	No. of PV's injected	Q (cc/min)	T (°C)	ΔP (psig)	D (in)	L (in)	K_d (md)	K_i (md)	k_d/k_i
10	4.74	21.61	50	200	1	3	13.63	13.70	0.9949
20	9.44	21.43	50	200	1	3	13.52	13.70	0.9872
30	14.09	21.21	50	200	1	3	13.38	13.70	0.9769
40	18.71	21.07	50	200	1	3	13.29	13.70	0.9702
50	23.31	20.97	50	200	1	3	13.23	13.70	0.9657
60	27.83	20.61	50	200	1	3	13.00	13.70	0.9487
70	32.35	20.59	50	200	1	3	12.99	13.70	0.9482
80	36.80	20.31	50	200	1	3	12.81	13.70	0.9354
90	41.25	20.31	50	200	1	3	12.81	13.70	0.9350
100	45.66	20.12	50	200	1	3	12.69	13.70	0.9263
110	50.03	19.92	50	200	1	3	12.57	13.70	0.9176
120	54.37	19.77	50	200	1	3	12.47	13.70	0.9099

Table B.15: Experimental data of core flood at normal barium: Run # 13

Injected Time (min)	No. of PV's injected	Q (cc/min)	T (°C)	ΔP (psig)	D (in)	L (in)	K_d (md)	K_i (md)	k_d/k_i
10	2.94	12.83	70	100	1	3	12.52	12.53	0.9989
20	5.85	12.71	70	100	1	3	12.41	12.53	0.9902
30	8.76	12.70	70	100	1	3	12.40	12.53	0.9893
40	11.64	12.57	70	100	1	3	12.27	12.53	0.9794
50	14.49	12.47	70	100	1	3	12.17	12.53	0.9713
60	17.33	12.42	70	100	1	3	12.12	12.53	0.9675
70	20.15	12.31	70	100	1	3	12.02	12.53	0.9600
80	22.97	12.31	70	100	1	3	12.02	12.53	0.9593
90	25.76	12.21	70	100	1	3	11.92	12.53	0.9512
100	28.54	12.17	70	100	1	3	11.88	12.53	0.9483
110	31.31	12.14	70	100	1	3	11.85	12.53	0.9456
120	34.08	12.07	70	100	1	3	11.78	12.53	0.9403

Table B.16: Experimental data of core flood at normal barium: Run # 14

Injected Time (min)	No. of PV's injected	Q (cc/min)	T (°C)	ΔP (psig)	D (in)	L (in)	K_d (md)	K_i (md)	k_d/k_i
10	3.88	20.78	70	150	1	3	13.52	13.55	0.9976
20	7.72	20.59	70	150	1	3	13.40	13.55	0.9891
30	11.53	20.44	70	150	1	3	13.30	13.55	0.9812
40	15.33	20.36	70	150	1	3	13.25	13.55	0.9776
50	19.09	20.16	70	150	1	3	13.12	13.55	0.9682
60	22.83	20.04	70	150	1	3	13.04	13.55	0.9621
70	26.55	19.92	70	150	1	3	12.96	13.55	0.9564
80	30.24	19.78	70	150	1	3	12.87	13.55	0.9498
90	33.90	19.62	70	150	1	3	12.77	13.55	0.9425
100	37.54	19.53	70	150	1	3	12.71	13.55	0.9383
110	41.17	19.47	70	150	1	3	12.67	13.55	0.9347
120	44.78	19.36	70	150	1	3	12.60	13.55	0.9301

Table B.17: Experimental data of core flood at normal barium: Run # 15

Injected Time (min)	No. of PV's injected	Q (cc/min)	T (°C)	ΔP (psig)	D (in)	L (in)	K_d (md)	K_i (md)	k_d/k_i
10	4.49	25.32	70	200	1	3	12.36	12.41	0.9961
20	8.94	25.12	70	200	1	3	12.26	12.41	0.9881
30	13.36	24.94	70	200	1	3	12.17	12.41	0.9805
40	17.76	24.79	70	200	1	3	12.10	12.41	0.9752
50	22.12	24.59	70	200	1	3	12.00	12.41	0.9670
60	26.48	24.57	70	200	1	3	11.99	12.41	0.9662
70	30.77	24.18	70	200	1	3	11.80	12.41	0.9512
80	35.03	24.05	70	200	1	3	11.74	12.41	0.9462
90	39.26	23.87	70	200	1	3	11.65	12.41	0.9389
100	43.47	23.75	70	200	1	3	11.59	12.41	0.9342
110	47.68	23.75	70	200	1	3	11.59	12.41	0.9337
120	51.84	23.48	70	200	1	3	11.46	12.41	0.9238

Table B.18: Experimental data of core flood at normal barium: Run # 16

Injected Time (min)	No. of PV's injected	Q (cc/min)	T (°C)	ΔP (psig)	D (in)	L (in)	K_d (md)	K_i (md)	k_d/k_i
10	3.08	14.80	80	100	1	3	12.95	12.96	0.9994
20	6.15	14.74	80	100	1	3	12.90	12.96	0.9957
30	9.20	14.65	80	100	1	3	12.82	12.96	0.9893
40	12.23	14.55	80	100	1	3	12.73	12.96	0.9823
50	15.25	14.49	80	100	1	3	12.68	12.96	0.9784
60	18.27	14.48	80	100	1	3	12.67	12.96	0.9779
70	21.26	14.34	80	100	1	3	12.55	12.96	0.9685
80	24.24	14.29	80	100	1	3	12.50	12.96	0.9646
90	27.21	14.27	80	100	1	3	12.49	12.96	0.9634
100	30.16	14.16	80	100	1	3	12.39	12.96	0.9561
110	33.10	14.10	80	100	1	3	12.34	12.96	0.9523
120	36.03	14.07	80	100	1	3	12.31	12.96	0.9496

Table B.19: Experimental data of core flood at normal barium: Run # 17

Injected Time (min)	No. of PV's injected	Q (cc/min)	T (°C)	ΔP (psig)	D (in)	L (in)	K_d (md)	K_i (md)	k_d/k_i
10	3.99	21.98	80	150	1	3	12.82	12.83	0.9989
20	7.96	21.86	80	150	1	3	12.75	12.83	0.9936
30	11.9	21.70	80	150	1	3	12.66	12.83	0.9864
40	15.84	21.69	80	150	1	3	12.65	12.83	0.9857
50	19.72	21.39	80	150	1	3	12.48	12.83	0.9731
60	23.59	21.33	80	150	1	3	12.44	12.83	0.9695
70	27.44	21.21	80	150	1	3	12.37	12.83	0.9640
80	31.29	21.19	80	150	1	3	12.36	12.83	0.9637
90	35.10	20.98	80	150	1	3	12.24	12.83	0.9539
100	38.89	20.88	80	150	1	3	12.18	12.83	0.9492
110	42.66	20.78	80	150	1	3	12.12	12.83	0.9450
120	46.41	20.69	80	150	1	3	12.07	12.83	0.9411

Table B.20: Experimental data of core flood at normal barium: Run # 18

Injected Time (min)	No. of PV's injected	Q (cc/min)	T (°C)	ΔP (psig)	D (in)	L (in)	K_d (md)	K_i (md)	k_d/k_i
10	5.71	28.34	80	200	1	3	12.42	12.45	0.9978
20	11.39	28.18	80	200	1	3	12.33	12.45	0.9902
30	17.04	28.00	80	200	1	3	12.25	12.45	0.9836
40	22.65	27.84	80	200	1	3	12.18	12.45	0.9780
50	28.22	27.61	80	200	1	3	12.08	12.45	0.9700
60	33.76	27.50	80	200	1	3	12.03	12.45	0.9663
70	39.27	27.34	80	200	1	3	11.96	12.45	0.9610
80	44.76	27.24	80	200	1	3	11.92	12.45	0.9574
90	50.22	27.08	80	200	1	3	11.85	12.45	0.9521
100	55.65	26.95	80	200	1	3	11.79	12.45	0.9467
110	61.05	26.79	80	200	1	3	11.72	12.45	0.9413
120	66.42	26.63	80	200	1	3	11.65	12.45	0.9356

APPENDIX C

EXPERIMENTAL DATA AND RESULTS OF CALCIUM AND STRONTIUM SULFATES

Table C.1: Experimental data of core flood at high salinity: Run # 19

Injected Time (min)	No. of PV's injected	Q (cc/min)	T (°C)	ΔP (psig)	D (in)	L (in)	K_d (md)	K_i (md)	k_d/k_i
10	1.87	10.26	50	100	1	3	12.96	12.98	0.9986
20	3.72	10.18	50	100	1	3	12.85	12.98	0.9902
30	5.56	10.09	50	100	1	3	12.74	12.98	0.9812
40	7.37	9.95	50	100	1	3	12.57	12.98	0.9685
50	9.14	9.74	50	100	1	3	12.30	12.98	0.9476
60	10.90	9.64	50	100	1	3	12.18	12.98	0.9382
70	12.60	9.32	50	100	1	3	11.77	12.98	0.9068
80	14.28	9.21	50	100	1	3	11.63	12.98	0.8959
90	15.94	9.10	50	100	1	3	11.49	12.98	0.8853
100	17.58	9.03	50	100	1	3	11.40	12.98	0.8779
110	19.20	8.92	50	100	1	3	11.26	12.98	0.8675
120	20.81	8.81	50	100	1	3	11.13	12.98	0.8574

Table C.2: Experimental data of core flood at high salinity: Run # 20

Injected Time (min)	No. of PV's injected	Q (cc/min)	T (°C)	ΔP (psig)	D (in)	L (in)	K_d (md)	K_i (md)	k_d/k_i
10	2.44	15.20	50	150	1	3	12.80	12.85	0.9963
20	4.86	15.06	50	150	1	3	12.68	12.85	0.9864
30	7.24	14.78	50	150	1	3	12.44	12.85	0.9682
40	9.59	14.61	50	150	1	3	12.30	12.85	0.9572
50	11.89	14.30	50	150	1	3	12.04	12.85	0.9368
60	14.15	14.05	50	150	1	3	11.83	12.85	0.9203
70	16.35	13.71	50	150	1	3	11.54	12.85	0.8980
80	18.53	13.55	50	150	1	3	11.41	12.85	0.8876
90	20.67	13.29	50	150	1	3	11.19	12.85	0.8712
100	22.80	13.26	50	150	1	3	11.16	12.85	0.8682
110	24.90	13.09	50	150	1	3	11.02	12.85	0.8575
120	26.98	12.92	50	150	1	3	10.88	12.85	0.8465

Table C.3: Experimental data of core flood at high salinity: Run # 21

Injected Time (min)	No. of PV's injected	Q (cc/min)	T (°C)	ΔP (psig)	D (in)	L (in)	K_d (md)	K_i (md)	k_d/k_i
10	3.62	19.49	50	200	1	3	12.31	12.47	0.9875
20	7.18	19.19	50	200	1	3	12.12	12.47	0.9723
30	10.68	18.85	50	200	1	3	11.90	12.47	0.9541
40	14.13	18.59	50	200	1	3	11.74	12.47	0.9412
50	17.52	18.27	50	200	1	3	11.54	12.47	0.9258
60	20.83	17.82	50	200	1	3	11.25	12.47	0.9024
70	24.08	17.53	50	200	1	3	11.07	12.47	0.8875
80	27.29	17.31	50	200	1	3	10.93	12.47	0.8767
90	30.44	16.99	50	200	1	3	10.73	12.47	0.8607
100	33.58	16.90	50	200	1	3	10.67	12.47	0.8559
110	36.68	16.72	50	200	1	3	10.56	12.47	0.8467
120	39.73	16.45	50	200	1	3	10.39	12.47	0.8336

Table C.4: Experimental data of core flood at high salinity: Run # 22

Injected Time (min)	No. of PV's injected	Q (cc/min)	T (°C)	ΔP (psig)	D (in)	L (in)	K_d (md)	K_i (md)	k_d/k_i
10	2.76	12.82	70	100	1	3	12.51	12.55	0.9971
20	5.49	12.69	70	100	1	3	12.39	12.55	0.9872
30	8.16	12.40	70	100	1	3	12.10	12.55	0.9642
40	10.79	12.23	70	100	1	3	11.94	12.55	0.9516
50	13.38	12.04	70	100	1	3	11.75	12.55	0.9364
60	15.91	11.76	70	100	1	3	11.48	12.55	0.9147
70	18.38	11.51	70	100	1	3	11.23	12.55	0.8949
80	20.79	11.19	70	100	1	3	10.92	12.55	0.8703
90	23.16	11.02	70	100	1	3	10.76	12.55	0.8576
100	25.50	10.90	70	100	1	3	10.64	12.55	0.8479
110	27.81	10.74	70	100	1	3	10.48	12.55	0.8352
120	30.08	10.54	70	100	1	3	10.29	12.55	0.8201

Table C.5: Experimental data of core flood at high salinity: Run # 23

Injected Time (min)	No. of PV's injected	Q (cc/min)	T (°C)	ΔP (psig)	D (in)	L (in)	K_d (md)	K_i (md)	k_d/k_i
10	3.84	20.72	70	150	1	3	13.48	13.57	0.9936
20	7.62	20.41	70	150	1	3	13.28	13.57	0.9786
30	11.32	19.98	70	150	1	3	13.00	13.57	0.9584
40	14.96	19.65	70	150	1	3	12.79	13.57	0.9423
50	18.53	19.29	70	150	1	3	12.55	13.57	0.9245
60	22.03	18.90	70	150	1	3	12.30	13.57	0.9062
70	25.42	18.32	70	150	1	3	11.92	13.57	0.8785
80	28.70	17.73	70	150	1	3	11.54	13.57	0.8502
90	31.94	17.52	70	150	1	3	11.40	13.57	0.8398
100	35.11	17.13	70	150	1	3	11.15	13.57	0.8214
110	38.24	16.90	70	150	1	3	11.00	13.57	0.8103
120	41.36	16.84	70	150	1	3	10.96	13.57	0.8076

Table C.6: Experimental data of core flood at high salinity: Run # 24

Injected Time (min)	No. of PV's injected	Q (cc/min)	T (°C)	ΔP (psig)	D (in)	L (in)	K_d (md)	K_i (md)	k_d/k_i
10	5.26	24.98	70	200	1	3	12.19	12.43	0.9805
20	10.46	24.69	70	200	1	3	12.05	12.43	0.9691
30	15.52	24.03	70	200	1	3	11.73	12.43	0.9436
40	20.51	23.69	70	200	1	3	11.56	12.43	0.9301
50	25.40	23.23	70	200	1	3	11.34	12.43	0.9123
60	30.15	22.54	70	200	1	3	11.00	12.43	0.8852
70	34.75	21.84	70	200	1	3	10.66	12.43	0.8576
80	39.24	21.31	70	200	1	3	10.40	12.43	0.8367
90	43.65	20.96	70	200	1	3	10.23	12.43	0.8228
100	47.96	20.45	70	200	1	3	9.98	12.43	0.8026
110	52.23	20.28	70	200	1	3	9.90	12.43	0.7963
120	56.46	20.10	70	200	1	3	9.81	12.43	0.7889

Table C.7: Experimental data of core flood at high salinity: Run # 25

Injected Time (min)	No. of PV's injected	Q (cc/min)	T (°C)	ΔP (psig)	D (in)	L (in)	K_d (md)	K_i (md)	k_d/k_i
10	3.50	15.77	80	100	1	3	13.80	13.87	0.9952
20	6.91	15.39	80	100	1	3	13.47	13.87	0.9712
30	10.28	15.21	80	100	1	3	13.31	13.87	0.9593
40	13.58	14.90	80	100	1	3	13.04	13.87	0.9401
50	16.84	14.72	80	100	1	3	12.88	13.87	0.9285
60	20.03	14.38	80	100	1	3	12.58	13.87	0.9068
70	23.15	14.05	80	100	1	3	12.29	13.87	0.8862
80	26.19	13.69	80	100	1	3	11.98	13.87	0.8635
90	29.14	13.31	80	100	1	3	11.65	13.87	0.8402
100	32.05	13.13	80	100	1	3	11.49	13.87	0.8286
110	34.92	12.94	80	100	1	3	11.32	13.87	0.8165
120	37.74	12.72	80	100	1	3	11.13	13.87	0.8024

Table C.8: Experimental data of core flood at high salinity: Run # 26

Injected Time (min)	No. of PV's injected	Q (cc/min)	T (°C)	ΔP (psig)	D (in)	L (in)	K_d (md)	K_i (md)	k_d/k_i
10	4.89	23.07	80	150	1	3	13.46	13.63	0.9874
20	9.61	22.27	80	150	1	3	12.99	13.63	0.9534
30	14.24	21.87	80	150	1	3	12.76	13.63	0.9361
40	18.83	21.67	80	150	1	3	12.64	13.63	0.9271
50	23.30	21.12	80	150	1	3	12.32	13.63	0.9036
60	27.67	20.62	80	150	1	3	12.03	13.63	0.8824
70	31.96	20.26	80	150	1	3	11.82	13.63	0.8673
80	36.12	19.63	80	150	1	3	11.45	13.63	0.8402
90	40.21	19.32	80	150	1	3	11.27	13.63	0.8265
100	44.22	18.93	80	150	1	3	11.04	13.63	0.8098
110	48.17	18.63	80	150	1	3	10.87	13.63	0.7976
120	52.06	18.36	80	150	1	3	10.71	13.63	0.7856

Table C.9: Experimental data of core flood at high salinity: Run # 27

Injected Time (min)	No. of PV's injected	Q (cc/min)	T (°C)	ΔP (psig)	D (in)	L (in)	K_d (md)	K_i (md)	k_d/k_i
10	6.91	30.60	80	200	1	3	13.39	13.73	0.9750
20	13.61	29.69	80	200	1	3	12.99	13.73	0.9464
30	20.16	29.03	80	200	1	3	12.70	13.73	0.9250
40	26.63	28.68	80	200	1	3	12.55	13.73	0.9143
50	32.93	27.91	80	200	1	3	12.21	13.73	0.8893
60	39.00	26.90	80	200	1	3	11.77	13.73	0.8571
70	44.94	26.33	80	200	1	3	11.52	13.73	0.8393
80	50.73	25.67	80	200	1	3	11.23	13.73	0.8179
90	56.36	24.96	80	200	1	3	10.92	13.73	0.7956
100	61.90	24.55	80	200	1	3	10.74	13.73	0.7821
110	67.39	24.30	80	200	1	3	10.63	13.73	0.7745
120	72.82	24.04	80	200	1	3	10.52	13.73	0.7661

Table C.10: Experimental data of core flood at normal salinity: Run # 28

Injected Time (min)	No. of PV's injected	Q (cc/min)	T (°C)	ΔP (psig)	D (in)	L (in)	K_d (md)	K_i (md)	k_d/k_i
10	1.47	10.72	50	100	1	3	12.86	12.87	0.9991
20	2.94	10.16	50	100	1	3	12.82	12.87	0.9962
30	4.40	10.09	50	100	1	3	12.73	12.87	0.9892
40	5.85	10.04	50	100	1	3	12.66	12.87	0.9835
50	7.29	9.98	50	100	1	3	12.59	12.87	0.9786
60	8.73	9.94	50	100	1	3	12.54	12.87	0.9747
70	10.16	9.89	50	100	1	3	12.48	12.87	0.9698
80	11.59	9.85	50	100	1	3	12.43	12.87	0.9656
90	13.01	9.83	50	100	1	3	12.40	12.87	0.9633
100	14.43	9.81	50	100	1	3	12.37	12.87	0.9614
110	15.85	9.79	50	100	1	3	12.35	12.87	0.9594
120	17.26	9.77	50	100	1	3	12.32	12.87	0.9576

Table C.11: Experimental data of core flood at normal salinity: Run # 29

Injected Time (min)	No. of PV's injected	Q (cc/min)	T (°C)	ΔP (psig)	D (in)	L (in)	K_d (md)	K_i (md)	k_d/k_i
10	2.46	15.51	50	150	1	3	12.68	12.72	0.9972
20	4.91	15.20	50	150	1	3	12.61	12.72	0.9914
30	7.34	14.91	50	150	1	3	12.54	12.72	0.9862
40	9.76	14.81	50	150	1	3	12.46	12.72	0.9792
50	12.16	14.70	50	150	1	3	12.36	12.72	0.9718
60	14.54	14.62	50	150	1	3	12.30	12.72	0.9670
70	16.91	14.54	50	150	1	3	12.23	12.72	0.9613
80	19.27	14.48	50	150	1	3	12.18	12.72	0.9578
90	21.63	14.45	50	150	1	3	12.15	12.72	0.9549
100	23.98	14.40	50	150	1	3	12.11	12.72	0.9522
110	26.32	14.34	50	150	1	3	12.06	12.72	0.9485
120	28.66	14.32	50	150	1	3	12.04	12.72	0.9465

Table C.12: Experimental data of core flood at normal salinity: Run # 30

Injected Time (min)	No. of PV's injected	Q (cc/min)	T (°C)	ΔP (psig)	D (in)	L (in)	K_d (md)	K_i (md)	k_d/k_i
10	4.72	19.75	50	200	1	3	12.27	12.38	0.9913
20	9.40	19.38	50	200	1	3	12.16	12.38	0.9823
30	14.04	19.13	50	200	1	3	12.07	12.38	0.9751
40	18.64	18.96	50	200	1	3	11.96	12.38	0.9662
50	23.21	18.83	50	200	1	3	11.88	12.38	0.9598
60	27.75	18.69	50	200	1	3	11.79	12.38	0.9524
70	32.26	18.60	50	200	1	3	11.73	12.38	0.9475
80	36.74	18.47	50	200	1	3	11.65	12.38	0.9407
90	41.20	18.39	50	200	1	3	11.60	12.38	0.9367
100	45.62	18.28	50	200	1	3	11.53	12.38	0.9316
110	50.04	18.20	50	200	1	3	11.48	12.38	0.9277
120	54.44	18.12	50	200	1	3	11.43	12.38	0.9236

Table C.13: Experimental data of core flood at normal salinity: Run # 31

Injected Time (min)	No. of PV's injected	Q (cc/min)	T (°C)	ΔP (psig)	D (in)	L (in)	K_d (md)	K_i (md)	k_d/k_i
10	2.90	13.69	70	100	1	3	12.39	12.42	0.9979
20	5.79	12.74	70	100	1	3	12.34	12.42	0.9932
30	8.65	12.52	70	100	1	3	12.22	12.42	0.9842
40	11.49	12.44	70	100	1	3	12.14	12.42	0.9776
50	14.30	12.33	70	100	1	3	12.03	12.42	0.9684
60	17.09	12.23	70	100	1	3	11.94	12.42	0.9617
70	19.87	12.19	70	100	1	3	11.90	12.42	0.9579
80	22.64	12.12	70	100	1	3	11.83	12.42	0.9523
90	25.39	12.06	70	100	1	3	11.77	12.42	0.9476
100	28.13	11.99	70	100	1	3	11.70	12.42	0.9419
110	30.85	11.93	70	100	1	3	11.64	12.42	0.9372
120	33.55	11.84	70	100	1	3	11.56	12.42	0.9311

Table C.14: Experimental data of core flood at normal salinity: Run # 32

Injected Time (min)	No. of PV's injected	Q (cc/min)	T (°C)	ΔP (psig)	D (in)	L (in)	K_d (md)	K_i (md)	k_d/k_i
10	3.70	20.44	70	150	1	3	13.30	13.36	0.9956
20	7.37	20.30	70	150	1	3	13.21	13.36	0.9886
30	10.99	20.04	70	150	1	3	13.04	13.36	0.9764
40	14.56	19.76	70	150	1	3	12.86	13.36	0.9623
50	18.10	19.59	70	150	1	3	12.75	13.36	0.9543
60	21.62	19.47	70	150	1	3	12.67	13.36	0.9482
70	25.11	19.32	70	150	1	3	12.57	13.36	0.9405
80	28.57	19.16	70	150	1	3	12.47	13.36	0.9332
90	32.00	18.99	70	150	1	3	12.36	13.36	0.9248
100	35.41	18.84	70	150	1	3	12.26	13.36	0.9174
110	38.79	18.67	70	150	1	3	12.15	13.36	0.9093
120	42.14	18.55	70	150	1	3	12.07	13.36	0.9032

Table C.15: Experimental data of core flood at normal salinity: Run # 33

Injected Time (min)	No. of PV's injected	Q (cc/min)	T (°C)	ΔP (psig)	D (in)	L (in)	K_d (md)	K_i (md)	k_d/k_i
10	5.44	24.89	70	200	1	3	12.15	12.32	0.9865
20	10.83	24.69	70	200	1	3	12.05	12.32	0.9781
30	16.10	24.16	70	200	1	3	11.79	12.32	0.9571
40	21.32	23.89	70	200	1	3	11.66	12.32	0.9464
50	26.42	23.38	70	200	1	3	11.41	12.32	0.9259
60	31.48	23.17	70	200	1	3	11.31	12.32	0.9182
70	36.50	22.99	70	200	1	3	11.22	12.32	0.9106
80	41.44	22.64	70	200	1	3	11.05	12.32	0.8967
90	46.36	22.52	70	200	1	3	10.99	12.32	0.8918
100	51.25	22.37	70	200	1	3	10.92	12.32	0.8865
110	56.10	22.23	70	200	1	3	10.85	12.32	0.8803
120	60.92	22.09	70	200	1	3	10.78	12.32	0.8754

Table C.16: Experimental data of core flood at normal salinity: Run # 34

Injected Time (min)	No. of PV's injected	Q (cc/min)	T (°C)	ΔP (psig)	D (in)	L (in)	K_d (md)	K_i (md)	k_d/k_i
10	2.92	14.55	80	100	1	3	12.73	12.78	0.9961
20	5.80	14.37	80	100	1	3	12.57	12.78	0.9832
30	8.65	14.17	80	100	1	3	12.40	12.78	0.9703
40	11.47	14.06	80	100	1	3	12.30	12.78	0.9621
50	14.27	13.97	80	100	1	3	12.22	12.78	0.9565
60	17.06	13.87	80	100	1	3	12.14	12.78	0.9498
70	19.82	13.75	80	100	1	3	12.03	12.78	0.9415
80	22.57	13.68	80	100	1	3	11.97	12.78	0.9370
90	25.30	13.59	80	100	1	3	11.89	12.78	0.9302
100	28.02	13.54	80	100	1	3	11.85	12.78	0.9276
110	30.72	13.46	80	100	1	3	11.78	12.78	0.9215
120	33.41	13.39	80	100	1	3	11.72	12.78	0.9174

Table C.17: Experimental data of core flood at normal salinity: Run # 35

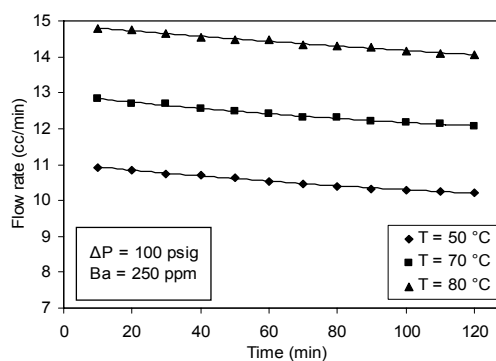
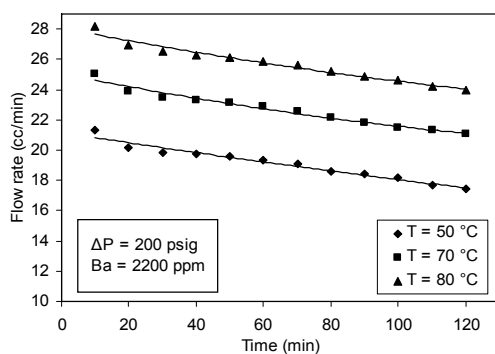
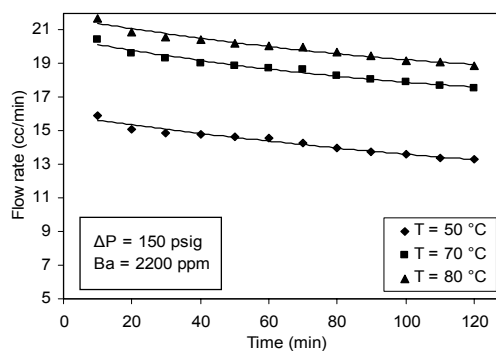
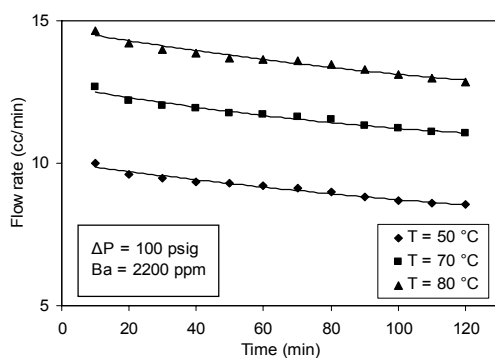
Injected Time (min)	No. of PV's injected	Q (cc/min)	T (°C)	ΔP (psig)	D (in)	L (in)	K_d (md)	K_i (md)	k_d/k_i
10	4.26	23.87	80	150	1	3	13.34	13.48	0.9894
20	8.45	22.53	80	150	1	3	13.14	13.48	0.9751
30	12.56	22.05	80	150	1	3	12.86	13.48	0.9543
40	16.63	21.87	80	150	1	3	12.76	13.48	0.9469
50	20.65	21.57	80	150	1	3	12.58	13.48	0.9336
60	24.64	21.41	80	150	1	3	12.49	13.48	0.9266
70	28.60	21.24	80	150	1	3	12.39	13.48	0.9195
80	32.52	21.07	80	150	1	3	12.29	13.48	0.9120
90	36.42	20.95	80	150	1	3	12.22	13.48	0.9065
100	40.29	20.79	80	150	1	3	12.13	13.48	0.8998
110	44.14	20.66	80	150	1	3	12.05	13.48	0.8936
120	47.95	20.49	80	150	1	3	11.95	13.48	0.8868

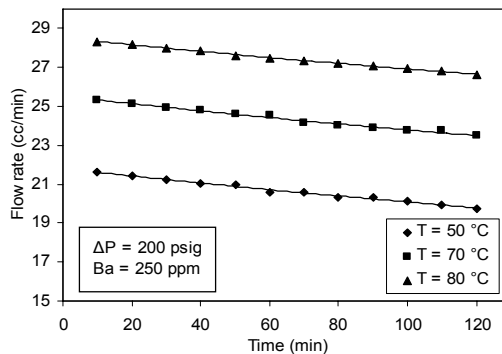
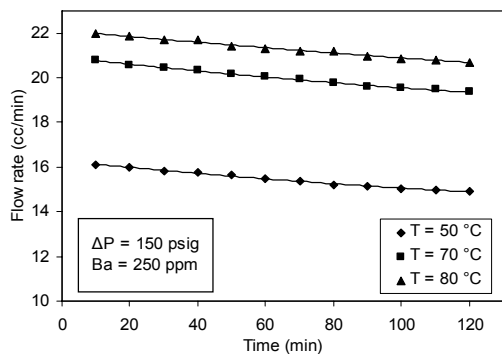
Table C.18: Experimental data of core flood at normal salinity: Run # 36

Injected Time (min)	No. of PV's injected	Q (cc/min)	T (°C)	ΔP (psig)	D (in)	L (in)	K_d (md)	K_i (md)	k_d/k_i
10	7.54	31.33	80	200	1	3	13.27	13.54	0.9803
20	14.99	30.94	80	200	1	3	13.10	13.54	0.9674
30	22.27	29.28	80	200	1	3	12.81	13.54	0.9461
40	29.46	28.91	80	200	1	3	12.65	13.54	0.9340
50	36.54	28.46	80	200	1	3	12.45	13.54	0.9193
60	43.50	27.98	80	200	1	3	12.24	13.54	0.9041
70	50.41	27.77	80	200	1	3	12.15	13.54	0.8973
80	57.17	27.47	80	200	1	3	12.02	13.54	0.8879
90	63.93	27.18	80	200	1	3	11.89	13.54	0.8781
100	70.61	26.86	80	200	1	3	11.75	13.54	0.8680
110	77.23	26.60	80	200	1	3	11.64	13.54	0.8596
120	83.80	26.42	80	200	1	3	11.56	13.54	0.8536

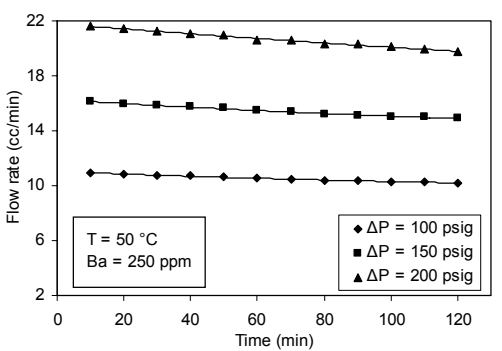
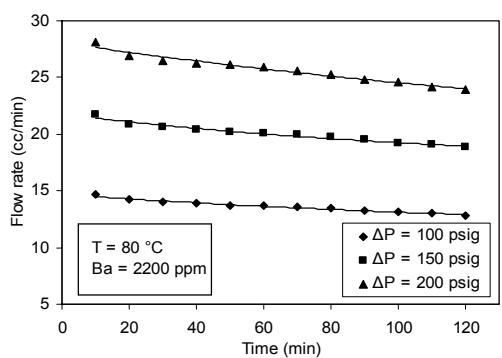
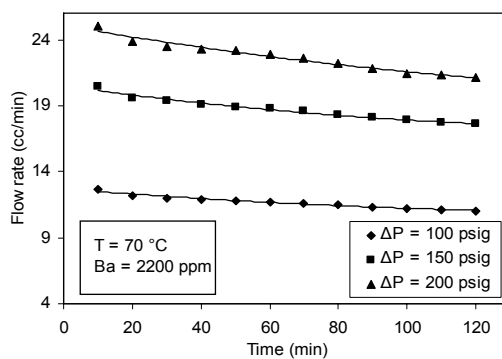
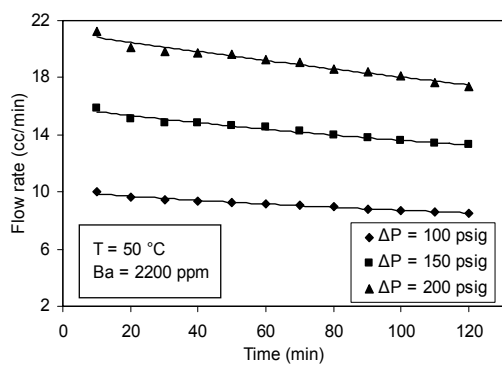
APPENDIX D

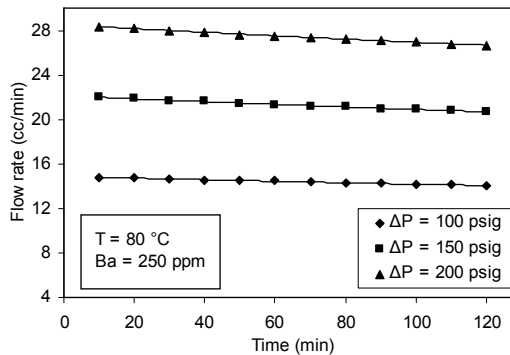
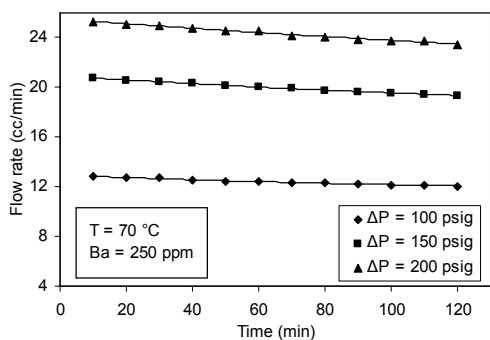
EFFECTS OF TEMPERATURE, CONCENTRATION OF BRINE, AND DIFFERENTIAL PRESSURES ON PERMEABILITY REDUCTION BY DEPOSITION OF BARIUM SULFATE



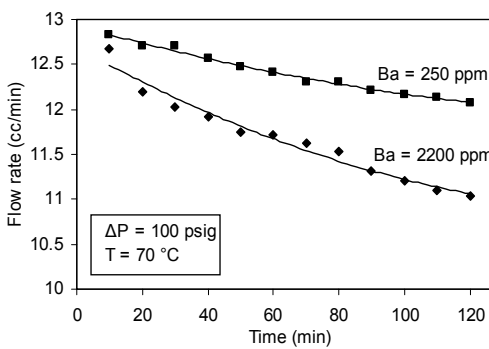
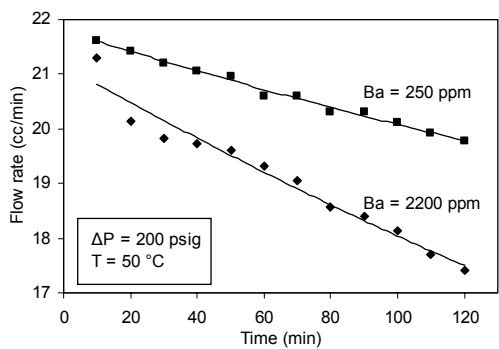
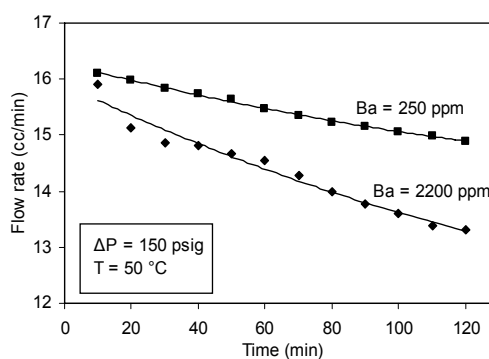
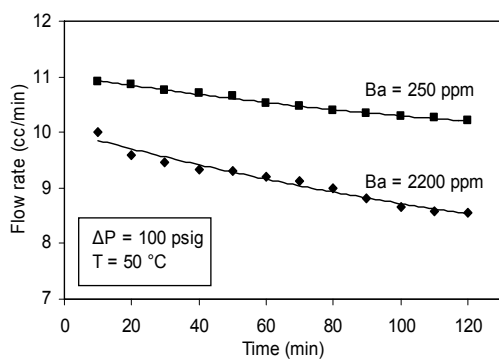


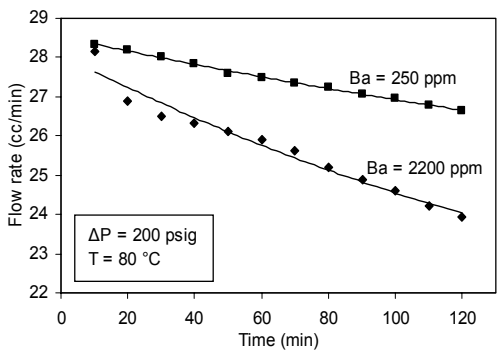
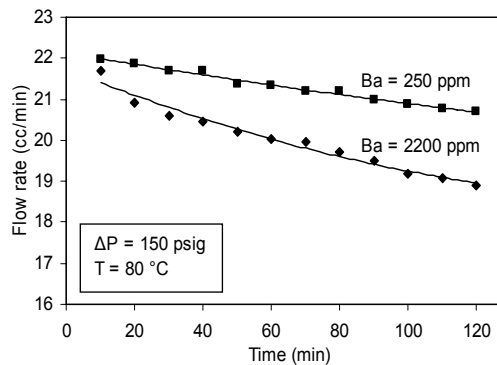
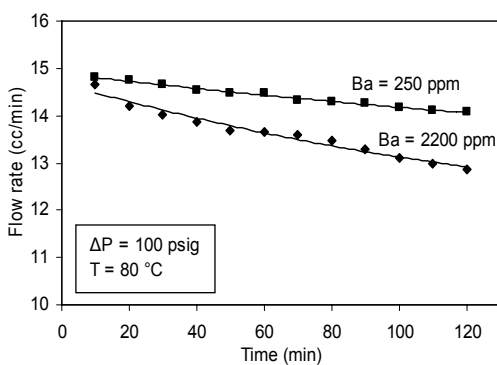
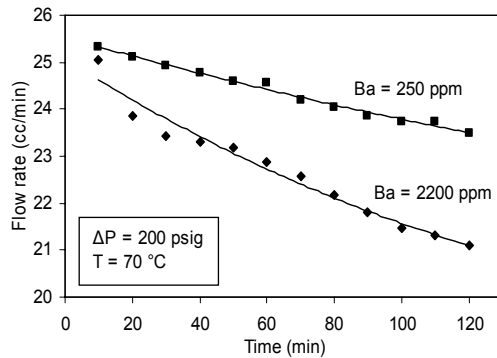
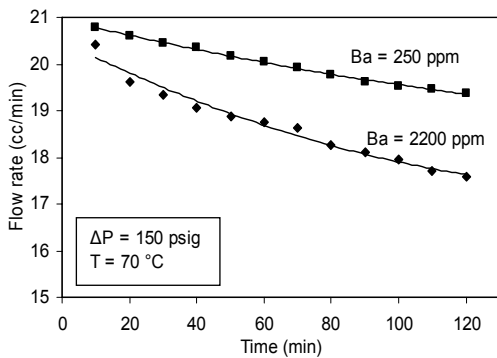
Figures D 1 - 6 Variation of flow rate as a function of time showing the effect of temperature



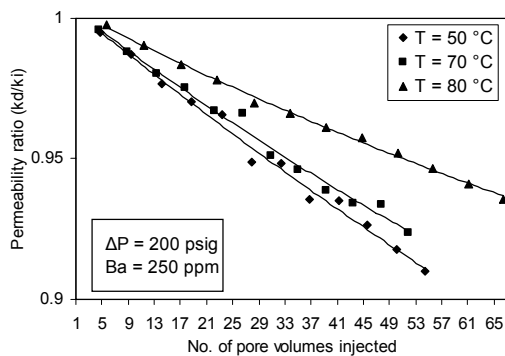
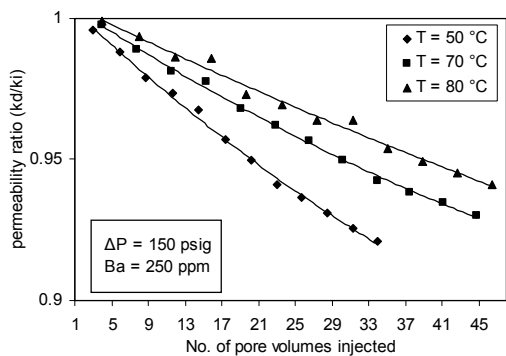
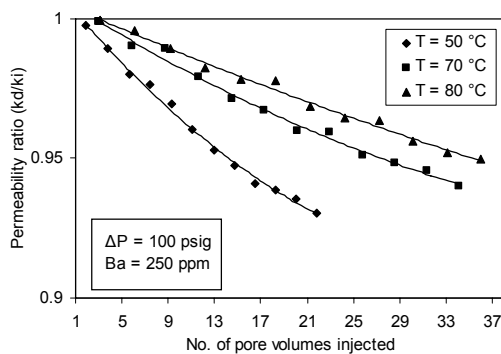
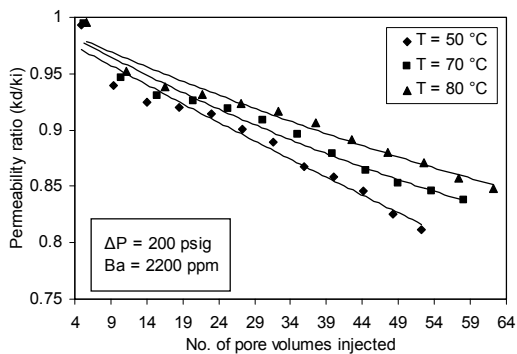
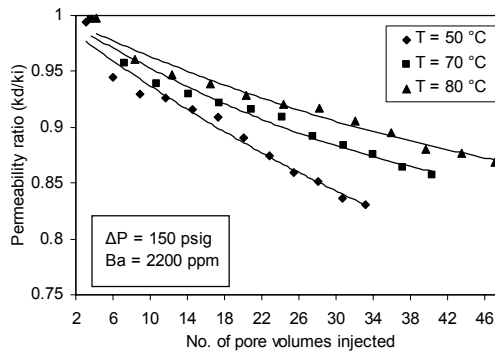
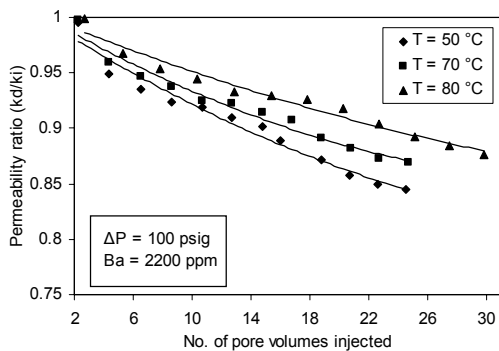


Figures D.7 – 12 Variation of flow rate as a function of time showing the effect of differential pressure





Figures D.13 - 21 Variation of flow rate as a function of time showing the effect of concentration



Figures D. 22 - 27 Variation of permeability ratio as a function of no. of pore volumes injected showing the effect of temperature

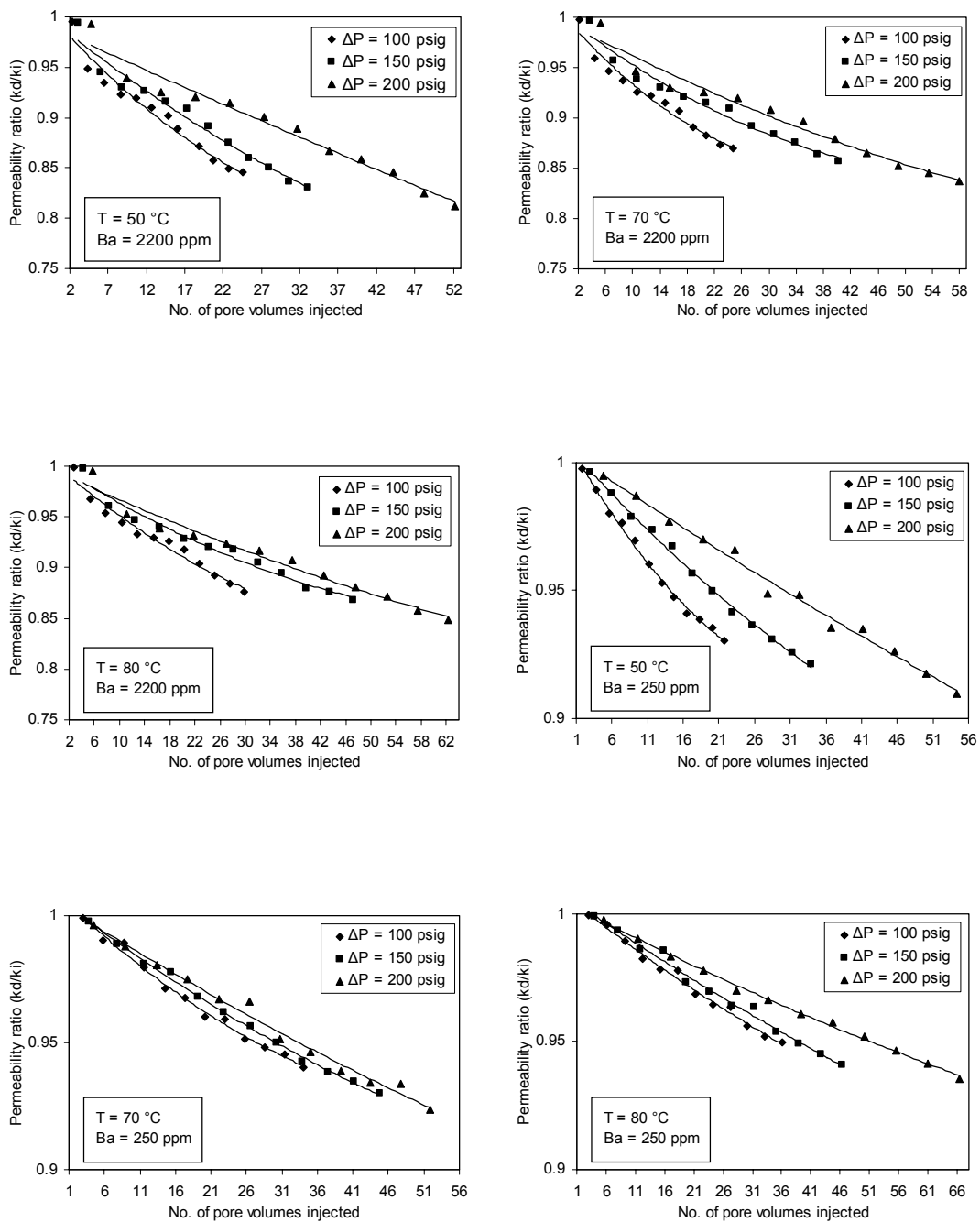
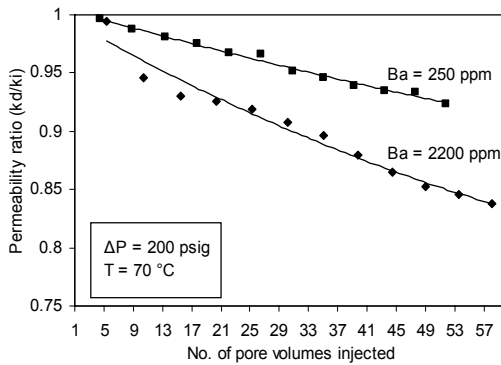
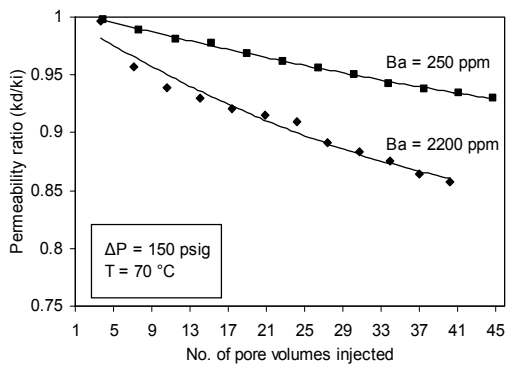
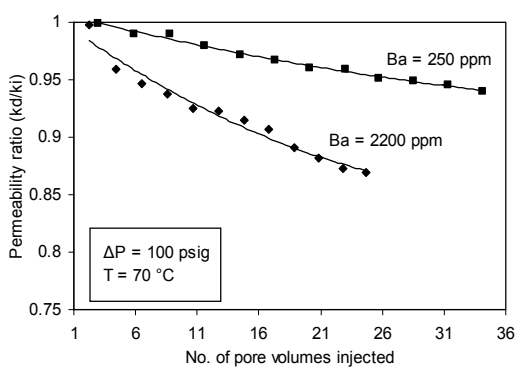
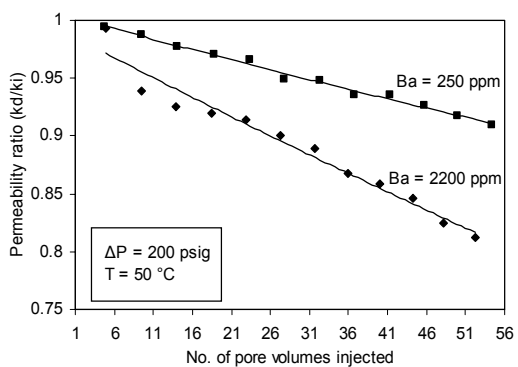
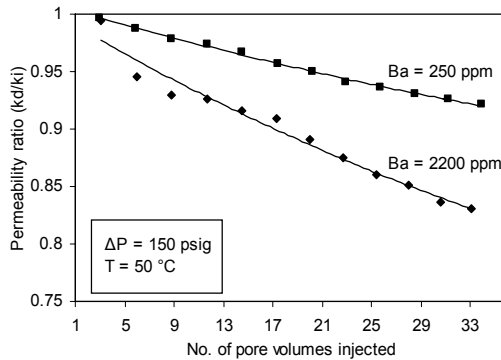
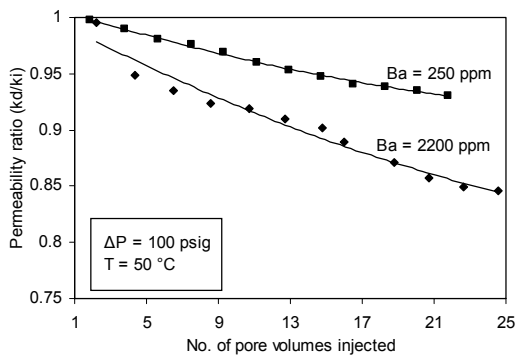


Figure D. 28 - 33 Variation of permeability ratio as a function of no. of pore volumes injected showing the effect of differential pressure



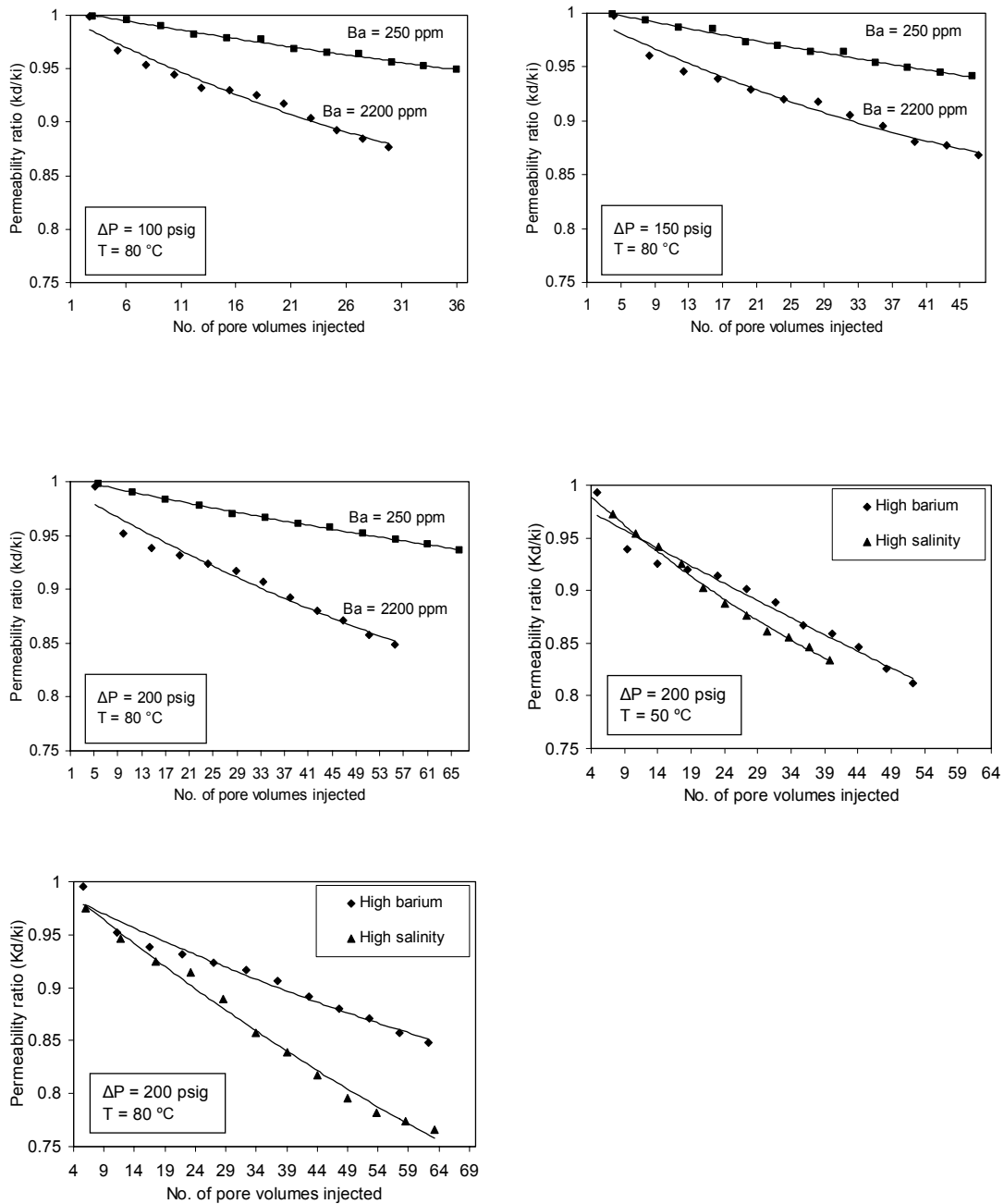
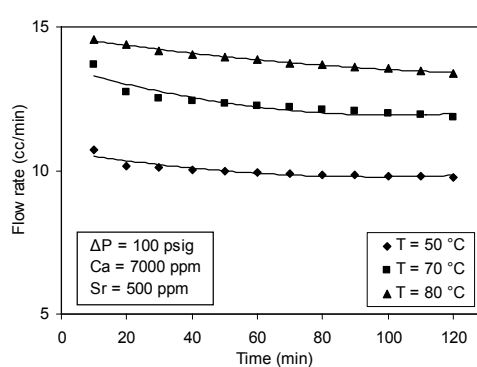
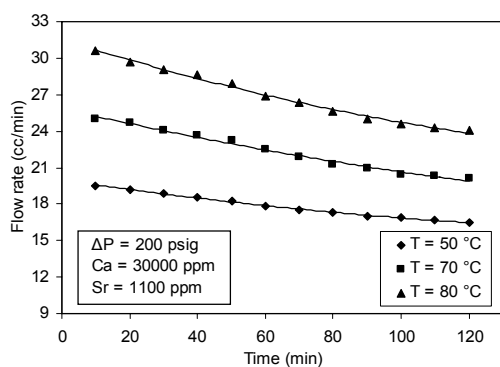
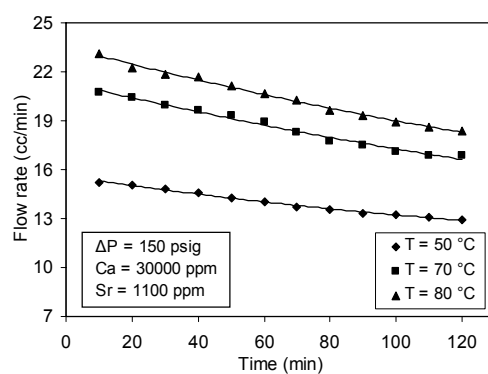
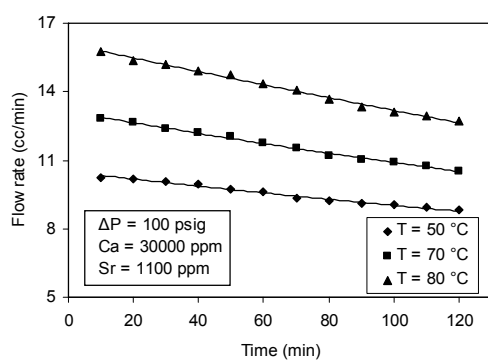
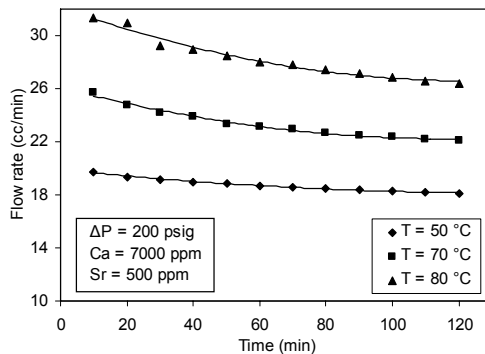
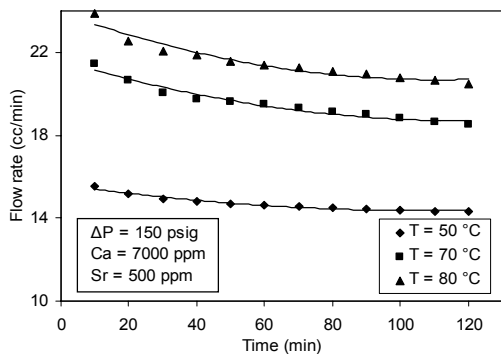


Figure D. 34 - 44 Variation of permeability ratio as a function of no. of pore volumes injected showing the effect of concentration

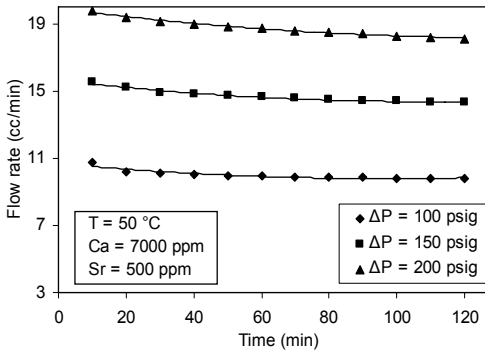
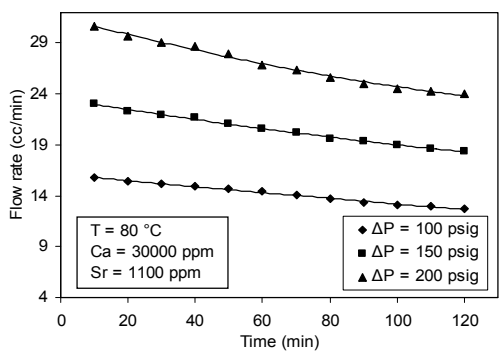
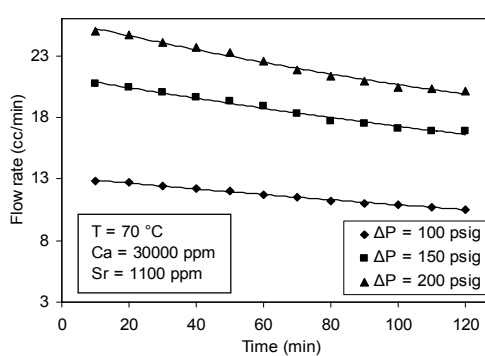
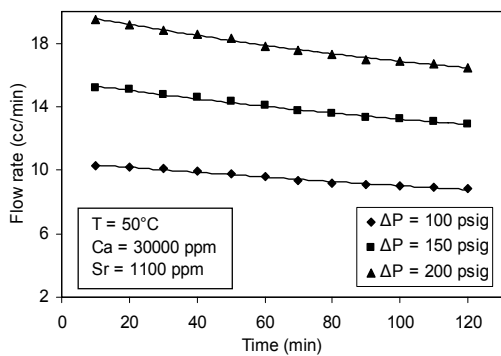
APPENDIX E

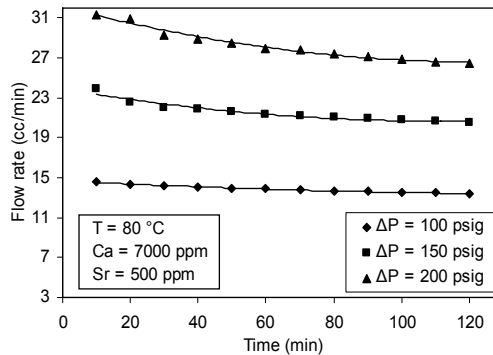
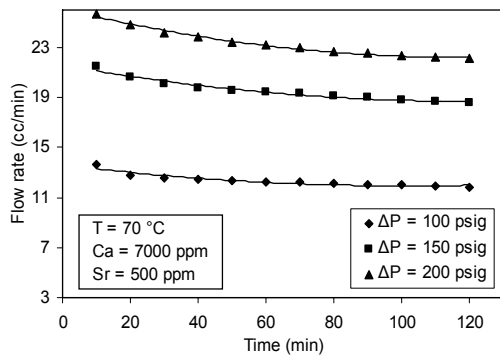
EFFECTS OF TEMPERATURE, CONCENTRATION OF BRINE, AND DIFFERENTIAL PRESSURES ON PERMEABILITY REDUCTION BY DEPOSITION OF CALCIUM AND STRONTIUM SULFATES



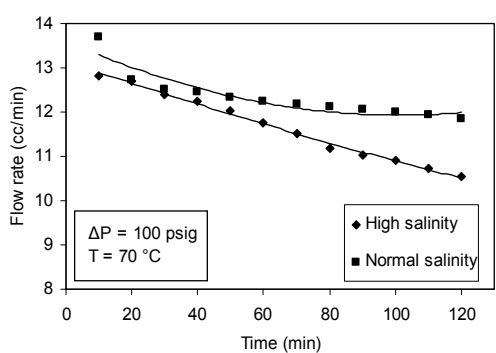
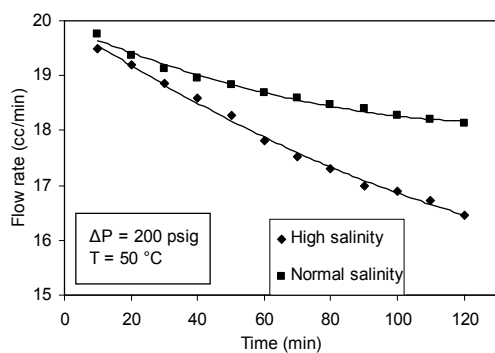
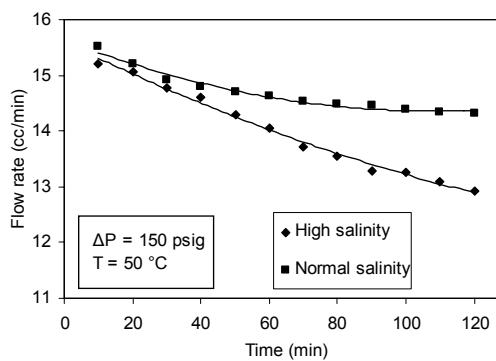
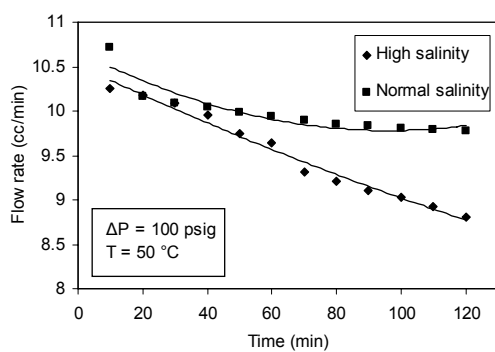


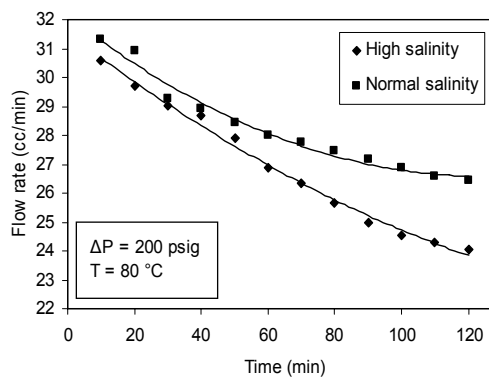
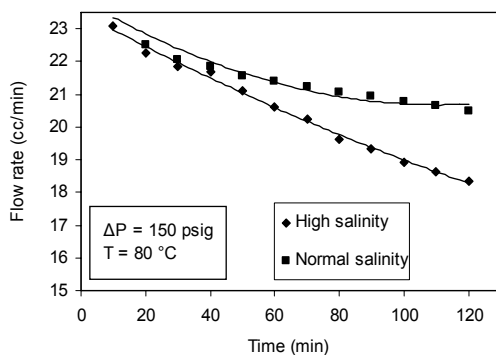
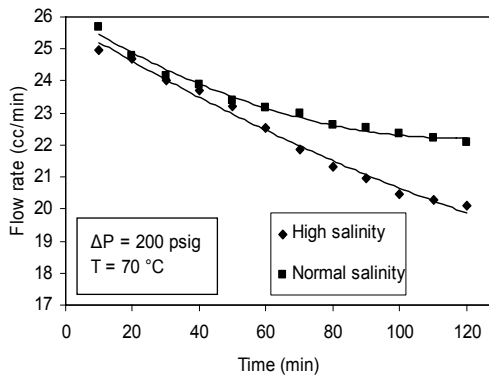
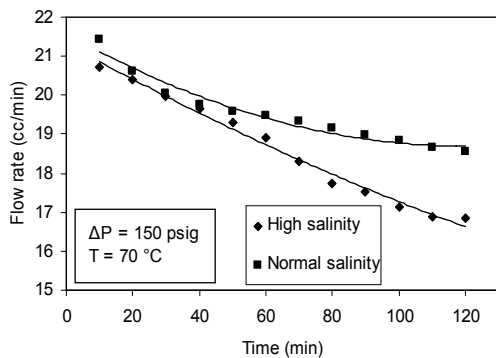
Figures E. 1 - 6 Variation of flow rate as a function of time showing the effect of temperature



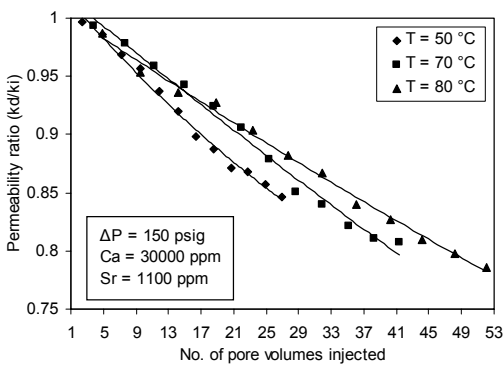
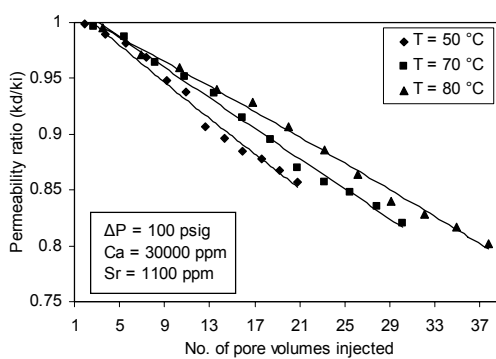


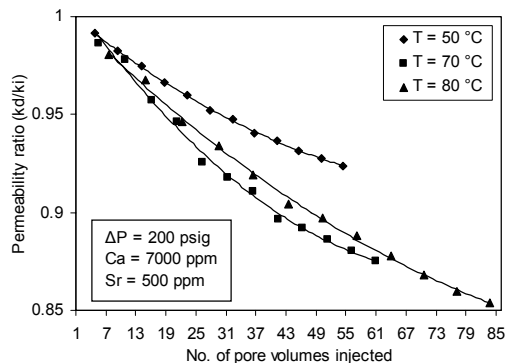
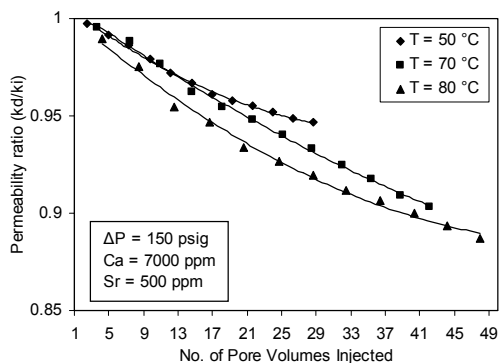
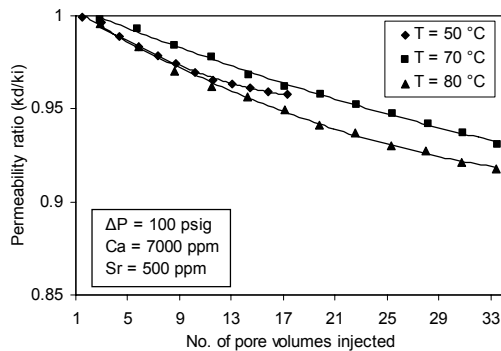
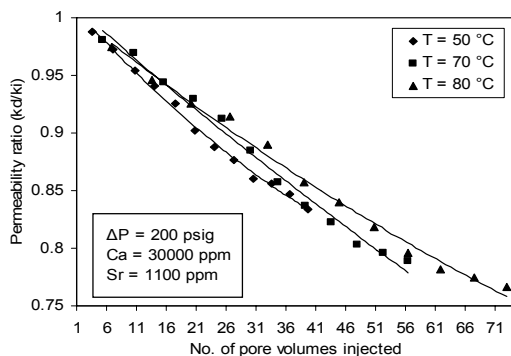
Figures E.7 - 12 Variation of flow rate as a function of time showing the effect of differential pressure



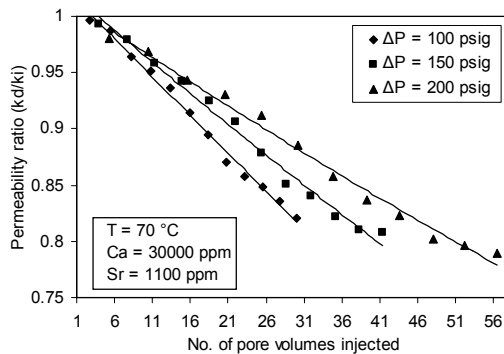
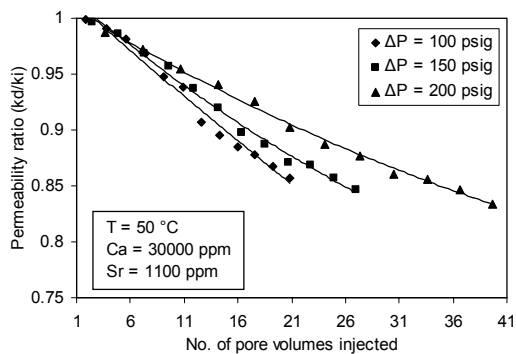


Figures E.13 - 20 Variation of flow rate as a function of time showing the effect of concentration





Figures E. 21 - 26 Variation of permeability ratio as a function of no. of pore volumes injected showing the effect of temperature



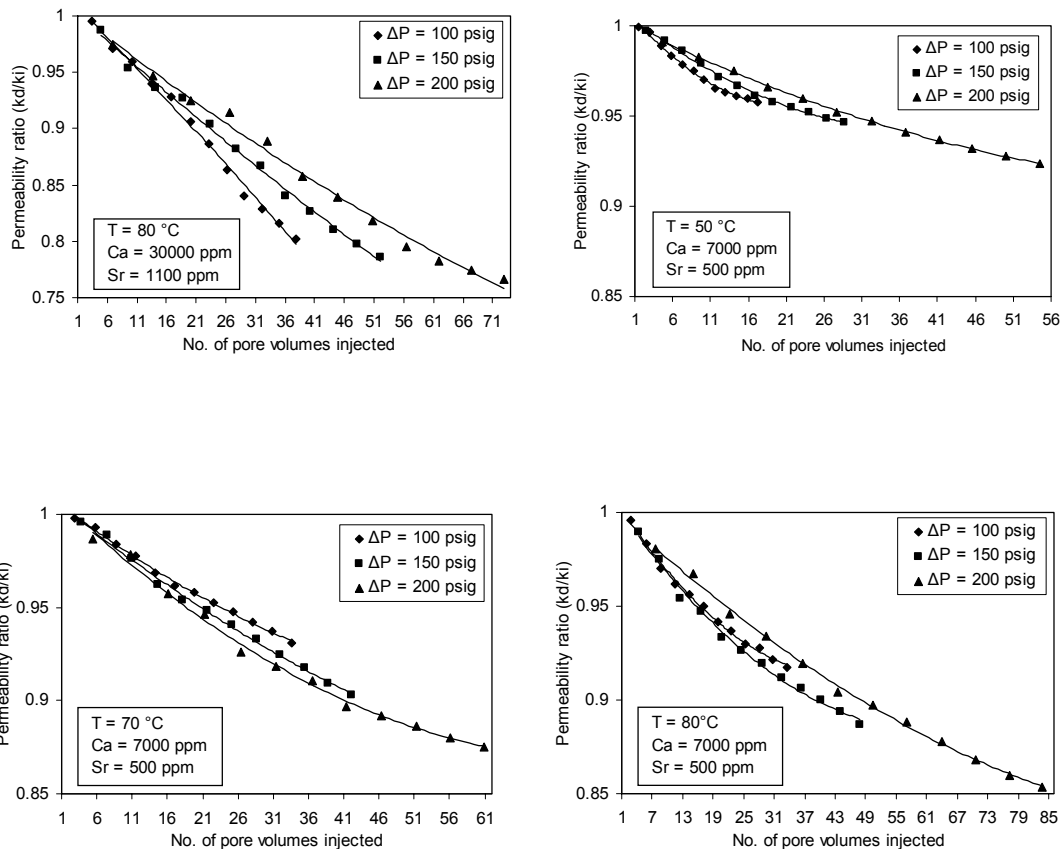
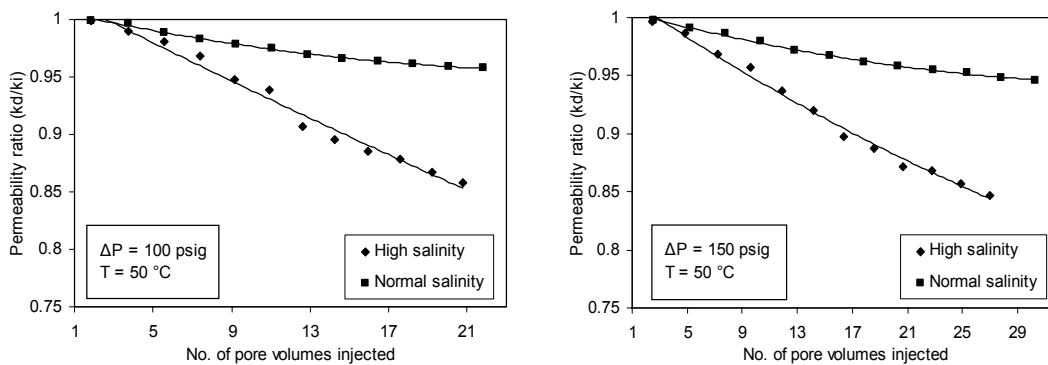
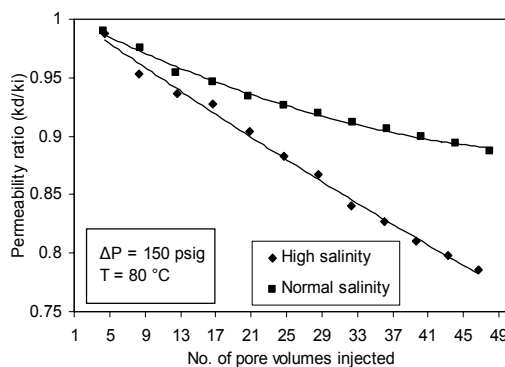
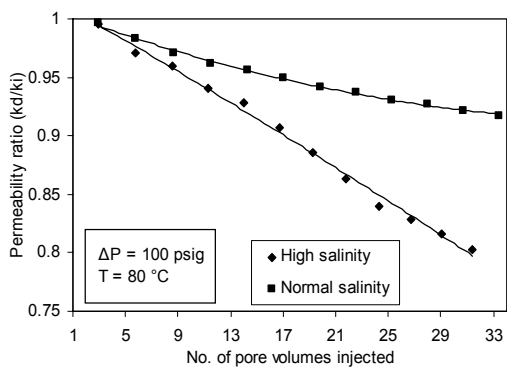
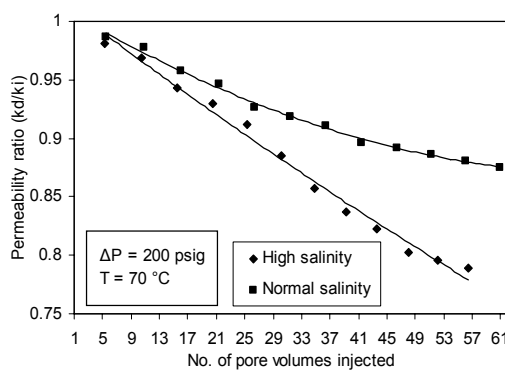
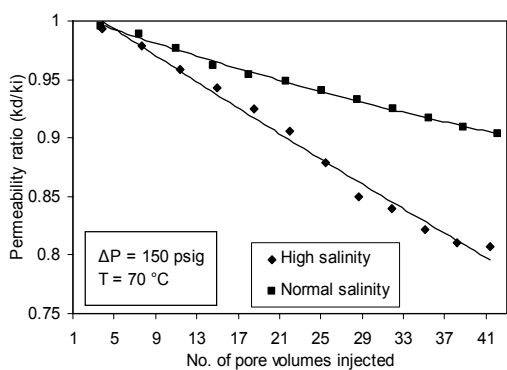
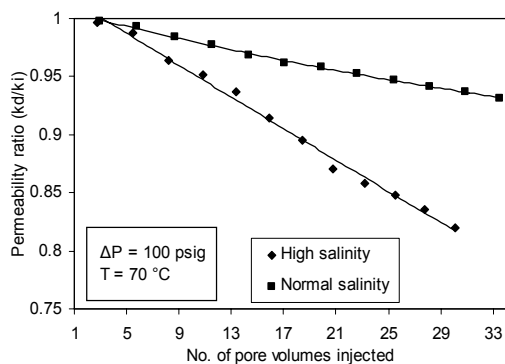
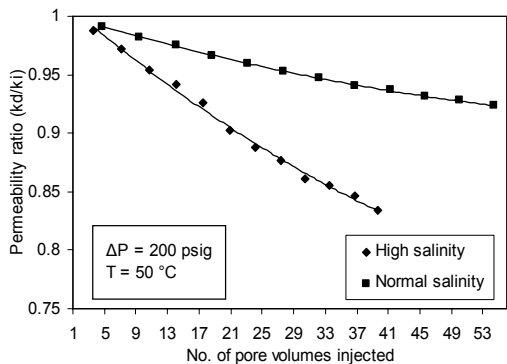


Figure E. 27 - 32 Variation of permeability ratio as a function of no. of pore volumes injected showing the effect of differential pressure





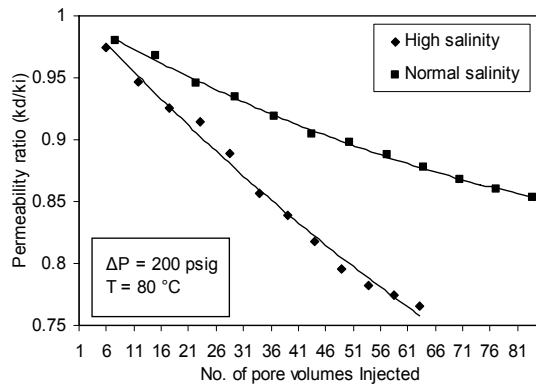


Figure E. 33 - 41 Variation of permeability ratio as a function of no. of pore volumes injected showing the effect of concentration